INFORMATION TO USERS

This manuscript has been reproduced from the microfilm master. UMI films the text directly from the original or copy submitted. Thus, some thesis and dissertation copies are in typewriter face, while others may be from any type of computer printer.

The quality of this reproduction is dependent upon the quality of the copy submitted. Broken or indistinct print, colored or poor quality illustrations and photographs, print bleedthrough, substandard margins, and improper alignment can adversely affect reproduction.

In the unlikely event that the author did not send UMI a complete manuscript and there are missing pages, these will be noted. Also, if unauthorized copyright material had to be removed, a note will indicate the deletion.

Oversize materials (e.g., maps, drawings, charts) are reproduced by sectioning the original, beginning at the upper left-hand corner and continuing from left to right in equal sections with small overlaps.

ProQuest Information and Learning
300 North Zeeb Road, Ann Arbor, MI 48106-1346 USA
800-521-0600

AN ASYMMETRIC TURBULENT FLUID FLOW INDUCED BY RECTANGULAR RIBBED SURFACE ROUGHNESS

by

Md. Amanullah Bhuiyan

A thesis submitted to the School of Graduate Studies in partial fulfillment of the requirements of the degree of

MASTER OF APPLIED SCIENCE

in the

Department of Mechanical Engineering
University of Ottawa
Ottawa, Canada

1977

AN ASYMMETRIC TURBULENT FLUID FLOW INDUCED BY RECTANGULAR RIBBED SURFACE ROUGHNESS

(Dr. Yung Lee)
Supervisor

(Md. Amanullah Bhuiyan)
Candidate

A B S T R A C T

The present thesis presents a theoretical as well as experimental investigation of fully developed turbulent fluid flow in partially roughened surfaced channel. The fluid properties were assumed to be constant throughout the analysis.

In the theoretical study of the problem the momentum integral method together with a turbulence model based on Prandtl's mixing length theory is adopted. The closure of the equations with one empirical constant was not possible and it was required to use empirical functions for the parameters describing the maximum velocity and zero shear stress points. The mean flow parameters of interests were given due considerations in the investigation.

The experimental study involves the measurements of mean and turbulent characteristics of the flow in a partially roughened surfaced channel. The asymmetric flow between parallel planes was developed by roughening one of the planes with rectangular ribs while the other was left smooth.

The most important parameters in the analysis are the locations of zero shear stress and maximum mean velocity points, since they

are the main experimental inputs used in the prediction of mean flow parameters.

The positions of the zero shear and maximum velocity points deviate more from the centre line of the channel towards the smooth wall for a lower roughness density as well as for increased Reynolds numbers corresponding to the same channel width.

A C K N O W L E D G E M E N T S

The author wishes to express his deep sense of gratitude to Dr. Yung Lee who initiated and supervised the present work. His valuable help, guidance and painstaking discussions which were extremely helpful in getting the end results of this project, are deeply appreciated. I am particularly grateful to Dr. Lee for the generous financial support I received during the course of my works.

Sincere thanks are also due to all the staff members, specially the technical staffs, of the Department of Mechanical Engineering, who extended their help and cooperation to me in various ways.

Last, but not the least, a special debt of gratitude is due to the author's wife who was a constant source of inspiration during the trying days.

TABLE OF CONTENTS

Contents

Contents

Contents

L I S T O F T A B L E S

L I S T O F F I G U R E S

NOMENCLATURE

A	Cross sectional area of channel ; constant , Equation (4.1)
a	Constant, Equation (4.8)
B	Constant, Equation (4.1)
b	Constant, Equation (4.8)
C	Constant, Equation (3.19)
C_1	Constant, Equation (3.18)
D	Diameter
F	Body force
f	Friction factor
g	Gravitational acceleration
k	Von karman's constant
k_s	Sand roughness
L	Dimension of length
l	Mixing length
M	Dimension of mass
m	$\frac{z_{or}}{\epsilon}$
n	Constant, Equation (4.1)
P	Pressure ; electrical power
p	Pitch ; distance between tips of roughness elements
Q	Flow rate ; heat transfer by convection from hot wire probe
R	Gas constant ; electrical resistance ; pipe radius

Re	Reynolds number, $\frac{u_{av} D_{hyd}}{\nu}$
s	Distance between channel walls
T	Temperature ; dimension of time
Tu	Turbulence intensity, $\frac{\sqrt{\overline{u'^2}}}{u}$ etc.
t	Time
u	Velocity in x- direction
u_{av}	Average velocity in the channel
u^+	Non-dimensionalized velocity, $\frac{u}{u_\tau}$
V	Anemometer output voltage
Vo	Zero velocity voltage signal from anemometer
v	Velocity in y-direction
w	Velocity in z-direction
x	Coordinate in the axial direction
x1,x2,x3,x4	Constants, Appendix A.14
y	Coordinate perpendicular to the channel walls
y1,y2,y3,y4	Constants, Appendix A.14
y^+	Non-dimensionalized length, $\frac{y u_\tau}{\nu}$
z	Coordinate parallel to the channel walls
z1,z2,z3,z4	Constants, Appendix A.14
z_{or}	Parameter defined by the equation $z_{or} = m\varepsilon$, hydrodynamic roughness, Equation (2.8)

Greek Symbols

γ	Specific weight
Δ	Difference
δ	Hydrodynamic boundary layer thickness
ϵ	Physical roughness height
ϵ_M	Eddy diffusivity
μ	Absolute viscosity
ν	Kinematic viscosity
ρ	Density
σ	Normal stress
τ	Shear stress
τ_ω	Wall shear stress
ϕ	Function
$\Pi 1, \Pi 2, \Pi 3, \Pi 4$	Dimensionless parameters, Appendix A.14

Superscripts

'	Fluctuating component
-	Time averaged quantity
+	Non-dimensionalized quantity, Equation (2.5)
++	Quantity non-dimensionalized by using the friction velocity of the opposite wall, Equation (3.24)

Subscripts

dp	Double pitot tube
i	Instantaneous
m	Corresponding to the meximum velocity point
r	Rough wall
rms	Root mean square
s	Smooth wall
t	Turbulent
0 (zero)	Corresponding to the zero shear stress point
δ	Corresponding to conditions at δ, edge of boundary layer
∞	Corresponding to conditions outside the boundary layer, potential flow

CHAPTER 1

INTRODUCTION

In the past most of the works related to turbulent flow were confined to the experimental investigations of the structure of turbulent shear flows for comparatively simple flows. The choice of simple geometries such as flow in circular cross sectional pipes and plane symmetric channels is due to the obvious reason of simplicity in handling turbulent flow problems. This is because some of the features of turbulent flow could most readily be discerned if the influences of others were small or absent.

Since the flows especially related to heat transfer are of more complex nature, the mathematical models of turbulence formulated with reference to the earlier experimental data cannot be used to predict such complex flows. In recent works [1, 2], therefore, attentions have been put to undertake a thorough examination of the turbulence structure in a flow which, in at least one respect, is substantially more complex than those which attracted earlier workers.

In theoretical approaches to the problem of predicting characteristics of turbulent shear flows, integral analyses were the main tools till recently [1], because of the lack of availability

of practical methods for the solution of a set of simultaneous partial differential equations closed with a set of empirical constants. This approach, however, was used successfully for the solution of more complex turbulent shear problems with the advent of high speed computers [3]. Due to the complexity of this approach an approximate solution using integral analyses together with a turbulence model based on prandtl's mixing length theory is attempted in the present study.

In this study particular emphasis was given on asymmetric flows related to heat transfer, where the characteristic flow properties exhibit stationary values, because it is these flow situations where some of the structural flow features, that are concealed in simple flows by virtue of symmetry become prominent.

Asymmetric flows are encountered in many practical situation where technological requirements impose dissimilar boundary conditions. An example is the use of partially roughened or finned annulus in compact heat exchangers.

Since the roughness of the wall, as a consequence of the higher turbulence produced in flow, not only increases the heat

transfer but also produces additional losses of pressure, it is meaningful to use optimum geometrical shapes and arrangements of the artificial roughness. This requires detailed knowledge of the relation between the efficiency and geometry of the wall roughness. An important parameter, which also determines the loss of pressure, is the roughness parameter which can be determined from isothermal pressure drop measurements or from measurements of velocity distributions. The roughness parameter is investigated in more detail for rectangular roughness in the present study. The geometry selected is a rectangular duct of sufficiently large aspect ratio for the flow along the mid-plane to be considered as that developed between infinite parallel planes.

CHAPTER 2

LITERATURE SURVEY

2.1 VELOCITY PROFILE :

In the theoretical study of turbulent fluid flow, precise determinations of the velocity profiles are quite important. As a fluid flows through a duct its velocity profile undergoes a change from its initial entrance form to that of a fully developed profile at an axial location of the duct far down stream from the entrance. Thus two distinct fields of turbulent fluid flow studies, one in developing region and the other in fully developed regions, for different geometries of test sections are available in the literature.

One of the most rigorous studies of turbulent flow in a circular pipe was carried out by Deissler [4] . An investigation by Laufer [5] covers the structure of turbulent pipe flow quite thoroughly. Cremers and Eckert [6] measured the turbulence correlations in a triangular duct and Clark [7] studied the turbulent boundary layers in channel flow.

Quite a few experimental or analytical studies for fully developed turbulent flow in a concentric annulus have

been done by Barrow [8], Lee and Barrow [9], Brighton and Jones [10], Levy [11], Quarmby [12, 13], Michiyoshi and Nakajima [14], and Randhava [15]. The studies of turbulent flow in rough surface ducts have been done by Kjellstro"m and Hedberg [16], and Robertson et al [17].

The earliest analytical studies on the entrance region of the turbulent flow in a circular duct appear to be these of Deissler [18] and Holdhuson [19]. Deissler used Von Karman integral techniques along with his own logarithmic velocity distributions. The influence of entrance configuration on turbulent velocity profile was observed by Knudson and Katz [20]. A semi-empirical method for predicting the flow and heat transfer in rough pipes is formulated by Hatton and Walklate [21]. In this method the mixing length model is used to describe the turbulence effects and the Van Driest [22] modification is included for the region near to the wall.

An equation describing shear stress, together with an eddy diffusivity model, has been extensively used to predict turbulent transport for a wide variety of flow geometries [2, 11, 23-26]. The shear stress τ in the direction of flow x, may be related to the time-averaged parameters of the

velocity field by the equation ,

$$\frac{\tau}{\rho} = \nu \frac{\partial u}{\partial y} + (- \overline{u' v'}) \qquad (2.1)$$

The term $\overline{u' v'}$ is the time-averaged value of the products of the fluctuating velocity components in x and y directions and may be expressed through the concept of the eddy diffusivity of momentum ε_M , by the equation

$$\overline{u' v'} = - \varepsilon_M \frac{\partial u}{\partial y} \qquad (2.2)$$

Hence equation (2. 1) can be written as

$$\frac{\tau}{\rho} = (\nu + \varepsilon_M) \frac{\partial u}{\partial y} \qquad (2.3)$$

τ varies from a maximum at the wall to zero somewhere in the main stream. However, in the region not too far from the wall where most velocity change takes plaee τ will not vary markedly from its wall value τ_0 [27] . Then the equation (2. 3) may be written as approximately ,

$$\frac{\tau_0}{\rho} = (\nu + \varepsilon_M) \frac{\partial u}{\partial y} \qquad (2.4)$$

2. 1. 1. SMOOTH SURFACE :

In order to deduce a possible form for the turbulent

velocity a profile from equation (2. 4), the relation between ϵ_M and the mean flow parameters has to be known. There are many expressions available in literature for [22,23,28,29,30-32] the one proposed by Reichardt [23] takes the form,

$$\frac{\epsilon_M}{\nu} = \{ (1 + k\, y^+)^{-1} + (\frac{7.8}{11}) [\exp (- \frac{y^+}{11}) + (\frac{1}{3} y - 1) \exp (- \frac{1}{3}\, y^+)] \}^{-1} - 1 \qquad (2.5)$$

The corresponding velocity profile is,

$$u^+ = \frac{1}{k} \ln (1 + k\, y^+) + 7.8 [1 - \exp (- \frac{y^+}{11}) - (\frac{y^+}{11}) \exp (- \frac{1}{3} y^+)] \text{ , for } y^+ \geq 0 \qquad (2.6)$$

These equations were originally developed for fully developed turbulent flow over a smooth surface. It has been shown that with proper modifications on y^+ these also work for developing turbulent flow in pipes [33] and in annuli [34, 35]. Also these equations have the virtue of providing continuity throughout the region of laminar sublayer where momentum is transfered virtually by molecular process into the region of turbulent core where turbulence dominates the mechanism of momentum transfer. This continuity characteristic is preferable because the limits of these regions distinguished by different momentum transfer processes are not well defined.

2. 1. 2. ROUGH SURFACE :

Due to the imposition of roughness on one side of the

channel, the flow may be turbulent starting from the beginning and the equation (2. 4) becomes

$$\frac{\tau_0}{\rho} = \epsilon_M \frac{\partial u}{\partial y} \tag{2.7}$$

Applying either Prandtl's mixing length hypothesis or Von Karman's similarity hypothesis [27] the following expression for the velocity distribution can be deduced from equation (2. 7)

$$\frac{u}{u_\tau} = \frac{1}{k} \ln \frac{y}{z_0} \tag{2.8}$$

where z_0 is known as the roughness length or the dynamic roughness [33, 36, 37].

2.2. DYNAMIC ROUGHNESS :

The logarithmic velocity profile consists of two parameters; a shear velocity u_τ and a dynamic roughness z_0 . Although the numerical value of z_0 can be easily evaluated, the physical interpretation of z_0 is not yet clear. The increase in z_0 with u_τ can be observed from the logarithmic velocity profile. As indicated by equation (2. 8) for a constant u , the shear velocity is directly proportional to the dynamic roughness.

2.3. FRICTION FACTOR :

A wealth of information regarding friction factor calculations is available in literature. But most of them are purely experimental and confined to symmetric flows in pipes.

It has been experimentally shown by Streeter [38] that in artificially roughened pipes , f is mainly a function of Re and s/ε and he also concluded that the shape of roughness has as much effect as the size of the roughness. Sheriff and Gumley [39] reported empirical correlations for friction factors, in an attempt to find the optimum heat transfer surfaces over a wire wrapped tube. Webb , Eckert and Goldstein [40] reported a friction factor correlation based on the law of the wall similarity,together with experimental pressure drop measurements in tubes with repeated- rib roughness. For rectangular channels with rough walls, friction factor and pressure drop measurements are reported by Wilkie , Burnett and Burgoyne [41] and Furber and Cox [42] respectively. In these two works a method due to Hall [43] was introduced to separate the friction factor due to each surface.

It is interesting to note that the above mentioned literatures contain little or no theoretical analysis. However ,

the study reported by Launder and Hanjalic [1] on turbulence structure in an asymmetric rectangular channel is a notable exception with theoretical predictions of mean flow parameters. This research has put main emphasis on establishing the turbulent structure , particularly in the central region of the channel where the two dissimilar wall flows, generated by the smooth and rough surfaces , interact. The striking feature of this interaction was that stationary values of mean velocity gradient and zero shear stress were non-coincident — the plane of zero shear lying substantially nearer the smooth wall than the plane of maximum velocity.

CHAPTER 3

ANALYTICAL STUDIES

3.1. BASIC EQUATIONS :

The mechanism of the turbulent momentum transfer process is governed by the general momentum equation which can be derived from the corresponding equations for laminar flow following the method initiated by Reynolds [44] . The Navier-Stokes equations for conservation of mass and momentum of an incompressible fluid with constant viscosity can be written in the following from [45] ,

$$\rho\left(\frac{\partial u}{\partial t} + u\frac{\partial u}{\partial x} + v\frac{\partial u}{\partial y} + w\frac{\partial u}{\partial z}\right) = -\frac{\partial p}{\partial x} + \mu \nabla^2 u + F_x \qquad (3.1)$$

$$\rho\left(\frac{\partial v}{\partial t} + u\frac{\partial v}{\partial x} + v\frac{\partial v}{\partial y} + w\frac{\partial v}{\partial z}\right) = -\frac{\partial p}{\partial y} + \mu \nabla^2 v + F_y \qquad (3.2)$$

$$\rho\left(\frac{\partial w}{\partial t} + u\frac{\partial w}{\partial x} + v\frac{\partial w}{\partial y} + w\frac{\partial w}{\partial z}\right) = -\frac{\partial p}{\partial z} + \mu \nabla^2 w + F_z \qquad (3.3)$$

The continuity equation for constant property steady flow is ,

$$\frac{\partial u}{\partial x} + \frac{\partial v}{\partial y} + \frac{\partial w}{\partial z} = 0 \qquad (3.4)$$

Since for turbulent flow the fluctuations are random and chaotic, Reynolds modified the momentum equation by introducing the mean fluctuating values of the flow quantities in place of the instantaneous values. As the instantaneous velocity component is

the sum of the mean component and fluctuating velocity component in the same direction, the transformation of the above Navier - Stokes equations can be obtained by introducing :

$$u_i = \bar{u} + u' ; \; v_i = v + v' ; \; w_i = w + w' \quad \text{and} \quad P_i = P + P' .$$

Hence, Reynolds equations for incompressible steady flow in a straight two dimensional duct of uniform cross section neglecting body forces, assume the following vector forms after replacing ,

$$\nabla = \frac{\partial}{\partial x} + \frac{\partial}{\partial y} + \frac{\partial}{\partial z} -$$

$$\rho \left[(\vec{v} . \nabla) \vec{v} \right] = - \nabla P + \mu \nabla^2 v \qquad (3.5)$$

Even for moderately higher Reynolds numbers, the flow in the vicinity of the inlet is preceded by a laminar boundary layer. According to Prandtl [46], in the presence of a laminar boundary layer near the entrance of a duct, the turbulent portion of the boundary layer behaves as if the boundary layer were turbulent all the way from the entrance. The two-dimensional flow in the entrance region of a duct belongs to a boundary layer class of flows. The so called " boundary layer approximations " after Prandtl [47], if introduced into equations (3. 4) and (3.5) will yeild :

$$\frac{\partial u}{\partial x} + \frac{\partial v}{\partial y} = 0 \qquad (3.7)$$

$$\rho \left(u \frac{\partial u}{\partial x} + v \frac{\partial u}{\partial y} \right) = - \frac{dP}{dx} + \mu \frac{\partial^2 u}{\partial y^2} - \rho \left(\frac{\overline{\partial u'^2}}{\partial x} + \frac{\overline{\partial u' v'}}{\partial y} \right) \qquad (3.8)$$

For fully developed flow sufficiently far from the entrance, the flow is essentially one-dimensional with velocity field invariant in the streamwise (x) direction. The conditions $\frac{\partial}{\partial x} = 0$, $v = 0$, characteristing fully developed flow, if imposed on equation (3. 8), results :

$$\mu \frac{\partial^2 u}{\partial y^2} - \rho \overline{\frac{\partial u'v'}{\partial y}} - \frac{dP}{dx} = 0 \qquad (3.9)$$

with boundary conditions ,

at $y = 0$; $u = 0$; $u'v' = 0$; $\mu \left(\frac{\partial u}{\partial y} \right) = \tau_\omega$, and

at $y = y_o$; $\tau = \mu \frac{\partial u}{\partial x} - \rho \overline{u'v'} = 0 \qquad (3.10)$

It may be noted here that in the last boundary condition, y_o represents the position of zero shear stress. It is not necessarily true that the position of maximum velocity coincides with the point of zero shear stress [7] .

3. 2 PHYSICAL MODEL AND ASSUMPTIONS :

The physical model and assumptions selected for the present study are as follows :-

(1) The flow is steady and turbulent everywhere in the duct.

(2) The flow is of an incompressible Newtonian fluid and the fluid properties are constant.

(3) The flow is uniform at the entrance.

(4) The flow in the region outside the boundary layer is a potential flow.

(5) The body forces are neglected for the flow.

(6) The following boundary layer approximations are valid :-

$$\frac{\partial u}{\partial y} >> \frac{\partial u}{\partial x} , \quad \frac{\partial w}{\partial x} , \quad \frac{\partial v}{\partial y}$$

$$\frac{\partial P}{\partial x} \simeq \frac{dP}{dx} , \quad \frac{\partial P}{\partial y} \simeq 0 .$$

3. 3. MOMENTUM INTEGRAL EQUATIONS :

Because of the nonlinearities involved in the equations (3. 1) to (3. 3), as manifested particularly by the terms such as $u \left(\frac{\partial u}{\partial x} \right)$, etc on the left hand side, very few exact analytical solutions are available. The two general types of flow for which most of the exact solutions have been found are ,

(1) Steady, two-dimensional, laminar, constant property, fully developed internal flow in ducts and tubes, and

(2) Steady, two-dimensional, laminar, constant property, external boundary layer-type flow over bodies immersed in the fluid [48]

The momentum integral method for the boundary layer due

to Von Karman [49] has been a powerful tool for the prediction of boundary layers so far. Together with an assumed velocity field it forms the basis of many existing solutions of the boundary layer . It can infact be derived through a partial integration of equation (3. 8) [45].

In deriving the momentum integral equations for the present study due considerations relevant to channels with both smooth and rough walls are given. However, depending upon the type of roughness, the local flow mechanism in the vicinity of rough wall may not fully satisfy the boundary layer approximations. Large scale roughness may cause flow recirculation in the wake zone of the roughness elements, where some of the terms usually neglected in the momentum equations become important. In this analysis, the momentum integral equation has been broken into smooth and rough side equations and to take care of the above mentioned complication, the parameter z_{or} is introduced in the rough side equation.

The basic integral equations for conservation of mass and momentum of incompressible fluid flow in a duct can be written from the diagram of the idealized model shown in figure (3. 1).

Conservation of mass equation :-

$$\frac{d}{dx} (u_{av} s) = \frac{d}{dx} \int_0^s u \, dy = 0 \qquad (3.11)$$

Conservation of momentum equation :-

Middle portion (potential flow) :

$$\frac{dp}{dx} = - \rho u_\infty \frac{du_\infty}{dx} \qquad (3.12)$$

Rough side :

$$\tau_{\omega r} = - \delta r \frac{dp}{dx} - \frac{d}{dx} \int_{z_{or}}^{\delta r} \rho u_r^2 \, dy_r + \rho u_\infty \frac{d}{dx} \int_{z_{or}}^{\delta r} u_r \, dy_r \qquad (3.13)$$

Smooth side :

$$\tau_{\omega s} = - \delta s \frac{dp}{dx} - \frac{d}{dx} \int_0^{\delta s} \rho u_s^2 \, dy_s + \rho u_\infty \frac{d}{dx} \int_0^{\delta s} u_s \, dy_s \qquad (3.14)$$

The details of the derivations are presented in Appendix A. 1.

For the fully developed region the momentum equations simplify to :

Rough side :

$$\tau_{\omega r} = - y_{or} \frac{dp}{dx} \qquad (3.15)$$

Smooth side :

$$\tau_{\omega s} = - y_{os} \frac{dp}{dx} \qquad (3.16)$$

where $y_{os} + y_{or} = s$.

The details of the derivations can be seen in Appendix A. 2.

By using the equations (3. 15) and (3. 16), the wall shear stresses can be calculated from the measured pressure gradient and the zero shear point y_o .

3. 4. MEAN VELOCITY FIELD :

The simplified equations of motions presented in the preceding section are not quite enough to predict the mean flow parameters which the present study is seeking for. A turbulence model is essential to give the velocity profiles encountered in the flow situations involved. In this study a model based on Prandtl's mixing length theory [48] is adopted. A physical interpretation of the mixing length can be given as - the mixing length is that distance in the transverse direction which must be covered by an agglomeration of fluid particles travelling with its original mean velocity in order to make the difference between its velocity and the velocity in the new lamina equal to the mean transverse fluctuation in turbulant flow [45] . By using this

concept of mixing length an expression for turbulent shear stress can be obtained :

$$\tau_t = \rho l^2 \left| \frac{du}{dy} \right| \frac{du}{dy} \qquad (3.17)$$

With the assumptions that mixing length is proportional to the wall distance through a constant k and that shear stress does not change with wall distance, the following expression for the velocity profile in turbulent flow near wall is obtained :

$$u = \frac{u_\tau}{k} \ln y + C_1 \qquad (3.18)$$

By dimensional analysis consideration the above equation can better be written for hydrodynamically smooth wall as [30] ;

$$\frac{u_s}{u_{\tau_s}} = \frac{1}{k} \ln \frac{y_s u_{\tau_s}}{\nu} + C \qquad (3.19)$$

and for rough walls as :

$$\frac{u_r}{u_{\tau_r}} = \frac{1}{k} \ln \frac{y_r}{z_{or}} \qquad (3.20)$$

where $z_{or} = m\varepsilon$ is also termed as hydrodynamic or characteristic roughness. Here m is a function introduced to incorporate the roughness shape and density into the theory . The expression for velocity profile derived by Reichardt equation (2. 6) among many others as shown in Table 3.1 [18, 22, 30 - 32, 37, 49 - 53] can be used with confidence since they have been verified by

experimental data for various flow passages [11, 54, 55]. The equation (2. 6) simplifies to the expression due to Prandtl and Taylor [29] for large y^+ ($\gtrsim$ 100, see Table 3. 2 and Table 3. 3 for the theoretical $y^+_{ms} = s^+ - y^{++}_{mr}$ values) -

$$u^+ = \frac{1}{k} \ln y^+ + C \qquad (3.21)$$

with k = 0.4, Von Karman's constant and the value of C = 5. 52 , adjusted to have numerical agreement with equation (2. 6). For the rough wall profile, equation (3. 20) , a number of and varying values of m are reported in the literature for different shape and density of roughness elements.

For sand roughness Nikuradse [56] reports a value $m = \frac{1}{30}$. For camouflage paints on aeroplanes $m = \frac{1}{18.75}$ [57], for different types of vegetations on earth $m = \frac{1}{7.5}$ [58] Geffroy, Jude, Paumard [59] reported values of m varying from $\frac{1}{7.65}$ to $\frac{1}{3400}$ with $\frac{p}{\epsilon}$ varying between 9 and 20, respectively, for sinusoidal undulations in a pipe. Through a survey to determine the effect of roughness density λ ; Simpson [60] found $m = \frac{1}{9400}$ for $\lambda = 1$ varying to $m = \frac{1}{3.45}$ for $\lambda = 5$, for different roughness shapes. In this case λ was defined as the ratio of the total surface area to the total roughness frontal

area normal to the flow. In a detailed experimental survey of flow in an asymmetric rectangular channel with rectangular ribs ($\frac{p}{\epsilon} = 10$), Hanjalic [61] suggests a value of $m = \frac{1}{3.83}$. All the above values of m were calculated through reported data so as to fit the nomenclature of the present study.

From the above it is clear that there is a wide range covering the values of m and no correlation is available in the literature. So further experimental work is necessary to establish relations between roughness structures on walls and velocity profiles.

The parameter z_{or} in the equation (3. 20) can be interpreted as a hypothetical distance from the wall where the velocity is assumed to be zero. It has been shown by Clauser [62] that this shift of the reference point for the rough wall velocity profile depends on the roughness Reynolds number $\frac{\epsilon u_\tau}{\nu}$, which is a measure of the roughness structure through the wall shear stress. This finding was based on the experiments conducted with two-dimensional roughness elements. Subsequently Hama [63] has varified Clauser's generalization for three-dimensional roughness elements. Also Perry and Joubert [64] have extended experimentally their results to the boundary layer with adverse pressure gradient.

A similar shift for a rough surface with uniform spherical particles arranged in a random and compact form was reported by Shaw [55] and Wu [65].

According to the reported data the above mentioned reference point is somewhere between the root and the tip of the physical roughness height. The exact position for a particular roughness structure remains to be found out through experiments.

3. 5. EDDY FIFFUSIVITY MODEL :

The analysis of the present study requires a solution for velocity profile and the value of such a solution depends very much upon the accuracy of the description of the eddy diffusivity for momentum along and across the duct. The concept of eddy diffusivity was first initiated by Bussinesq [66] and this can be introduced into the analysis by writing the equation (3. 9) as -

$$\frac{\partial}{\partial y} \left(\mu \frac{\partial u}{\partial y} - \rho \, u'v' \right) - \frac{dp}{dx} = 0 \qquad (3.22)$$

The quantity in the parantheses of the above equation corresponds to the shear stress , τ in the channel -

$$\tau = \mu \frac{\partial u}{\partial y} - \rho \, \overline{u'v'} \qquad (3.23)$$

This equation (3. 23) is the same as the equation (2. 1)

which results the equation (2, 3) . This equation (2, 3) with the help of an eddy diffusivity model, has been widely used to predict turbulent transport for a large variety of flow parameters. However, the concept of eddy diffusivity as used above presents some difficulties, especially in asymmetric flows, where the stationary values of the mean and fluctuating velocities do not coincide. According to Lee and Barrow [9], at points where the velocity gradient is zero, shear stress is not necessarily zero, where as equation (2, 3) suggests it to be zero.

As indicated by the appearance of turbulent stresses in the mean momentum equation, and mean velocity gradients in the stress equations, the mean and fluctuating motions are closely interconnected. It seems that the statistically averaged fluctuating velocities will follow the behavior of the mean motion and that both mean and fluctuating fields can be treated uniquely. But the reported non-coincidence of the stationary values of the mean and fluctuating velocities [16 , 61 , 67] infers that universal treatment of the two fields together is not possible. A partial explanation for this non-universality may be obtained from Townsend's [68] suggestion that the fluctuating motion consists of an "active" component which interacts locally with the mean motion and, also of an " inactive " component, governed by

far-away conditions and , therefore, not directly correlated with the mean motion . Kjellstrom and Headberg [16] discussed the reason why the zero shear and zero velocity gradient points are not necessarily coincident in turbulent flows through an analysis of Navier-Stokes and Von Karman's momentum equations.

3.6. FRICTION FACTOR :

A friction factor is defined by the expression ,

$$f = \frac{\tau}{\frac{1}{2}\rho u_{av}^2}$$

Considering rough side of the channel ,

$$f_r = \frac{2\,\tau_{\omega r}}{\rho\, u_{av}^2} \tag{3.24}$$

and using equation (3. 15) ,

$$f_r = \frac{2\,y_{or}}{\rho\, u_{av}^2}\left(-\frac{dp}{dx}\right) \tag{3.25}$$

Considering smooth side of the channel ,

$$f_s = \frac{2\,\tau_{\omega s}}{\rho\, u_{av}^2} \tag{3.26}$$

and using equation (3. 16) ,

$$f_s = \frac{2\,y_{os}}{\rho\, u_{av}^2}\left(-\frac{dp}{dx}\right) \tag{3.27}$$

Now making a fully developed momentum balance on a fluid element of thickness dx and height s , (see Appendix A. 1 and Appendix A. 2) -

$$\tau_{\omega r} + \tau_{\omega s} = s\left(-\frac{dp}{dx}\right) \tag{3.28}$$

Hence , the friction factor for the whole channel can be defined as,

$$f = \frac{\tau_{\omega r} + \tau_{\omega s}}{\rho\, u_{av}^2} \tag{3.29}$$

which becomes ,

$$f = \frac{s}{\rho u_{av}^2} \left(- \frac{dp}{dx} \right) \qquad (3.30)$$

When equation (3. 28) is substituted in equation (3. 29). And from equations (3. 24) and (3. 26) ,

$$f = \frac{f_r + f_s}{2} \qquad (3.31)$$

3.7. RELATION AMONG FLOW PARAMETERS :

A large number of mean flow parameters are considered in the present study , a list of which together with a summary of the expressions relating them , is given in Appendix A. 11. These expressions constitute a system of 17 equations , containing 32 parameters . To solve these equations , 15 of these parameters , therefore , have to be supplied , experimentally or otherwise . For this the following four groupings may be considered -

(a) Physical properties of working fluid : ρ and μ .

(b) G eometrical parameters : A, D_{hyd}, s, ε, and p .

(c) Independent variables : y_s and y_r .

(d) Experimental flow variables : $\frac{dp}{dx}$, y_{or} , y_{mr} , $\frac{du_s}{dy_s}$, $\frac{du_r}{dy_r}$ and Q .

With the chosen velocity field i.e. equations (2. 6) and (3. 20) and u_{av} , the expression for Re in terms of the mean flow

parameters is derived as shown in Appendix A. 7 ,

$$Re = \frac{2\,(1 + k\,y^{+}_{ms})}{k^2}\left[\ln\,(1 + k\,y^{+}_{ms}) - 1\right] + 15.6\left\{y^{+}_{ms} - 11\left[1 - \exp\left(-\frac{y^{+}_{ms}}{11}\right)\right] + \frac{9}{11}\left(1 + \frac{y^{+}_{ms}}{3}\right)\exp\left(-\frac{y^{+}_{ms}}{3}\right) - \frac{9}{11}\right\} + \frac{2\,y^{++}_{mr}}{\kappa}\left[\ln y^{+}_{ms} + C\,k - \frac{u_{\tau_r}}{u_{\tau_s}}\right] + \frac{2\,z^{++}_{or}}{k}\,\frac{u_{\tau_r}}{u_{\tau_s}} \qquad (3.32)$$

The main purpose of the analysis is to find velocity field and hence to predict the friction factor f as a function of Re for the particular flow geometry in consideration . The expression for f can also be deduced by using its definition in terms of the parameters encountered in equation (3. 24) as shown in Appendix A. 8.

The ratio $\frac{u_{\tau_r}}{u_{\tau_s}}$ can be obtained by using the equations (3. 15) and (3. 16) (see Appendix A.8) The unknown parameter z^{++}_{or} can be eliminated by matching the rough and smooth wall profiles at maximum velocity point as can be seen in Appendix A.9 . The velocity profiles were assumed to be valid from the wall until

the maximum velocity point in the above derivations .

3. 8. METHOD OF CALCULATIONS :

3. 8. 1. CALCULATIONS BASED ON CONSTANT m :

In the theoritical analysis an attempt was made to predict the friction factors without any new emperical input into the equations. The commonly used assumtion of the coincidence of the stationary values of the mean and fluctuating velocity feilds was introduced into the equations by putting $y_0 = y_m$. In addition to this assumption a constant value of $m = \frac{1}{30}$, based on Nikuradse's [45] experiments on rough pipes in complete rough flow regime , was used to solve the equations.

The equations derived on the basis of the above considerations are shown in Appendix A. 10. The values of f and y_m can be calculated from the system of equations (3. 24),(A. 8. 1), (A. 8. 2) , (A. 10. 2) and (A. 10. 3) by independently assigning the values of Re . From a computational point of views , however, it was found more economical to assign u_{τ_s} and compute y_m and u_{τ_s} . The computation was carried out numerically on the University of Ottawa, IBM 360 , model 65, computer. A simplified

flowchart of the programme is reproduced in Appendix A. 12. The results of two sets of calculations with $m = \frac{1}{30}$ and $m = \frac{1}{40}$ are shown in figure 3. 2.

3. 8. 2. CALCULATIONS BASED ON VARIABLE m :

Because of the disagreements of the results obtained in previous section with experimental results, it was decided to use m as a variable function of Re and s/ε . The assumption $y_o = y_m$ was disregarded, instead empirical values of y_o and y_m were assigned. The computations were done in a similar manner as was described in the previous section, the only exception being the equations (A. 10. 2) and (A. 10. 3) were replaced by the equation (A. 9. 4). The flowchart of this computer programme is reproduced in Appendix A. 13 and the results are shown in the figure 3. 3.

CHAPTER 4

EXPERIMENTAL STUDIES

4. 1. APPARATUS :

The general experimental set up was initially installed by Alp [54] for his Master degree thesis. The new test section along with the setup of the auxiliary apparatus is shown schematically in figure 4. 1 and photographs of the channel assembly are shown in figure 4. 2. The details of the experimental set up are similar to that of Alp but re-presented here for the completeness. The channel walls were made of 1.2 7 cm thick aluminium plate, 3.353 m long and 41.593 cm wide. Asymmetry was introduced by artificially roughening one side of channel only partially. Roughening was done by machining rectangular grooves on the plate in the transverse direction on a milling machine. The height of the grooves, shown in figure 4. 3, is 0.244 cm. The pitch to height ratios ($\frac{p}{\epsilon}$) for the present study are 2, 4, 8 and 16.

The roughened plate was provided with 5 velocity measuring ports of 4.445 cm diameter with centre pieces to fit these ports, as shown in figure 4. 4. A round 8.573 cm diameter and 1.2 7 cm thick aluminium piece was welded on the main rough plate to provide support to be base of the traversing mechanism which was fixed to the plate by allan screws. Holes of 0.318 cm diameter were provided

in the middle of the centre pieces for smooth movement of pitot tubes and hot-wire probes. The machining was done with these centre pieces fixed to place, to provide a flush fit with the grooves. The smooth plate consisting the other side of the channel was provided with static pressure holes of 0.064 cm diameter at 10.16 cm intervals along the centre line.

The two plates were mounted vertically on their sides to avoid the problem of sagging on a steel frame specifically designed for the purpose of changing the spacing between the plates. The top and bottom of the channel were closed with 1.2 7 cm thick transparent plexiglass pieces through which the position of the probes could be examined. The ratio $\frac{s}{\varepsilon}$ of the channel could be controlled by using different widths of the plexiglass spacers with discrete intervals. Four different sized spacers, 3.334 cm , 4.604 cm, 7.144 cm, 8.414 cm were respectively used to provide $\frac{s}{\varepsilon}$ ratios of 8.61 , 13.82 , 24.24 and 29.45.

Air was drawn through the test section, by a centrifugal fan driven by a 19.8 HP , 1785 rpm A/C motor. A diffuser box connected to the channel through a diffuser section is equipped with two movable gates inside, on the fan side, to facilitate the control of flow rate of air.

4. 2. INSTRUMENTATION :

4. 2. 1. ORIFICE PLATE :

An orifice plate was put between two pieces of aluminium pipe of 15.405 cm I. D. to measure the flow rate in the channel. The orifice plate was designed according to ISO recommendation R541 with vena contracta taps [69,70].

4. 2. 2. PITOT TUBE AND PRESSURE MEASUREMENT SYSTEM :

The mean velocity profiles across the test section were measured by means of flattened-tip pitot tube made of hypodermic stainless steel tubing , 0.089 cm O. D. and 0.051 cm I. D. . The internal tip height was about 0.015 cm.

The static pressure holes were connected to the pressure measuring network of tubes through 0.318 cm I. D. pressure connectors, which were fixed onto the plate by screws. Jayflex- 180 plastic tubing of 0.953 cm O. D. and 0.635 cm I. D. was used for this purpose. The ends of each of these tubes were connected to a common mainfold with one output going to the pressure measuring instrument. The signals through these pressure taps could be turned on and off by clamps which were placed before the manifold.

The MKS differential pressure transducers types 77 H - 1 and 77 H - 1000 with the MKS Baratron type 77 electronic pressure meter [71] were used for pressure measurements .

4. 2. 3. DOUBLE PITOTTUBE AND POSITION OF MAXIMUM VELOCITY :

To determine the position of maximum velocity, a double pitot tube consisting of two flatened tipped tubes with centres 2 mm apart was employed [61,72].

4. 2. 4. HOT WIRE PROBE AND ANEMOMETER :

A DISA 55D00 series hot-wire anemometer system in conjunction with miniature hot wire probes was used to measure mean velocity profiles and to detect the longitudinal turbulence intensity. The probes were of type 55P11 and made of platinum plated tungsten wires, 5 microns in diameter and 1.25 mm long [73] .

The signal from the constant temperature hot wire probe was fed to the Anemometer, DISA 55D01 , which was in turn connected to the Auxiliary Unit, DISA 55D25, and the output signal was fed to the Linearizer, DISA 55D10. The linearized turbulence signal was then integrated by RMS voltmeter, DISA 55D35, and finally root mean squared values were either read on the dial of RMS meter, DISA 55D35,

or on a digital voltmeter, DISA 55D30. Flowchart of these measurements are shown in figures 4.5 and 4.6.

Basically, the velocity measurements with a constant temperature Anemometer are performed by measuring the electric power. The power has to be supplied to the probe from the anemometer in order to keep the probe sensor at a certain temperature, usually higher than the temperature of the flow medium under measurement. The required amount of power, P, from the Anemometer, is thus equal to the power, Q, removed by the flow. Assuming everything else to be constant, the amount of heat, Q, removed per unit time then corresponds to the measure of the velocity of the flow. The power, P, which is proportional to the output voltage of the Anemometer is a nonlinear function of the flow velocity u under measurement. This non-linearity is not very significant in measurements of small degrees of turbulence, in which case a small section of the calibration curve may be considered sufficiently linear . However, at higher degrees of turbulence, the distortion caused by the curvature of the calibration curve becomes noticeable. Also measurements at varying degrees of mean flow velocity are rendered difficult by the consequent sensitivity variations. Since mathematical treatment of results obtained in both of the cases mentioned above does not give a satisfactory solution, an electronic circuit to take care of linearization problem is preferred [73].

The fundamental relationship between the flow velocity u and the amount of heat, Q, removed per unit of time can be formulated as

$$Q = P = A + B\,(u)^n \tag{4.1}$$

where A and B are constants, assuming constant temperature and constant density. Over a wide range of Re, the exponent n has an almost constant value. The above equation can be put into the following form (see Appendix A. 3),

$$\ln\left(\frac{V^2}{V_0^2} - 1\right) = n \ln u + C \tag{4.2}$$

where V_0 is constant and hence a linear calibration curve can be drawn. The relationship between the fluctuating and the mean components of hot wire signals and the velocity, then becomes relatively complicated as (see Appendix A. 4) :

$$\frac{u'}{u} = \frac{V'}{V}\,\frac{1}{n}\left(\frac{V^2}{V^2 - V_0^2}\right) \tag{4.3}$$

But with help of an electronic linearizer which takes care of the non-linear dependence of V on u the following simple form can be obtained :

$$V = B\,u \tag{4.4}$$

where B is another constant and thus the following relationship

can be used :

$$\frac{u'}{u} = \frac{V'}{V} \qquad (4.5)$$

4. 2. 5. TRAVERSING MECHANISM :

A DISA 55H01 Traversing mechanism supported by a base which could be secured onto the plate carrying the velocity measuring ports by three capscrews, was used to traverse both hot wire probes and pitot tubes. The traversing mechanism could be operated either manually or by a DISA 52C01 stepper motor. The DISA 52B01 Sweep Drive Unit was used as a remote control for the stepper motor. The output could be read on a 3-digit mechanical counter or recorded automatically on a HP digital recorder.

4. 2. 6. DATA ACQUISITION SYSTEM :

The static pressure drops were recorded on a Baratron Pressure meter manually. However, all other measurements were suitable for automatic recording through a Hewlett-Packard HP-5050B digital recorder in conjunction with an HP 2901A Input Scanner and an HP 2401C Integrating digital voltmeter as shown in figure 4. 7. An HP 7004B X-Y recorder was used for graphical representation of the recorded variables (see figure 4. 8).

4. 3. CALIBRATION OF INSTRUMENTS :

4. 3. 1. ORIFICE PLATE :

The calibration of the orifice plate was done by connecting the downstream end of the entrance box to a settling chamber-copper pipe assembly [74] . A traversing mechanism located at about 30 equivalent diameters from the bell-mouthed entrance to the pipe facilitated the measurement of velocity profiles throughout the cross section of the pipe. These velocity profiles, measured by using a single pitot tube, were integrated numerically using the trapezoid rule to give the flow rate for a given pressure drop across the orifice plate. From Bernoulli's equation it can be shown that the flow rate is proportional to the square root of the orifice pressure drop [75] . The calibration curve Q versus $\Delta P_{orifice}$ drawn on this basis is shown in figure 4. 9. The accuracy of the calibration was estimated to be ± 1.5% in the range considered.

4. 3. 2. HOT WIRE PROBES :

The calibration of the hot wire probe was done by placing the probe in an air stream of known velocity and measuring the linearized voltage output from the Anemometer. A known velocity

was supplied to the probe by using a DISA 55D 41/42 calibration unit. A DISA 55A67 adopter was used to match the geometry of the flow in the experimental apparatus ; figure 4.10. A typical calibration curve is shown in figure 4.11.

4. 4. EXPERIMENTAL PROCEDURE :

The main experimental variables for the present study are the pitch of roughness, p and the width of the channel, s. To see the effect of the intensity of roughness on the flow parameters, four different pitches of the roughness elements were studied. The pitches were varied by machining the rough plate. All the electronic instruments were switched on for about two hours before every experimental set up of measurements were taken to attain steady state conditions and to avoid drift due to warm up. Steady state conditions were obtained by running the experiment for about one-half hour before any measurement was taken. For each roughness pitch and four different channel widths the following measurements were taken :

(i) Static pressure drops across channel length, x for three different Res.

(ii) Static pressure drops at fully developed conditions for ten different Res.

(iii) Velocity profiles U versus y along x at five different

locations, using pitot tube or hot wire probe for three different Res.

(iv) Velocity profiles U versus y at fully developed conditions for ten different Res.

(v) $\sqrt{\overline{u'^2}}$ versus y along x at five different locations for three different Res.

(vi) $\sqrt{\overline{u'^2}}$ versus y at fully developed conditions for ten different Res.

(vii) Double pitot tube readings ΔP_{dp} versus y at fully developed conditions for ten different Res.

The range of Reynolds number covered was from 10,000 to 150,000 approximately. The hot-wire calibrations were done before each run. The pressure and temperature of the ambient were also recorded before each run.

4. 4. 1. STATIC PRESSURE MEASUREMENTS :

The measurements of static pressure were made with the help of an MKS pressure transducer. The calibration of the transducer was checked against a inclined-arm micromanometer at frequent intervals. Due to rapid random fluctuations in the pressure readouts both from the inclined-arm micromanometer and the electronic meter, an estimate of the average readout had to be made

Considering the maximum and minimum values of the instantaneons readouts, the error introduced in this manner was estimated to be less than ± 0.5%.

A FORTRAN program was written to calculate $\frac{dp}{dx}$ values as a function of x. The subroutine REGR from the IBM Scientific Subroutine Package (SSP) [76] was used for the straight line fit. $\frac{dp}{dx}$ versus x were calculated by fitting a straight line into the data points taken six at a time by polynomial regression and taking the slope of this line as $\frac{dp}{dx}$ in the middle of the range of the six points ; figures 5.1 and 5.2 . $\frac{dp}{dx}$ values for fully developed conditions were calculated by using the same program and subroutine, but the data used was only for five points covering an x range of about five feet at the extreme down stream and of the test section ; figure 5.3 (A to D). Friction factors were also computed in the same program using the following relation derived from the momentum balance for a fully developed flow as shown in section 3.6.

$$f = \frac{2\,\tau_\omega}{\rho\, u_{av}^2} = \frac{s}{\rho\, u_{av}^2}\left(\frac{dp}{dx}\right) \qquad (4.6)$$

4. 4. 2. TURBULENCE MEASUREMENTS :

The velocity fluctuations were measured with DISA hot wire

probes. The turbulence intensities were computed for uniform flow at the entrance through the relations :-

$$Tu = \frac{\sqrt{\overline{u'^2}}}{u} = \frac{Vrms}{V} \qquad (4.7)$$

The data of the Vrms values of the signals from a hot wire probe located at $x = 0$ recorded, were fed in a computer program and the results obtained for Tu versus Re is shown in figure 5.4 .

4. 4. 3. DETERMINATION OF THE PROBE POSITION RELATIVE TO THE WALLS :

The starting position of the probe relative to the channel walls was determined by advancing the probe towards the smooth wall until the probe just touched the wall and this point was taken as the reference point for the y - cordinate. The touching of the probe was checked visually through the transparent top wall of the channel. Since for the hot wire probes, actual touching could not be done, so a dummy probe was used for this purpose and the reference point was noted. Then the working probe was mounted onto the probe support and the traverse carried out. The repeatability of the position of the probe was given as ± 0.2 mm for the stepper motor [73] , and a resolution of 0.01 mm and 0.02 mm for the manual drive and the stepper motor respectively. Thus the uncertainty in the y_s measurement was estimated to be less than

± 1.5% of channel width for the smallest channel.

4. 4. 4. MEAN VELOCITY PROFILES :

The data for the mean velocity profiles were recorded both manually as well as through HP 5050B data acquisition system and HP 7004B X-Y recorder. The graphs displayed on the X-Y recorder are shown in figures 4.12 and 4.13 respectively as examples for developing and developed regions. The fluctuations shown are a qualitative measure of the fluctuations of instantaneous velocity, and hence, are not representative of the actual magnitudes and frequency. This is due to damping of the signal through the various electronic apparatus.

The numerical data from these graphical displays were fed into a computer program and the velocity profiles were plotted in the form (see section 3.4)-

$$u = a \ln y + b \qquad (4.8)$$

This was repeated for both $y = y_s$ and $y = y_r$. A straight line was fit by least squares method to the portions close to the walls and the corresponding slopes and u-axis intersections were computed ; figure 5.8 . If the velocity profiles of equations (3.19) and (3.20) are considered, u_{τ_s} and u_{τ_r} can be

calculated from the slopes mentioned above and C and z_{or} from the intersections. A value of k = 0.4 was chosen for this purpose.

4. 4. 5. MAXIMUM VELOCITY POINTS :

The maximum mean velocity points were determined by making a double pitot tube traverse in y direction and recording the pressure difference between the pitot tubes ; figure 4.14. This reading is a measure of the velocity gradient and the place where the curve cuts the $\Delta P_{dpitot} = 0$ line corresponds to the maximum velocity point. The uncertainity involved, in this case, was extimated to be ± 1 mm which is much better than the estimate from the velocity profile itself where the uncertainity could be as high as ± 3 mm for flatter profile.

4. 4. 6. EDDY DIFFUSIVITY :

The experimental outputs corresponding to double pitot tube traverses of the channel width were used for calculation of eddy diffusivity distribution. From equations (2.3) and (A. 5. 2), the following equation is obtained :

$$\frac{\varepsilon_m}{\nu} = \frac{\tau_\omega}{\mu} \frac{\left(1 - \frac{y}{y_o}\right)}{\frac{du}{dy}} - 1 \qquad (4.9)$$

For the computation of the smooth and rough wall portions of the flow, the corresponding wall shear stress was used. The conversion of the double pitot tube results into $\frac{du}{dy}$ was made through the use of the relation (see Appendix A.6) -

$$\frac{du}{dy} = \frac{1}{\rho_{air}} \frac{1}{u} \frac{\Delta P_{dpitot}}{\Delta y} \qquad (4.10)$$

Considering the fluctuations in the output from the double pitot tube, the uncertainity in $^{\Delta P}dpitot$ is estimated to be less than ± 2.5% of maximum reading drawn on the x-y recorder. The results for one set of calculations is shown in figure 5.5 . At maximum velocity point, the eddy diffisivity becomes indeterminable and it becomes negative near this point.

4. 4. 7. $\sqrt{\overline{u'^2}}$ MEASUREMENTS :

The longitudinal fluctuating velocity components were measured with hot wire probes and recorded either manually or through the data acquisition system simultaneously with the mean velocity. The minimum Vrms point was estimated from graphs drawn on the x-y recorder (figure 4. 13.). In this case the uncertainty involved was estimated to be ± 1.5 mm.

4. 4. 8. ZERO SHEAR STRESS POINTS :

The zero shear stress points were measured making a hot wire probe traverse in y-direction across the channel. The traversings were ploted on the x-y recorder; figure 4. 13. The position of zero shear stress point corresponds to the point where the fluctuations of axial velocity component is minimum.

4. 4. 9. FLOW PARAMETERS :

The only independent quantities among the geometrical parameters described in section 3.7 are s, p and ϵ . s could be measured to an accuracy of ± 0.002 inch with a knowledge of ϵ ± 0.001 inch. The values of dynamic viscosity (μ) was taken from Reference [77] corresponding to the ambient temperature. The ideal gas equation of state $P = \rho RT$ was used to calculate the density of air (ρ), corresponding to the ambient conditions. The accuracy of P and T measurements was estimated to be ± 0.1 mm Hg and ± 0.5^{o} C respectively.

The accuracy of the flow rate (Q) measurement was estimated to be ± 1.5% 54 in section 4.3.1. Due to the higher accuracies in measurements of geometrical parameters, it may be concluded that the uncertainity involved in the u_{av} and Re

largely depends on the flow rate measurements .

A consideration of dimensional analysis techniques along with a closer examination of the 15 inputs of the flow parameters mentioned in section 3.7 reveals that the effects of all these parameters can be incorporated in the effects of the following four main dimensionless groups ; Appendix A.14 -

$$\frac{s}{\varepsilon} \ , \ \frac{p}{s} \ , \ Re \ , \ f \ .$$

The first two groups are geometric parameters and Re and f are used to relate the geometric properties, fluid properties and flow variables. To find a correlations among the above dimensionless groups is the major interest from the type of experiments undertaken in the present study. The rest of the parameters considered are mainly for further understanding of the related flow properties . The results of the experimental investigations in terms of the relevent dimensionless groups are presented in figures 5.6 (A to D) The results regarding other variables of inter-est are given in figures 5.1 to 5.20 and Tables 5.1 (A to D)

CHAPTER 5

EXPERIMENTAL RESULTS AND DISCUSSIONS

5. 1 ZERO SHEAR STRESS AND MAXIMUM MEAN VELOCITY POINT :

The locations of the zero shear stress and maximum mean velocity points are the most important parameters in the present study, since they are the only experimental inputs used in the prediction of mean flow parameters. As shown in figures 5.9 to 5..16 , the variation of the position of these points indicates strong dependence on Re, s/ε and p/ε . It may be observed that these two points donot coincide. With the increase of Re and p/ε, and decrease of s/ε, they get proportionately closer to the smooth wall. The variation with s/ε reflects the greater effect of a physical roughness element as it occupies a larger portion of the space between the walls. And the variation with Re indicates stronger diffusion of turbulent eddies from the rough towards the smooth side as the velocity is increased and as the momentum exchange near the rough wall becomes more vigorous.

5. 2. ROUGHNESS DENSITY :

The effect of p/ε on zero shear stress and maximum velocity points was first found indirectly by comparing with

Hanjalic's [61] results ; figures 5.11 and 5.13 . The Re used in these figures is based on maximum velocity in the channel rather than the average velocity, as Hanjalic's results were not available in terms of u_{av} . Hence, the present data were translated into Hanjalic's terms using the actual measured u_m in a channel corresponding to a particular u_{av} . It may be observed that the positions of the zero shear and maximum velocity points deviate more from the centre line of the channel towards the smooth wall for a larger p/ϵ , i.e. for a lower roughness density at the same s/ϵ ratio. At first instance, it may seem unexpected since a higher roughness density would seem to imply a more vigorous momentum exchange than a lower roughness density, and hence a smaller $\frac{y_{os}}{s}$ ratio . However, a closer examination of flow separation patterns between roughness elements of different pitches [78,79] reveals the possibility that at a higher roughness density the flow will tend to pseudo-smooth over the tips of the elements, but at a lower density the flow will find some time to re-attach and when it faces a new element it will be thrown into the stream, shedding vigorous eddies. Thus the points under consideration are even further displaced from the rough wall. The noncoincidence of the two points and the larger displacement of the zero-shear point than the maximum velocity point simply indicate the stronger effect of dissimilar boundary conditions on the turbulent flow field rather

than the mean motion .

5. 3. MEAN VELOCITY FIELDS :

Except very near the rough wall, in a region of about 1.5 ε from the roughness root as shown in figure 5.8 , the logarithmic velocity profiles chosen for the present study represent well the actual velocity fields encountered . This deviation may be due to the flow separation structures mentioned in the previous section, which possibly prevail between the roughness elements. This is an indication of the failure of the mixing length hypothesis and the assumptions used in the derivation of the logarithmic law (section 3.4) very near a rough wall.

Near the maximum velocity point, the experimental velocity profile seems flatter than those that the logarithmic profiles indicate. In this region the velocity field is influenced by the two dissimilar wall and the flow is retarded by the effect of the opposite wall. It is quite possible that this flattering will introduce some error in the calculation of z_{or} and m since they are computed by matching the two wall profiles at the maximum velocity point. However, this error is probably much less than the errors involved in the calculations through the profile method, see the

scatter of the results presented in Table 4.1.

The velocity profiles accord well with the law-of-the wall profiles, between the sublayers very near the walls and the above mentioned region. Thus the fluid particles within these regions are unaware of the nature of the opposite surface.

A large variation of the parameter m was cited in section 3.4 refering to the relevant literature. But the mention of variation of m with Re was hardly found in any of the references, although in some, variation with roughness density p/ε was reported. The observed Re dependence of m as shown in Tables 5.1 (A to D) during the present experimental program led to a further survey of more recent literature and a similar reported behaviour was found in the work of Wang and Tullis [80]. A variation of m from $\frac{1}{29}$ to $\frac{1}{33.6}$ for a Re range of 7.20×10^5 to 2.53×10^6 was calculated through the data reported in [80] to match the present nomenclature. Almost the same type of variation was found in the present study, namely, a decrease of m with the increase of Re, see figure 5.17 (A to D) , and similar order of magnitude for m. The interpretation of $z_{or} = m\varepsilon$ as the point where the velocity is assumed to be zero leads to the conclusions that, first, the virtual origin of velocity is under the roughness

top, near the root, and second, as the velocity in the channel is increased, this origin is further suppressed towards the roughness roots, at least in the range of Reynolds numbers considered.

5. 4. FRICTION FACTORS :

The values of the friction factors obtained from the experimental measurements are in the same order of magnitude as the ones obtained from the classical Moody diagram corresponding to the same relative roughness in a circular pipe ; figure 5.6A . The differences, which might be significant in certain critical applications, are in the shape of the function f versus Re. In the range of Reynolds' number considered, Moody diagram predicts a constant friction factor, since the flow in a pipe is completely rough in this range [45,81] . However, the present study as shown in figure 5.6 (A to D) indicates a seemingly transition range type of flow, between completely smooth and completely rough regimes. This is due to the asymmetry in the roughness distribution on the channel walls. The combination of completely smooth flow on one side and rough flow on the other produces the type of observed behaviour, namely the variation of total friction factor with both Re and s/ε (or ε/D).

It is difficult to use Moody diagram in the cases where unfamiliar roughness structures are encountered. From a strictly design point of view, if the test channel had rough walls on both sides, one would still tend to use the same relative roughness value used above in order to calculate the friction factor from the Moody diagram. This in turn would obviously predict the same friction factor for both rough-rough and rough-smooth channels. Naturally, this cannot be the case. The problem arises due to the use of the concept of equivalent sand roughness in the classical diagram. An equivalent sand roughness has to be defined for the particular roughness structure on a wall to be able to use the Moody diagram. This sand roughness should also be a function of Reynolds number in case of asymmetric roughness distribution.

In the present study, the use of parameter z_{or} , which is connected to the equivalent sand roughness through the logarithmic rough wall profile, is introduced to provide a step in the theoretical analysis of the behavior of flow near a rough wall. It is conceptually easier to visualize z_{or} as a point where the average velocity profile reaches zero near roughness root where as an equivalent sand roughness has no sound physical basis. An equivalent sand roughness is defined as that value which gives the actual coefficient of resistance when inserted into the equation [45] ,

$$f = \left(2 \ln \frac{R}{k_s} + 1.74 \right)^{-2} / 4 .$$

Thus $z_{or} = m \varepsilon$ is more amenable to theoretical analysis than k_s.

Since no theoretical prediction of the above mentioned parameters were available for the particular geometry used in the present study, empirical inputs of m, or y_o and y_m were employed. Friction factors calculated with m as a constant did not agree at all with the experimentally measured values, figure 3.2 . Those calculated with experimental values of y_o and y_m , on the other hand, gave excellent results in predicting the friction factors as shown in figure 3.3 , again proving the strong dependence of m on Re, s/ε and p/ε.

5. 5. CORRELATION OF EXPERIMENTAL RESULTS :

The functional relationship derived in terms of dimensionless groups as shown in Appendix A. 14 can be written as-

$$\phi \left(Re, \frac{v}{s} , \frac{s}{\varepsilon} , \frac{p}{s} \right) = 0 \qquad (5.1)$$

Replacing $\frac{v}{s} = A$, $Re = B$, $\frac{s}{\varepsilon} = C$ and $\frac{p}{s} = D$, the equation (5. 1) can be given as -

$$A = \phi (B, C, D) \qquad (5.2)$$

We can assume that equation (5.2) can take a form as follows -

$$A = G\, B^{l}\, C^{m}\, D^{n}\,, \qquad (5.3)$$

where G, l, m and n are constants. In order to find the numerical values for these constants, a computer program named Statistical Package for the Social Sciences version H (SPSSH) [82] was used. This package uses the multiple regression which is a general Statistical technique through which an analysis is done for the relationship between a dependent variable and a set of independent variables. Thus 160 sets of experimental data consisting of dependent variable A and independent variables B, C and D were fed into the computer program. The program was run twice, once with the dependent variable A based on zero shear stress point and next with A based on maximum velocity point, the same sets of data being used for the independent variables B, C and D for both the cases. The values of G, l, m and n thus obtained when substituted in equation (5.3) , give

$$\frac{y_{or}}{s} = 0.418\ Re^{0.033}\ \left(\frac{s}{\varepsilon}\right)^{0.157}\ \left(\frac{p}{s}\right)^{0.158} \qquad (5.4)$$

and

$$\frac{y_{mr}}{s} = 0.299\ Re^{0.066}\ \left(\frac{s}{\varepsilon}\right)^{0.140}\ \left(\frac{p}{s}\right)^{0.201} \qquad (5.5)$$

The correlations of the experimental datas based on

equations (5.4) and (5.5) are shown in figures 5.20 a,b and 5.21 a,b respectively.

The maximum deviation of the data from the correlations given by equations (5.4) and (5.5) are 10% and 12% respectively.

CHAPTER 6

CONCLUSION

The following conclusions were drawn from both the analytical and experimental studies of the turbulent fluid flow in a partially roughened surfaced channel :

1. In general, a substantial agreement was obtained between the analysis and the experimental results of the particular turbulent fluid flow studied.
2. The fact that the locations of maximum velocity and zero shear stress are the non-coincident for asymmetric turbulent velocity profiles was further established.
3. The locations of zero shear stress and maximum velocity points shift towards smooth wall side for a larger p/ϵ i.e. for a lower roughness density at the same s/ϵ ratio.
4. Experimentally calculated friction factors of the present study show that f decreases with the increase of s/ϵ but increases with the increase of p/ϵ.
5. The point z_o , where the average velocity profile reaches zero near a rough wall and hence the parameter m, which is a function of Re , s/ϵ and p/ϵ , decreases

with the increase of Re and s/ϵ, but increases with the increase of p/ϵ , the exception being observed at higher $p/\epsilon = 16$ as well as at higher Reynolds number considered.

APPENDIX A.I

DERIVATION OF INTEGRAL EQUATIONS

Considering figure 3.I of idealized model -

A.1.1. MIDDLE PORTION :

Continuity equation :

$$(s_r - \delta_r + \delta_s) \frac{du_\infty}{dx} = V_{\delta_r} + V_{\delta_s} \qquad (A.1.1)$$

Momentum equation :

$$(s - \delta_r - \delta_s) dp + d (\rho u_\infty^2) (s - \delta_r - \delta_s)$$

$$= \rho (u_\infty v_{\delta_r} dx + u_\infty v_{\delta_s} dx)$$

$$\text{i.e. } (s - \delta_r - \delta_s) \frac{d}{dx} (p + \rho u_\infty^2) = \rho u_\infty (v_{\delta_r} + v_{\delta_s}) \qquad (A.1.2)$$

From equations (A.1.1) and (A.1.2),

$$(s - \delta_r - \delta_s) \left[\frac{dp}{dx} + 2 \rho u_\infty \frac{du_\infty}{dx} \right] = (s - \delta_r - \delta_s) \rho u_\infty \frac{du_\infty}{dx}$$

$$dp = - \rho u_\infty du_\infty \qquad (A.1.3)$$

A.1.2 ROUGH SIDE :

Continuity equation :

$$\frac{d}{dx} \int_{z_{or}}^{\delta_r} \rho\, u_r\, dy_r = - \rho\, v_{\delta_r} \qquad (A.1.4)$$

Momentum equation :

$$\tau_\omega\, dx + (\delta_r - z_{or})\, dp = - d \int_{z_{or}}^{\delta_r} \rho\, u_r^2\, dy_r - u_{\delta_r}\, \rho\, v_{\delta_r}\, dx \qquad (A.1.5)$$

From equations (A.1.4) and (A.1.5) and using $u_{\delta_r} = u_\infty$ and assuming $z_{or} \angle\angle \delta_r$,

$$\tau_{\omega r} = - \delta_r \frac{dp}{dx} - \frac{d}{dx} \int_{z_{or}}^{\delta_r} \rho\, u_r^2\, dy_r + \rho\, u_\infty \frac{d}{dx} \int_{z_{or}}^{\delta_r} u_r\, dy_r \qquad (A.1.6)$$

A.1.3 SMOOTH SIDE :

Continuity equation :

$$\frac{d}{dx} \int_0^{\delta_s} \rho\, u_s\, dy_s = - \rho\, v_{\delta_s} \qquad (A.1.7)$$

Momentum equation :

$$\tau_{\omega s}\, dx + \delta_s\, dp = - d \int_0^{\delta_s} \rho\, u_s^2\, dy_s - u_{\delta_s}\, \rho\, v_{\delta_s}\, dx \qquad (A.1.8)$$

From equation (A.1.7) and (A.1.8) and using $u_{\delta_s} = u_\infty$,

$$\tau_{\omega s} = - \delta_s \frac{dp}{dx} - \frac{d}{dx} \int_0^{\delta_s} \rho\, u_s\, dy_s + \rho\, u_\infty \frac{d}{dx} \int_0^{\delta_s} u_s\, dy_s \qquad (A.1.9)$$

A.1.4 WHOLE CHANNEL :

Adding equations (A.1.1) , (A.1.4) and (A.1.7) , the continuity equation for the whole channel becomes -

$$\frac{d}{dx} \int_0^s u\, dy = 0 ,$$

keeping in view that u is in three portions with corresponding upper and lower limits , of validity in the channel .

APPENDIX A.2

DERIVATION OF FULLY DEVELOPED REGION MOMENTUM EQUATIONS

From equation (3. 9) ,

$$\frac{\partial}{\partial y}\left(\mu \frac{\partial u}{\partial y} - \rho \, u' \, v' \right) = \frac{dp}{dx}$$

Integrating,

$$\mu \frac{\partial u}{\partial y} - \rho \, \overline{u' \, v'} = y \frac{dp}{dx} + C$$

Using the boundary conditions ,

at $y = 0$, $\overline{u' \, v'} = 0$, $\mu \frac{\partial u}{\partial y} = \tau_\omega$,

$$\mu \frac{\partial u}{\partial y} - \rho \, \overline{u' \, v'} = y \frac{dp}{dx} + \tau_\omega \qquad \text{(A.2.1)}$$

And using the other boundary conditions ,

at $y = y_o$, $\tau = \mu \frac{\partial u}{\partial x} - \rho \, \overline{u' \, v'} = 0$,

$$0 = y_o \frac{dp}{dx} + \tau_\omega$$

i.e. $$\tau_\omega = - y_o \frac{dp}{dx} \qquad \text{(A.2.2)}$$

APPENDIX A.3

RELATION BETWEEN AIR VELOCITY AND HOT-WIRE ANEMOMETER OUTPUT SIGNALS

For the removal of heat from a heated wire can be written as [73] -

$$Q = P = (A + B u^n) \Delta T \qquad (A.3.1)$$

The electric power input , $P = \frac{V^2}{R}$

Hence equation (A.3.1.) becomes ,

$$V^2 = R (A + B u^n) \Delta T$$

To keep the wire at constant temperature , at $u = 0$, $V = V_0$,

$$V^2 = V_0^2 + B R \Delta T u^n \qquad (A.3.2)$$

$$\text{i.e. } \frac{V^2}{V_0^2} = 1 + \frac{B R \Delta T u^n}{V_o^2}$$

$$\text{i.e. } \frac{V^2}{V_o^2} - 1 = C u^n \quad , \quad \text{where } C = \frac{B R \Delta T}{V_o^2}$$

$$\ln \left(\frac{V^2}{V_o^2} - 1 \right) = n \ln u + C \qquad (A.3.3)$$

APPENDIX A.4

RELATION BETWEEN THE FLUCTUATING AND THE MEAN COMPONENTS OF HOT-WIRE SIGNALS AND VELOCITIES

A. In the case of non-linearized signals , we get from equation (A.3.2) -

$$V^2 = V_0^2 + C_1 u^n \qquad (A.4.1)$$

Differentiating ,

$$2 V dV = C_1 n u^{n-1} du$$

Now dividing by $2 V^2$ and multiplying the right hand side by $\frac{u}{u}$,

$$\frac{dV}{V} = \frac{C_1 n u^n}{2 V^2} \frac{du}{u}$$

Rearranging ,

$$\frac{du}{u} = \frac{2 V^2}{n C_1 u^n} \frac{dV}{V}$$

$$\text{i.e.} \quad \frac{du}{u} = \frac{dV}{V} \frac{2}{n} \left(\frac{V^2}{V^2 - V_0^2} \right) \qquad (A.4.2)$$

To relate du and dv with u' and V' , we have to introduce ,

$V = \overline{V} + V'$ and $u = \overline{u} + u'$ in equation (A.4.1) .

Hence , $(\bar{V} + V')^2 = V_0^2 + C_1 (\bar{u} + u')^n$

Expanding the terms -

$$\bar{V}^2 + 2 \bar{V} V' + V'^2 = V_0^2 + C_1 (\bar{u}^n + n \bar{u}^{n-1} u' + \frac{n (n-1)}{2!} \bar{u}^{n-2} u'^2 + ...) \quad (A.4.3)$$

Keeping only the first two terms of expansions ,

$$\bar{V}^2 + 2 \bar{V} V' \simeq V_0^2 + C_1 \bar{u}^n + C_1 n \bar{u}^{n-1} u'$$

Since , $\bar{V}^2 = V_0^2 + C_I \bar{u}^n$,

$$2 \bar{V} V' \simeq C_1 n \bar{u}^{n-1} u'$$

$$\text{i.e. } V' \simeq \frac{n}{2} \frac{C_1 n \bar{u}^{n-1}}{V} u'$$

Multiplying the right hand side by $\frac{\bar{u}'}{\bar{u}}$ and recognizing that $C_1 \bar{u}^n = \bar{V}^2 - V_0^2$,

$$V' \simeq \frac{n}{2} \frac{\bar{V}^2 - V_0^2}{V} \frac{u'}{\bar{u}}$$

$$\text{i.e. } \frac{u'}{\bar{u}} \simeq \frac{V'}{\bar{V}} \frac{n}{2} \left(\frac{V^2}{\bar{V}^2 - V_0^2} \right) \quad (A.4.4)$$

Now comparisons of equations (A. 4.2) and (A. 4.4) will reveal that replacing du and dV by u' and V' , and u and V by u and V respectively , is equivalent to omitting the higher order terms in equation (A. 4.3) , which was done in the above derivation .

B. In the case of linearized signals voltage - velocity relationship is of the form :

$$V = B\,u$$

$$dV = B\,du$$

$$\frac{du}{u} = \frac{dV}{V}$$

$$\text{or, } V = B\,u$$

$$\bar{V} + V' = B\,(\bar{u} + u')$$

$$\bar{V} = B\,\bar{u}\,, \quad V' = B\,u'$$

$$\text{Hence , } \frac{u'}{\bar{u}} = \frac{V'}{\bar{V}}$$

APPENDIX A.5

FULLY DEVELOPED SHEAR STESS DISTRIBUTION

From eqution (3. 23) and (A.2.1) ,

$$\tau = y \frac{dP}{dx} + \tau_\omega \qquad (A.5.1)$$

$$\text{i.e. } \frac{\tau}{\tau_\omega} = \frac{y}{\tau_\omega} \frac{dp}{dx} + 1$$

Now substituting $\tau_\omega = - y_0 \frac{dp}{dx}$, (equation A.2.2) into the right hand side of the above eqution , and simplifying ,

$$\frac{\tau}{\tau_\omega} = 1 - \frac{y}{y_0} \qquad (A.5.2)$$

The relations A.5.1 and A.2.2 can directly be written down by a force balance on an infinitesimal fluid element of thickness dx and height y and y_0 respectively .

APPENDIX A.6

RELATION BETWEEN $\frac{du}{dy}$ AND DOUBLE PITOT TUBE MEASUREMENTS

In this case, $dy \simeq \Delta y = 2$ mm , which is the distance between two pitot tubes , Writing the Bernoulli equation ,

$$\frac{P_1 - P_{st}}{\gamma_{air}} = \frac{U_1^2}{2g} \quad , \quad \text{for pitot tube number 1 ,}$$

and $$\frac{P_2 - P_{st}}{\gamma_{air}} = \frac{U_2^2}{2g} \quad , \quad \text{for pitot tube number 2 .}$$

Subtracting the above relations from each other ,

$$\frac{P_1 - P_2}{\gamma_{air}} = \frac{U_1^2 - U_2^2}{2g}$$

$$\text{i.e.} \quad \frac{P_1 - P_2}{\gamma_{air}} = \frac{(U_1 + U_2)(U_1 - U_2)}{2g}$$

Assuming the velocity profile between the tips of the pitot tubes is linear , and the velocity at the centre is u and $U_1 - U_2 = \Delta u$,

$$\frac{P_1 - P_2}{\gamma_{air}} = \frac{2u\,\Delta u}{2g}$$

Putting $P_1 - P_2 = \Delta P_{dpitot}$ and dividing by Δy ,

$$\frac{u}{y} = \frac{1}{\rho_{air}} \frac{1}{u} \frac{\Delta P_{dpitot}}{\Delta y} \quad ,$$

$$\text{or} \quad , \quad \frac{du}{dy} \simeq \frac{1}{\rho_{air}} \frac{1}{u} \frac{\Delta P_{dpitot}}{\Delta}$$

APPENDIX A.7

REYNOLDS NUMBER IN TERMS OF MEAN FLOW PARAMETERS

From definition ,

$$u_{av} = \frac{\int u \, dA}{A} = \frac{\int_0^{y_{ms}} u_s \, dA + \int_{z_{or}}^{y_{mr}} u_r \, dA}{A} \qquad (A.8.1)$$

Now substituting $u_s^+ = \frac{u_s}{u_{\tau_s}}$ in equation (2. 6),

$$u_s = u_{\tau_s} \left\{ \frac{1}{k} \ln \left(1 + k \frac{y \, u_{\tau s}}{\nu} \right) + 7.8 \left[1 - \exp\left(- \frac{y \, u_{\tau s}}{11 \, \nu} \right) - \frac{y \, u_{\tau s}}{11 \, \nu} \exp \left(- \frac{y \, u_{\tau s}}{3 \, \nu} \right) \right] \right\}$$

Also from equation (3. 20) ,

$$u_r = u_{\tau_r} \left(\frac{1}{k} \ln \frac{y}{z_{or}} \right)$$

$$dA = 1.dy$$

$$A = 1.s$$

Substituting the above values in equation (A. 7. 1) and integrating ,

$$u_{av} = \frac{\nu}{s}\left\{ \frac{1 + k\, y^{+}_{ms}}{k^2}\left[\ln\left(1 + k\, y^{+}_{ms}\right) - 1\right] + \left[7.8 \quad y^{+}_{ms} - 11\left(1 - \exp\left(-\frac{y^{+}_{ms}}{11}\right)\right) + \frac{9}{11}\left(1 + \frac{y^{+}_{ms}}{3}\right)\exp\left(-\frac{y^{+}_{ms}}{3}\right) - \frac{9}{11}\right] + \frac{y^{++}_{mr}}{k}\left[\ln y^{+}_{ms} + C\,k - \frac{u_{\tau r}}{u_{\tau s}}\right] + \frac{z^{++}_{or}}{k}\,\frac{u_{\tau r}}{u_{\tau s}}\right\} \qquad (A.7.2)$$

From definition ,

$$Re = \frac{u_{av}\, D_{hyd}}{\nu}\,, \qquad (A.7.3)$$

Also from definition ,

$$D_{hyd} = \frac{4\, s\, w}{2(s + w)} = \frac{2\, s\, w}{s + w} \approx 2\, s$$

Now substituting the above values of u_{av} and D_{hyd} in equation (A. 7. 3) , the equation (3. 32) is obtained.

APPENDIX A.8

FRICTION FACTORS IN TERMS OF MEAN FLOW PARAMETERS

From equation (A. 2.2) ,

$$\frac{\tau_{\omega r}}{\tau_{\omega s}} = \frac{y_{or}}{y_{os}} = \frac{y_{or}}{s - y_{or}} \quad , \quad \text{since} \quad s = y_{or} + y_{os}$$

$$= \frac{1}{\frac{s}{y_{or}} - 1}$$

From definition ,

$$u_{\tau r} = \frac{\tau_{\omega r}}{\rho} \quad \text{and} \quad u_{\tau s} = \frac{\tau_{\omega s}}{\rho}$$

Hence ,

$$\frac{u_{\tau r}}{u_{\tau s}} = \frac{\tau_{\omega r}}{\tau_{\omega s}} = \frac{1}{\sqrt{\frac{s}{y_{or}} - 1}} \equiv \frac{1}{D} \qquad \text{(A.8.1)}$$

From equation (3. 24) ,

$$f_r = \frac{2\tau_{\omega r}}{\rho u_{av}^2}$$

$$= 2\left(\frac{u_{\tau r}}{u_{av}} \right)^2$$

$$= \frac{2}{D^2} \left(\frac{u_{\tau s}}{u_{av}} \right)^2$$

From equation (3. 26) ,

$$f_s = \frac{2\,\tau_\omega}{\rho\, u_{av}^2}$$

$$= 2\,\left(\frac{u_{\tau s}}{u_{av}}\right)^2$$

Let $\Omega = \frac{u_{\tau s}}{u_{av}}$, then from equation (A. 7.2) , Ω becomes ,

$$\Omega = \frac{s^+}{E} ,$$

where $$E = \frac{1 + k\, y^+_{ms}}{k^2}\left[\ln\left(1 + k\, y^+_{ms}\right) - 1\right] + 7.8\left[y^+_{ms} - 11\left(1 - \exp\left(-\frac{y^+_{ms}}{11}\right)\right) + \frac{9}{11}\left(1 + \frac{y^+_{ms}}{3}\right)\exp\left(-\frac{y^+_{ms}}{3}\right) - \frac{9}{11}\right.$$

$$\left. + \frac{1}{k}\left[y^{++}_{mr}\left(\ln y^+_{ms} + C\,k - \frac{1}{D}\right) + \frac{z^{++}_{or}}{D}\right]\right],$$

$$y^+_{ms} = s^+ - y^{++}_{mr}$$

and $$f = \Omega^2\left(1 + \frac{1}{D^2}\right) \qquad \text{(A.8.2)}$$

APPENDIX A.9

MATCHING OF SMOOTH AND ROUGH WALL VELOCITY PROFILES AT THE MAXIMUM VELOCITY POINT

From the equations (3. 19) and (3. 20) ,

$$u_m = \frac{u_{\tau r}}{k} \ln \left(\frac{y_{mr}}{z_{or}} \right)$$

$$= \frac{u_{\tau s}}{k} \ln \left(\frac{y_{ms}\, u_{\tau s}}{\nu} \right) + C\, u_{\tau s} \qquad \text{(A.9.1)}$$

Now rearranging equation (A. 9.1) and substituting $y_{ms} = s - y_{mr}$,

$$\ln y_{mr} - \ln z_{or} = \frac{u_{\tau s}}{u_{\tau r}} \left\{ \ln \left[\frac{(s - y_{mr})\, u_{\tau s}}{\nu} \right] + C\, k \right\}$$

Hence , $$z_{or} = y_{mr} \exp \left\{ - \frac{u_{\tau s}}{u_{\tau r}} \left[\ln \frac{(s - y_{mr})\, u_{\tau r}}{\nu} + C\, k \right] \right\} \qquad \text{(A.9.2)}$$

Multiplying equation (A. 9.2) by $\frac{u_{\tau s}}{\nu}$,

$$z_{or}^{++} = y_{mr}^{++} \exp \left\{ - \frac{u_{\tau s}}{u_{\tau r}} \left[\ln (s^{+} - y_{mr}^{++}) + C\, k \right] \right\} \qquad \text{(A.9.3)}$$

Substituting equation (A . 8.1) in equation (A . 9.3) ,

$$z_{or}^{++} = y_{mr}^{++} \exp \left\{ - D \left[\ln (s^{+} - y_{mr}^{++}) + C\, k \right] \right\} \qquad \text{(A.9.4)}$$

APPENDIX A.10

RELATIONS FOR f AND Re WITH m AS A CONSTANT

From equation (A . 10. 2) ,

$$z_{or} = y_{mr} \exp \left\{ - D \left[\ln \left(s^{+} - y_{mr}^{++} \right) + C\, k \right] \right\} \qquad (A.10.1)$$

For constant m , $y_o = y_m$,(see section 3.8.1). Hence D becomes ,

$$D = \sqrt{\frac{s}{y_{mr}} - 1} \qquad (A.10.2)$$

Substituting equation (A. 10. 2) into equation (A . 10. 1) ,

$$z_{or} = m\varepsilon$$

$$= y_{mr} \exp \left\{ - \sqrt{\frac{s}{y_{mr}} - 1} \left[\ln \frac{\left(s - y_{mr} \right) u_{\tau} s}{\nu} + C\, k \right] \right\} \qquad (A.10.3)$$

Equations (3 . 32) and (A . 8.2) stay the same , but the above equation (A . 10.2) should be used for constant m .

APPENDIX A.11

SUMMARY OF RELATIONS BETWEEN MEAN FLOW PARAMETERS

$$u_{\tau r} = \sqrt{\frac{\tau_{\omega r}}{\rho}} \qquad \text{(Definition)}$$

$$u_{\tau s} = \sqrt{\frac{\tau_{\omega s}}{\rho}} \qquad \text{(Definition)}$$

$$f_r = \frac{2\,\tau_{\omega r}}{\rho\, u_{av}^2} \qquad \text{(Definition)}$$

$$f_s = \frac{2\,\tau_{\omega s}}{\rho\, u_{av}^2} \qquad \text{(Definition)}$$

$$f = \frac{f_s + f_r}{2} \qquad \text{(Equation 3.31)}$$

$$\tau_{\omega r} = - y_{or} \frac{dP}{dx} \qquad \text{(Appendix A.2)}$$

$$\tau_{\omega s} = - y_{os} \frac{dP}{dx} \qquad \text{(Appendix A.2)}$$

$$\tau_{\omega r} + \tau_{\omega s} = - s \frac{dP}{dx} \qquad \text{(Equation 3.28)}$$

$$\frac{\tau_r}{\tau_{\omega r}} = \left(1 - \frac{y_r}{y_{or}} \right) \qquad \text{(Appendix A.5)}$$

$$\frac{\tau_s}{\tau_{\omega s}} = \left(1 - \frac{y_s}{y_{os}} \right) \qquad \text{(Appendix A.5)}$$

$$Re = \frac{u_{av} \; D_{hyd}}{\nu} \qquad \text{(Definition)}$$

$$z_{or} = y_{mr} \exp \left\{ - \frac{u_{\tau_s}}{u_{\tau_r}} \left[\ln \left(\frac{u_{\tau_s} \; s}{\nu} - \frac{u_{\tau_s} \; y_{mr}}{\nu} \right) + C \; k \right] \right\} \qquad \text{(Appendix 10)}$$

$$u_{av} = \frac{Q}{A} \qquad \text{(Definition)}$$

$$s = y_{or} + y_{os} \qquad \text{(Definition)}$$

$$m = \frac{z_{or}}{\varepsilon} \qquad \text{(Definition)}$$

$$\frac{\varepsilon_{Ms}}{\nu} = \frac{\tau_{\omega s}}{\mu} \; \frac{\left(1 - \frac{y_s}{y_{os}} \right)}{\frac{du_s}{dy_s}} - 1 \qquad \text{(Equation 4.9)}$$

$$\frac{\varepsilon_{Mr}}{\nu} = \frac{\tau_{\omega r}}{\mu} \; \frac{\left(1 - \frac{y_r}{y_{or}} \right)}{\frac{du_r}{dy_r}} - 1 \qquad \text{(Equation 4.9)}$$

APPENDIX A.12

FLOWCHART OF THEORETICAL CALCULATIONS WITH m AS CONSTANT

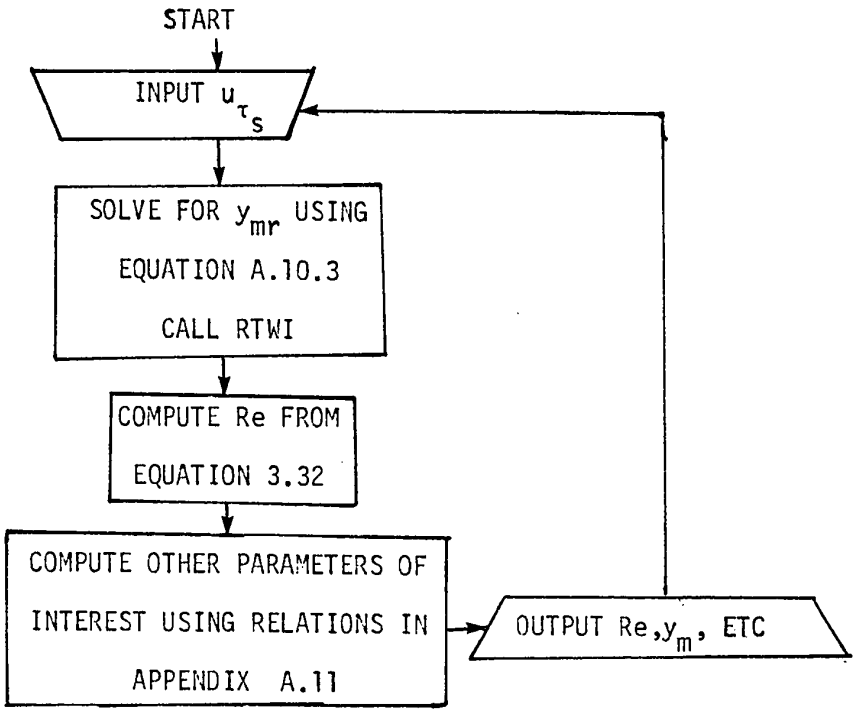

The programme is open ended. The non-linear equation (.A.10.3) was solved by the sub-routine RTWI, which utilizes the Wegstein's iteration method [41].

APPENDIX A.13

FLOWCHART OF THEORETICAL CALCULATIONS WITH m AS VARIABLE

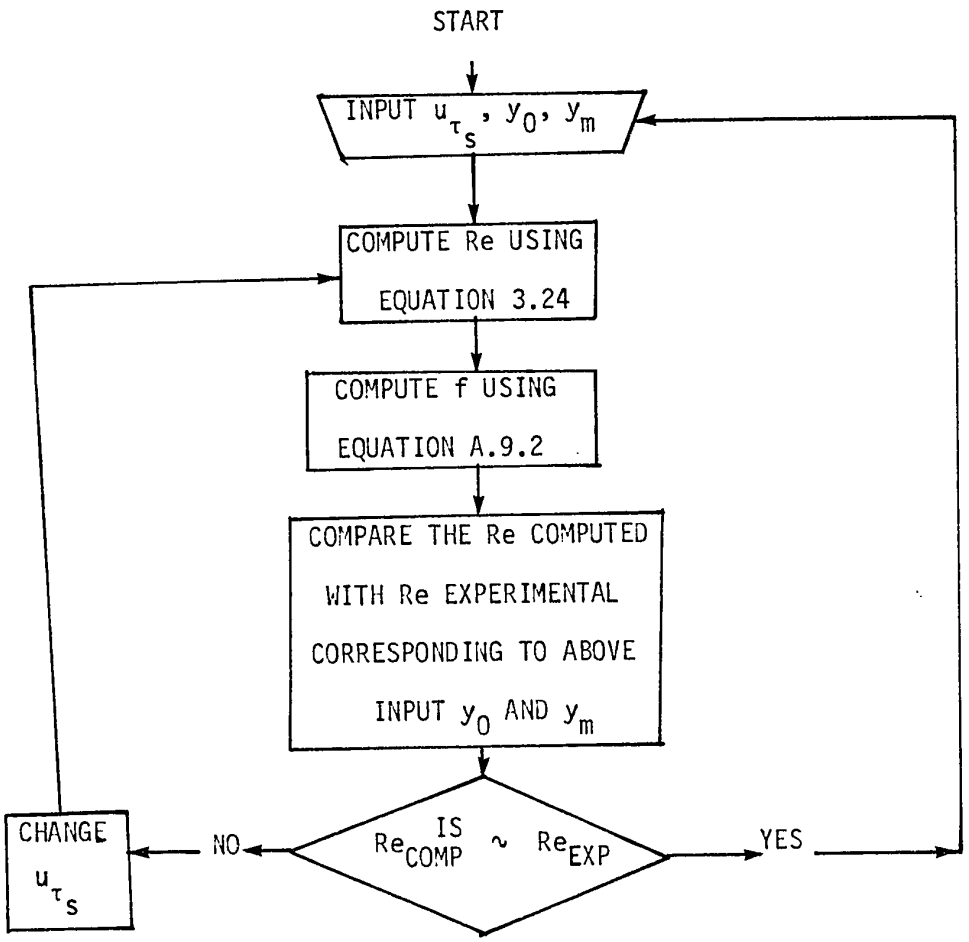

APPENDIX A.14

DIMENSIONAL ANALYSIS

The zero shear stress point (y_0), or the maximum velocity point (y_m) for a partially roughened surfaced channel assumed here to depend mainly on channel width s, roughness height ε, roughness pitch p, the hydraulic diameter D of the channel, the average velocity u of fluid, the density ρ and the dynamic viscosity μ. The relationship among the variables is expressed by an equation of the form,

$$\phi (y, s, \varepsilon, p, u, \rho, \mu) = 0 \qquad (A.14.1)$$

The dimensional matrix of the variables in equation (A.14.1) can be given as,

	y	s	ε	p	u	ρ	μ
M	0	0	0	0	0	1	1
L	1	1	1	1	1	-3	-1
T	0	0	0	0	-1	0	-1

According to Buckingham's Π theorem, since there are seven variables in equation (A.14.1) in which there are only three dimensions as shown in the above matrix, the variables may be arranged into four independent dimensionless Π parameters. If

u, ρ and s are the primary variables, four Π parameters are -

$$\Pi_1 = u^{x1}\ \rho^{y1}\ s^{z1}\ \mu$$

$$\Pi_2 = u^{x2}\ \rho^{y2}\ s^{z2}\ y$$

$$\Pi_3 = u^{x3}\ \rho^{y3}\ s^{z3}\ \varepsilon$$

$$\Pi_4 = u^{x4}\ \rho^{x4}\ s^{z4}\ p$$

By expanding the Π quantities into dimensions,

$$\Pi_1 = (M^0 L^1 T^{-1})^{x1}\ (M^1 L^{-3} T^0)^{y1}\ L^{z1}\ (M^1 L^{-1} T^{-1})$$

Since Π_1 is required to be dimensionless, the exponents of M,L and T must all be zero. Hence,

$$y1 + 1 = 0$$

$$x1 - 3y1 + z1 - 1 = 0$$

$$-x1 - 1 = 0$$

from which $x1 = -1$, $y1 = -1$ and $z1 = -1$. Therefore,

$$\Pi_1 = (u)^{-1}\ (\rho)^{-1}\ (s)^{-1}\ \mu$$

$$= \frac{\mu}{u\ \rho\ s}$$

Now $\Pi_2 = (M^0 L^1 T^{-1})^{x2}\ (M^1 L^{-3} T^0)^{y2}\ (L)^{z2}\ (L)$

i.e. $y2 = 0$

$$x2 - 3y2 + z2 + 1 = 0$$
$$- x2 = 0,$$

from which $x2 = 0$, $y2 = 0$ and $z2 = -1$. Therefore,

$$\Pi_2 = (u)^0 (\rho)^0 (s)^{-1} y$$

$$= \frac{y}{s}$$

Similarly, $\Pi_3 = \frac{\varepsilon}{s}$ and $\Pi_4 = \frac{p}{s}$. Hence, equation (A.14.1) becomes,

$$\phi \left(\frac{\mu}{u \rho s}, \frac{y}{s}, \frac{\varepsilon}{s}, \frac{p}{s} \right) = 0$$

It is convenient to invert some of the parameters and by doing so the above equation becomes,

$$\phi \left(\frac{u \rho s}{\mu}, \frac{y}{s}, \frac{s}{\varepsilon}, \frac{p}{s} \right) = 0 \qquad (A.14.2)$$

TABLE 3.1

LAW OF THE WALL [55]

	Range	Equation
Prandtl & Taylor [26,27]	$0 \leq y^+ \leq 11.5$	$u^+ = y^+$
	$11.5 \leq y^+$	$u^+ = 2.5 \ln y^+ + 5.5$
Von Karman [28]	$0 \leq y^+ \leq 5$	$u^+ = y^+$
	$5 \leq y^+ < 30$	$u^+ = 5 \ln y^+ - 3.05$
	$30 \leq y^+$	$u^+ = 2.5 \ln y^+ + 5.5$
Reichardt [25]	$0 \leq y^+$	$u^+ = 2.5 \ln (1 + 0.4 y^+) + 7.8 \left[1-\text{Exp}(-y^+/11)-(y^+/11)\text{Exp}(-0.33y^+) \right]$
Deissler [15]	$0 \leq y^+ \leq 26$	$u^+ = \int_0^{y^+} \frac{dy^+}{1+(0.124)^2 u^+ y^+ \left[1-\text{Exp}(0.124)^2 u^+ y^+\right]}$
	$26 \leq y^+$	$u^+ = 2.78 \ln y^+ + 3.8$
Van Driest [29]	$0 \leq y^+$	$u^+ \int_0^{y^+} \frac{2\, dy^+}{1+\{1+0.64y^{+2}\left[1-\text{Exp}(-y^+/26)\right]^2\}^{\frac{1}{2}}}$
Rannie [30]	$0 \leq y^+ \leq 27.5$	$u^+ = 14.54 \tanh (0.0688\, y^+)$
	$27.5 \leq y^+$	$u^+ = 2.5 \ln y^+ + 5.5$
Spalding [31]	$0 \leq y^+$	$y^+ = u^+ + 0.1108\left[\text{Exp}(0.4u^+)-1-0.4u^+ - (0.4u^+)^2/2! - (0.4u^+)^3/3! - (0.4u^+)^4/4!\right]$
Wasan et al [32]	$0 \leq y^+ \leq 20$	$u^+ = y^+ - 1.04\text{x}10^{-4}(y^+)^4 + 3.03\text{x}10^{-6}(y^+)^5$
	$20 \leq y^+$	$u^+ = 2.5 \ln y^+ + 5.5$

TABLE 3.2

VARIATION OF C WITH y^+

y_s^+	C
1	1.01
4	0.55
9	2.36
16	4.00
25	4.94
36	5.38
64	5.58
81	5.58
100	5.57
121	5.56
144	5.55
196	5.54
256	5.53
324	5.53
361	5.52
400	5.52
484	5.52
576	5.52
676	5.52
900	5.52

TABLE 3.3

RESULTS OF THEORETICAL COMPUTATIONS

$\frac{s}{\varepsilon} = 8.6$

Re	u_{av} ft/sec	s^+	$\frac{y^{++}_{mr}}{s^+}$	z^{++}_{or}	z_{or}	f	$\frac{1}{m}$
15067	18.97	511	0.62	1.1642	0.00188	0.01149	50.94
24284	30.57	773	0.63	1.4476	0.00155	0.01035	62.02
27116	34.14	855	0.64	1.6012	0.00155	0.01022	62.02
33322	41.95	1027	0.65	1.8090	0.00146	0.00986	65.90
47185	59.41	1397	0.65	2.1801	0.00129	0.00925	74.37
65004	81.84	1855	0.66	2.4953	0.00111	0.00867	86.31
75473	95.02	2124	0.67	2.8361	0.00110	0.00855	86.92
82299	103.61	2303	0.67	3.3424	0.00120	0.00867	79.97
88099	98.33	2203	0.67	3.6467	0.00137	0.00901	70.12
94405	118.86	2605	0.67	3.9796	0.00126	0.00869	76.00

TABLE 3.3 (CONTINUED)

$\frac{s}{\varepsilon} = 13.8$

Re	u_{av} ft/sec	s^+	$\frac{y^{++}_{mr}}{s^+}$	z^{++}_{or}	z_{or}	f	$\frac{1}{m}$
9790	7.92	355	0.57	0.7866	0.00294	0.01204	32.67
20272	16.40	665	0.58	1.0286	0.00205	0.01006	46.76
30241	24.46	944	0.58	1.2849	0.00181	0.00935	53.15
48737	39.42	1445	0.60	1.7329	0.00159	0.00865	60.32
63383	51.27	1829	0.61	2.1384	0.00155	0.00840	61.88
85178	68.90	2383	0.61	2.6696	0.00149	0.00811	64.58
102294	82.74	2825	0.62	3.5835	0.00168	0.00825	57.03
111045	89.82	3066	0.65	4.2333	0.00183	0.00836	52.39
129081	104.41	3529	0.66	5.2435	0.00197	0.00843	48.70
137395	111.13	3745	0.66	6.1838	0.00219	0.00864	43.81

TABLE 3.3 (CONTINUED)

$\frac{s}{\varepsilon} = 24.2$

Re	u_{av} ft/sec	s^+	$\frac{y^{++}_{mr}}{s^+}$	z^{++}_{or}	z_{or}	f	$\frac{1}{m}$
13111	6.63	442	0.31	0.2607	0.00132	0.00905	72.77
28686	14.49	889	0.38	0.4714	0.00119	0.00787	80.97
44816	22.67	1332	0.42	0.6830	0.00115	0.00740	83.72
51293	25.95	1524	0.48	0.9905	0.00145	0.00758	66.04
67407	34.10	1952	0.49	1.4368	0.00165	0.00760	58.30
76950	38.93	2207	0.50	1.7939	0.00182	0.00767	52.80
90835	45.96	2600	0.55	2.5765	0.00222	0.00787	43.30
104648	52.95	2963	0.56	3.1818	0.00240	0.00793	39.96
122108	61.78	3416	0.57	3.9553	0.00259	0.00799	37.06
143071	72.39	3965	0.59	5.0970	0.00288	0.00819	33.39

TABLE 3.3 (CONTINUED)

$\frac{s}{\epsilon} = 29.5$

Re	u_{av} ft/sec	s^+	$\frac{y^{++}_{mr}}{s^+}$	z^{++}_{or}	z_{or}	f	$\frac{1}{m}$
13638	5.64	472	0.36	0.0817	0.00049	0.00707	196.07
26318	10.89	851	0.43	0.1818	0.00060	0.00662	159.03
37218	15.40	1168	0.45	0.4292	0.00104	0.00698	92.37
59831	24.76	1798	0.49	0.6892	0.00108	0.00667	88.57
71314	29.51	2112	0.51	0.8505	0.00114	0.00661	84.31
98432	40.73	2822	0.52	1.0576	0.00106	0.00633	90.60
123891	51.26	3484	0.53	1.3368	0.00108	0.00623	88.49
128974	53.37	3644	0.56	1.8827	0.00146	0.00658	65.74
142341	58.90	3995	0.57	2.2517	0.00159	0.00665	60.25
155533	64.35	4355	0.58	2.9219	0.00190	0.00685	50.61

TABLE 4.1

RESULTS FROM PROFILE METHOD

$\frac{s}{\epsilon} = 8.6$ $\quad$ $x = 120$ inch

Re	C	f_r	f_s	f	z_{or} in	$\frac{1}{m}$
12502	27.71	0.03762	0.00123	0.01943	0.02676	3.59
23221	16.79	0.04277	0.00237	0.02257	0.02616	3.67
28645	15.65	0.04984	0.00244	0.02614	0.03012	3.19
35138	13.42	0.04156	0.00258	0.02207	0.02568	3.73
46441	15.51	0.01396	0.00201	0.00799	0.00384	25.27
53333	10.01	0.00573	0.00267	0.00420	0.00024	365.79
64960	25.06	0.00269	0.00145	0.00207	0.000003	31857.90
71160	20.08	0.0149	0.00142	0.00818	0.00490	19.61
79067	21.69	0.0240	0.00147	0.01275	0.01028	9.33
93218	18.99	0.03259	0.00171	0.01715	0.02118	5.46

TABLE 4.2

EFFECT OF A SMALL ERROR IN y MEASUREMENT ON RESULTS FROM PROFILE METHOD

$\frac{s}{\varepsilon}$ = 8.6 x = 120 inch

Re = 46441

RESULTS WITH EXPERIMENTAL Y_s	RESULTS WITH y_s + 0.1 mm	% CHANGE	RESULTS WITH y_s - 0.09 mm	% CHANGE
C = 15.51	13.73	-11.5	17.35	+ 11.8
u_{τ_r} = 5.258 ft/sec	5.168	-1.7	5.340	+ 1.6
τ_{or} = 0.062 lbf/ft^2	0.060	-3.2	0.064	+ 3.2
u_{τ_s} = 1.997 ft/sec	2.116	+6.0	1.885	- 5.6
τ_{os} = 0.009 lbf/ft^2	0.010	+11.1	0.008	- 11.1
f_r = 0.01396	0.01348	-3.4	0.01440	+ 3.2
f_s = 0.00201	0.00226	+12.5	0.00179	- 11.0
f = 0.00799	0.00787	-1.5	0.00810	+ 1.4
z_{or} = 0.00032 ft	0.00029	-9.4	0.00034	+ 6.3
$\frac{l}{m}$ = 25.27	27.64	+9.3	23.36	- 7.6

TABLE 5.1 A1

EXPERIMENTAL RESULTS

$\frac{s}{\varepsilon} = 8.6$ $\frac{p}{\varepsilon} = 2$

Re	$\frac{dp}{dx}$ lbf/ft^2/in	$\frac{y_{or}}{s}$	$\frac{y_{mr}}{s}$	$\tau_{\omega r}$ lbf/ft^2	$\tau_{\omega s}$ lbf/ft^2	u_{τ_r} ft/sec	u_{τ_s} ft/sec
12865	0.01162	0.640	0.622	0.00615	0.00346	1.628	1.221
24410	0.02717	0.647	0.628	0.01454	0.00793	2.502	1.848
29618	0.03343	0.649	0.640	0.01794	0.00970	2.780	2.044
36389	0.04874	0.653	0.647	0.02632	0.01399	3.367	2.454
47620	0.09171	0.659	0.653	0.04998	0.02586	4.639	3.337
56079	0.16282	0.661	0.659	0.08900	0.04565	6.191	4.434
65348	0.21649	0.666	0.665	0.11924	0.05980	7.166	5.074
72778	0.26154	0.675	0.671	0.14600	0.07030	7.929	5.502
81368	0.24463	0.682	0.671	0.13797	0.06433	7.708	5.263
95932	0.34442	0.684	0.671	0.19483	0.09001	7.100	6.226

TABLE 5.1 A1 (CONTINUED)

$\frac{s}{\varepsilon} = 8.6$ $\frac{p}{\varepsilon} = 2$

Re	u_m ft/sec	Rem	f_r	f_s	f	z_{or} in	$\frac{1}{m}$
12865	22.66	17208	0.01846	0.01038	0.01442	.00196	48.96
24410	36.15	27453	0.01212	0.00661	0.00936	.00160	59.84
29618	40.34	30631	0.01016	0.00549	0.00783	.00159	60.19
36389	49.43	37533	0.00987	0.00525	0.00756	.00151	63.73
47620	69.63	52877	0.01095	0.00566	0.00831	.00133	72.00
56079	95.47	72493	0.01406	0.00721	0.01063	.00114	84.08
65348	110.75	84102	0.01387	0.00695	0.01041	.00114	84.52
72778	120.95	91841	0.01369	0.00659	0.01014	.00124	77.24
81368	115.12	87418	0.01035	0.00483	0.00759	.00141	68.01
95932	138.78	105385	0.01051	0.00486	0.00769	.00129	74.16

TABLE 5.1 B1

EXPERIMENTAL RESULTS

$\frac{s}{\varepsilon} = 8.6$ $\frac{p}{\varepsilon} = 4$

Re	$\frac{dp}{dx}$ lbf/ft^2/in	$\frac{y_{or}}{s}$	$\frac{y_{mr}}{s}$	$\tau_{\omega r}$ lbf/ft^2	$\tau_{\omega s}$ lbf/ft^2	u_{τ_r} ft/sec	u_{τ_s} ft/sec
10254	0.01054	0.729	0.716	0.00635	0.00236	1.679	1.024
20509	0.03829	0.738	0.729	0.02337	0.00830	3.221	1.919
30445	0.07380	0.748	0.744	0.04565	0.01538	4.502	2.613
40636	0.12718	0.780	0.758	0.08204	0.02314	6.035	3.205
46700	0.19843	0.790	0.779	0.12964	0.03446	7.586	3.911
51158	0.21027	0.799	0.786	0.13894	0.03495	7.853	3.939
55818	0.27386	0.804	0.793	0.18209	0.04439	8.990	4.439
60890	0.29614	0.814	0.800	0.19935	0.04555	9.407	4.497
66044	0.38758	0.817	0.808	0.26187	0.05866	10.781	5.103
71699	0.42425	0.822	0.815	0.28840	0.06245	11.314	5.265

TABLE 5.1 B1 (CONTINUED)

$\frac{s}{\varepsilon} = 8.6$ $\frac{p}{\varepsilon} = 4$

Re	u_m ft/sec	Rem	f_r	f_s	f	z_{or} in	$\frac{1}{m}$
10254	17.75	13075	0.02911	0.01082	0.01996	0.00864	11.12
20509	36.06	26563	0.02677	0.00950	0.01814	0.00685	14.02
30445	50.74	37377	0.02373	0.00800	0.01586	0.00678	14.16
40636	63.42	46719	0.02394	0.00675	0.01534	0.00937	10.25
46700	78.80	58051	0.02864	0.00761	0.01813	0.01000	9.60
51158	78176	58022	0.02558	0.00643	0.01601	0.01177	8.16
55818	89.72	66094	0.02816	0.00686	0.01751	0.01211	7.93
60890	90.64	66776	0.02591	0.00592	0.01591	0.01402	6.85
66044	103.95	76579	0.02893	0.00648	0.01770	0.01412	6.79
71699	107.18	78961	0.02703	0.00585	0.01644	0.01524	6.29

TABLE 5.1 C1

EXPERIMENTAL RESULTS

$\frac{s}{\varepsilon} = 8.6$ $\frac{p}{\varepsilon} = 8$

Re	$\frac{dp}{dx}$ lbf/ft^2/in	$\frac{y_{or}}{s}$	$\frac{y_{mr}}{s}$	$\tau_{\omega r}$ lbf/ft^2	$\tau_{\omega s}$ lbf/ft^2	u_{τ_r} ft/sec	u_{τ_s} ft/sec
9920	0.01553	0.842	0.821	0.01081	0.00203	2.163	0.937
18112	0.04403	0.843	0.827	0.03084	0.00557	3.653	1.552
25615	0.08567	0.855	0.833	0.06057	0.01027	5.119	2.108
32018	0.13515	0.859	0.839	0.09601	0.01576	6.445	2.611
38422	0.18703	0.863	0.843	0.13348	0.02119	7.599	3.028
43432	0.24847	0.867	0.846	0.17815	0.02733	8.779	3.438
47921	0.30867	0.870	0.851	0.22209	0.03319	9.801	3.789
52024	0.33652	0.874	0.855	0.24324	0.03507	10.258	3.895
55826	0.46649	0.879	0.861	0.33910	0.04668	12.111	4.494
58690	0.49434	0.885	0.867	0.36180	0.04701	12.510	4.510

TABLE 5.1 C1 (CONTINUED)

$\frac{s}{\varepsilon} = 8.6$ $\frac{p}{\varepsilon} = 8$

Re	u_m ft/sec	Rem	f_r	f_s	f	z_{or} in	$\frac{1}{m}$
9920	15.01	11349	0.05432	0.01019	0.03226	0.04227	2.27
18112	26.70	20185	0.04648	0.00840	0.02744	0.03673	2.61
25615	37.69	28489	0.04564	0.00774	0.02669	0.03624	2.64
32018	47.84	36162	0.04630	0.00760	0.02695	0.03563	2.69
38422	56.40	42635	0.04470	0.00710	0.02590	0.03581	2.68
43432	64.98	49119	0.04669	0.00716	0.02693	0.03623	2.65
47921	72.21	54585	0.04781	0.00714	0.02748	0.03695	2.60
52024	74.23	56113	0.04443	0.00641	0.02542	0.03911	2.44
55826	86.78	65598	0.05379	0.00741	0.03060	0.04054	2.37
58690	86.63	65487	0.05193	0.00675	0.02934	0.04493	2.14

TABLE 5.1 D1

EXPERIMENTAL RESULTS

$\frac{s}{\varepsilon} = 8.6$ $\frac{p}{\varepsilon} = 16$

Re	$\frac{dp}{dx}$ lbf/ft^2/in	$\frac{y_{or}}{s}$	$\frac{y_{mr}}{s}$	$\tau_{\omega r}$ lbf/ft^2	$\tau_{\omega s}$ lbf/ft^2	u_{τ_r} ft/sec	u_{τ_s} ft/sec
11052	0.01579	0.804	0.741	0.01050	0.00256	2.135	1.054
18047	0.03703	0.808	0.750	0.02475	0.00588	3.278	1.598
25523	0.07304	0.813	0.753	0.04911	0.01130	4.617	2.214
31904	0.11126	0.816	0.759	0.07508	0.01693	5.709	2.711
38284	0.15836	0.817	0.764	0.10700	0.02397	6.816	3.226
43276	0.20614	0.821	0.767	0.13997	0.03052	7.795	3.640
47749	0.25529	0.825	0.771	0.17418	0.03695	8.696	4.005
51626	0.29318	0.831	0.775	0.20148	0.04098	9.352	4.218
55626	0.33789	0.836	0.779	0.23360	0.04583	10.070	4.460
59856	0.40922	0.839	0.786	0.28394	0.05449	11.102	4.864

TABLE 5.1 D1 (CONTINUED)

$\frac{s}{\epsilon} = 8.6$ $\frac{p}{\epsilon} = 16$

Re	u_m ft/sec	Rem	f_r	f_s	f	z_{or} in	$\frac{1}{m}$
11052	18.16	13680	0.04233	0.01032	0.02632	0.02038	4.71
18047	29.05	21884	0.03742	0.00889	0.02316	0.01789	5.37
25523	42.01	31642	0.03714	0.00854	0.02284	0.01636	5.87
31904	52.64	39647	0.03634	0.00819	0.02227	0.01571	6.11
38284	63.86	48099	0.03596	0.00806	0.02201	0.01489	6.45
43276	73.04	55015	0.03681	0.00803	0.02242	0.01495	6.42
47749	81.15	61125	0.03763	0.00798	0.02281	0.01525	6.29
51837	85.82	64642	0.03694	0.00751	0.02222	0.01632	5.88
55626	91.18	68681	0.03719	0.00730	0.02224	0.01722	5.57
59856	100.09	75387	0.03904	0.00749	0.02327	0.01766	5.44

TABLE 5.1 A2

EXPERIMENTAL RESULTS

$\frac{s}{\varepsilon} = 13.8$ $\frac{p}{\varepsilon} = 2$

Re	$\frac{dp}{dx}$ lbf/ft^2/in	$\frac{y_{or}}{s}$	$\frac{y_{mr}}{s}$	$\tau_{\omega r}$ lbf/ft^2	$\tau_{\omega s}$ lbf/ft^2	u_{τ_r} ft/sec	u_{τ_s} ft/sec
10901	0.00133	0.629	0.571	0.00111	0.00066	0.689	0.529
22865	0.00478	0.638	0.576	0.00405	0.00230	1.314	0.990
33891	0.00988	0.647	0.580	0.00848	0.00463	1.903	1.405
54576	0.02375	0.656	0.598	0.02068	0.01084	2.971	2.152
67549	0.03898	0.664	0.607	0.03434	0.01738	3.829	2.724
91114	0.06799	0.673	0.611	0.06072	0.02950	5.092	3.549
113702	0.09980	0.687	0.625	0.09098	0.04145	6.233	4.207
125870	0.11906	0.691	0.647	0.10917	0.04882	6.828	4.566
138799	0.16198	0.699	0.660	0.15025	0.06470	8.009	5.256
156099	0.18800	0.701	0.664	0.17663	0.07285	8.684	5.577

TABLE 5.1 A2 (CONTINUED)

$\frac{s}{\varepsilon} = 13.8$ $\frac{p}{\varepsilon} = 2$

Re	u_m ft/sec	Rem	f_r	f_s	f	z_{or} in	$\frac{1}{m}$
10901	9.52	11347	0.01135	0.00669	0.00902	0.00301	31.88
22865	19.34	23051	0.00939	0.00533	0.00736	0.00213	45.17
33891	28.66	34162	0.00896	0.00489	0.00693	0.00186	51.49
54576	45.92	54739	0.00843	0.00442	0.00642	0.00164	58.51
67549	59.58	71023	0.00913	0.00462	0.00688	0.00161	60.14
91114	79.89	95233	0.00888	0.00431	0.00659	0.00153	62.95
113702	96.10	114555	0.00854	0.00389	0.00622	0.00174	55.20
125870	104.53	124614	0.00836	0.00374	0.00605	0.00188	51.08
138799	121.70	145073	0.00946	0.00408	0.00677	0.00201	47.79
156099	129.79	154728	0.00880	0.00363	0.00621	0.00231	43.01

TABLE 5.1 B2

EXPERIMENTAL RESULTS

$\frac{s}{\varepsilon} = 13.8$ $\frac{p}{\varepsilon} = 4$

Re	$\frac{dp}{dx}$ lbf/ft^2/in	$\frac{y_{or}}{s}$	$\frac{y_{mr}}{s}$	$\tau_{\omega r}$ lbf/ft^2	$\tau_{\omega s}$ lbf/ft^2	u_{τ_r} ft/sec	u_{τ_s} ft/sec
12540	0.00205	0.684	0.589	0.00186	0.00086	0.831	0.565
26303	0.00922	0.698	0.620	0.00854	0.00369	1.178	1.171
39654	0.01749	0.702	0.631	0.01629	0.00692	2.459	1.602
50158	0.03003	0.711	0.668	0.02834	0.01152	3.243	2.068
61431	0.04454	0.726	0.673	0.04291	0.01619	3.991	2.452
73831	0.06758	0.735	0.683	0.06591	0.02376	4.946	2.970
102385	0.13311	0.744	0.694	0.13141	0.04522	6.984	4.097
115835	0.15631	0.753	0.705	0.15619	0.05124	7.614	4.361
127879	0.19522	0.762	0.715	0.19740	0.06166	8.560	4.784
138277	0.24027	0.771	0.726	0.24583	0.07302	9.552	5.206

TABLE 5.1 B2 (CONTINUED)

$\frac{s}{\varepsilon} = 13.8$ $\frac{p}{\varepsilon} = 4$

Re	u_m ft/sec	Rem	f_r	f_s	f	z_{or} in	$\frac{l}{m}$
12540	10.39	14246	0.01650	0.00762	0.01206	0.00525	18.28
26303	23.45	32155	0.01722	0.00745	0.01234	0.00423	22.68
39654	33.23	45569	0.01447	0.00614	0.01030	0.00376	25.51
50158	43.65	59862	0.01572	0.00639	0.01106	0.00407	23.60
61431	52.71	72286	0.01587	0.00599	0.01093	0.00453	21.18
73831	65.05	89200	0.01688	0.00609	0.01148	0.00471	20.40
102385	92.66	127067	0.0750	0.00602	0.01176	0.00456	21.03
115835	98.91	135644	0.01625	0.00533	0.01079	0.00518	18.53
127879	109.20	149754	0.01685	0.00526	0.01106	0.00577	16.65
138277	119.43	163772	0.01795	0.00533	0.01164	0.00648	14.80

TABLE 5.1 C2

EXPERIMENTAL RESULTS

$\frac{s}{\varepsilon} = 13.8$ $\frac{p}{\varepsilon} = 8$

Re	$\frac{dp}{dx}$ lbf/ft^2/in	$\frac{y_{or}}{s}$	$\frac{y_{mr}}{s}$	$\tau_{\omega r}$ lbf/ft^2	$\tau_{\omega s}$ lbf/ft^2	u_{τ_r} ft/sec	u_{τ_s} ft/sec
10778	0.00375	0.885	0.864	0.00441	0.00057	1.380	0.497
22608	0.01502	0.894	0.872	0.01782	0.00211	2.774	0.955
34083	0.03072	0.899	0.879	0.03664	0.00412	3.978	1.333
43112	0.05256	0.904	0.885	0.06305	0.00670	5.218	1.700
52801	0.07440	0.909	0.888	0.08975	0.00898	6.225	1.970
63459	0.11468	0.913	0.898	0.13894	0.01324	7.746	2.391
78711	0.17065	0.917	0.904	0.20766	0.01880	9.470	2.849
93133	0.24573	0.921	0.911	0.30033	0.02576	11.388	3.335
102627	0.28669	0.923	0.918	0.35114	0.02929	12.314	3.557
113519	0.34283	0.925	0.924	0.42082	0.03412	13.480	3.839

TABLE 5.1 C2 (CONTINUED)

$\frac{s}{\varepsilon} = 13.8$ $\frac{p}{\varepsilon} = 8$

Re	$\dot{u}_m$ ft/sec	Rem	f_r	f_s	f	z_{or} in	$\frac{l}{m}$
10778	7.43	8759	0.04554	0.00592	0.02573	0.13298	0.72
22608	15.68	18485	0.04182	0.00496	0.02339	0.12055	0.80
34083	22.82	26896	0.03785	0.00425	0.02105	0.11759	0.82
43112	29.92	35264	0.04070	0.00432	0.02251	0.11852	0.81
52801	35.25	41549	0.03863	0.00387	0.02125	0.12236	0.78
63459	43.39	51143	0.04140	0.00395	0.02267	0.12677	0.76
78711	52.52	61899	0.04022	0.00364	0.02193	0.13051	0.74
93133	62.16	73272	0.04155	0.00356	0.02256	0.13618	0.71
102627	66.13	77949	0.0400	0.00334	0.02167	0.14215	0.68
113519	71.38	84130	0.03918	0.00318	0.02118	0.14748	0.65

TABLE 5.1 D2

EXPERIMENTAL RESULTS

$\frac{s}{\varepsilon} = 13.8$ $\frac{p}{\varepsilon} = 16$

Re	$\frac{dp}{dx}$ lbf/ft^2/in	$\frac{y_{or}}{s}$	$\frac{y_{mr}}{s}$	$\tau_{\omega r}$ lbf/ft^2	$\tau_{\omega s}$ lbf/ft^2	u_{τ_r} ft/sec	u_{τ_s} ft/sec
10721	0.00277	0.873	0.778	0.00321	0.00047	1.181	0.450
22489	0.01348	0.878	0.781	0.01571	0.00218	2.611	0.973
33904	0.02722	0.880	0.782	0.03179	0.00433	3.715	1.372
42885	0.04693	0.883	0.784	0.05499	0.00729	4.886	1.779
52523	0.06775	0.885	0.787	0.07956	0.01034	5.877	2.119
63125	0.09625	0.887	0.791	0.11329	0.01443	7.013	2.503
78297	0.14471	0.890	0.794	0.17091	0.02112	8.614	3.028
92643	0.20887	0.892	0.796	0.24724	0.02994	10.360	3.605
102087	0.25529	0.894	0.798	0.30286	0.03591	11.466	3.948
116792	0.31126	0.898	0.800	0.37092	0.04213	12.689	4.277

TABLE 5.1 D2 (CONTINUED)

$\frac{s}{\varepsilon} = 13.8$ $\frac{p}{\varepsilon} = 16$

Re	u_m ft/sec	Rem	f_r	f_s	f	z_{or} in	$\frac{l}{m}$
10721	7.16	8399	0.03336	0.00485	0.01911	0.09121	1.05
22489	17.32	20311	0.03707	0.00515	0.02111	0.07296	1.32
33904	25.57	29984	0.03300	0.00450	0.01875	0.06609	1.45
42885	34.27	40181	0.03569	0.00473	0.02021	0.06290	1.53
52523	41.68	48864	0.03442	0.00447	0.01945	0.06123	1.57
63125	50.17	58817	0.03393	0.00432	0.01913	0.06003	1.60
78297	62.02	72720	0.03327	0.00411	0.01869	0.05913	1.62
92643	75.32	88307	0.03438	0.00416	0.01927	0.05766	1.66
102087	83.29	97658	0.03469	0.00411	0.01940	0.05794	1.66
116792	90.97	106657	0.03246	0.00369	0.01807	0.06034	1.59

TABLE 5.1 A3

EXPERIMENTAL RESULTS

$\frac{s}{\varepsilon} = 24.2$ $\frac{p}{\varepsilon} = 2$

Re	$\frac{dp}{dx}$ lbf/ft^2/in	$\frac{y_{or}}{s}$	$\frac{y_{mr}}{s}$	$\tau_{\omega r}$ lbf/ft^2	$\tau_{\omega s}$ lbf/ft^2	u_{τ_r} ft/sec	u_{τ_s} ft/sec
11211	0.00038	0.593	0.294	0.00052	0.00036	0.471	0.391
21468	0.00155	0.602	0.367	0.00218	0.00144	0.966	0.786
32148	0.00357	0.611	0.403	0.00507	0.00323	1.475	1.177
51241	0.00478	0.620	0.457	0.00689	0.00423	1.720	1.346
64079	0.00823	0.638	0.466	0.01221	0.00693	2.289	1.724
86843	0.01079	0.647	0.480	0.01624	0.00886	2.640	1.950
107536	0.01536	0.656	0.530	0.02345	0.01230	3.172	2.297
119120	0.02048	0.665	0.539	0.03169	0.01596	3.687	2.617
133076	0.02797	0.674	0.548	0.04387	0.02122	4.338	3.017
147983	0.03877	0.683	0.566	0.06162	0.02860	5.142	3.503

TABLE 5.1 A3 (CONTINUED)

$\frac{s}{\epsilon} = 24.2$ $\frac{p}{\epsilon} = 2$

Re	u_m ft/sec	Rem	f_r	f_s	f	z_{or} in	$\frac{l}{m}$
11211	7.76	15236	0.01363	0.00935	0.01149	0.00094	101.71
21468	16.77	32915	0.01560	0.01032	0.01296	0.00082	116.47
32148	26.14	51311	0.01622	0.01033	0.01327	0.00078	122.76
51241	30.04	58962	0.00868	0.00532	0.00700	0.00098	97.71
64079	39.46	77456	0.00983	0.00558	0.00771	0.00110	87.52
86843	45.09	88505	0.00712	0.00388	0.00550	0.00120	79.81
107536	53.48	104969	0.00670	0.00351	0.00511	0.00145	66.15
119120	61.67	121040	0.00738	0.00372	0.00555	0.00158	61.56
133076	72.02	141359	0.00819	0.00396	0.00608	0.00167	57.62
147983	84.57	165987	0.00930	0.00432	0.00681	0.00183	52.46

TABLE 5.1 B3

EXPERIMENTAL RESULTS

$\frac{s}{\varepsilon} = 24.2$ $\frac{p}{\varepsilon} = 4$

Re	$\frac{dp}{dx}$ lbf/ft^2/in	$\frac{y_{or}}{s}$	$\frac{y_{mr}}{s}$	$\tau_{\omega r}$ lbf/ft^2	$\tau_{\omega s}$ lbf/ft^2	u_{τ_r} ft/sec	u_{τ_s} ft/sec
10194	0.00051	0.700	0.552	0.00083	0.00036	0.609	0.399
21323	0.00179	0.709	0.617	0.00296	0.00121	1.147	0.735
31213	0.00341	0.714	0.663	0.00567	0.00227	1.588	1.005
49022	0.00802	0.719	0.695	0.01342	0.00524	2.443	1.528
62426	0.01229	0.724	0.700	0.02070	0.00789	3.035	1.874
82183	0.02543	0.728	0.716	0.04307	0.01609	4.378	2.676
101941	0.03328	0.733	0.720	0.05676	0.02068	5.025	3.033
111671	0.03771	0.738	0.729	0.06477	0.02299	5.368	3.198
128947	0.05495	0.743	0.733	0.09501	0.03286	6.501	3.824
142353	0.06826	0.747	0.741	0.11865	0.04019	7.266	4.228

TABLE 5.1 B3 (CONTINUED)

$\frac{s}{\varepsilon} = 24.2$ $\frac{p}{\varepsilon} = 4$

Re	u_m ft/sec	Rem	f_r	f_s	f	z_{or} in	$\frac{l}{m}$
10194	7.46	14113	0.02558	0.01096	0.01827	0.00960	10.00
21323	14.57	27584	0.02073	0.00851	0.01462	0.00891	10.78
31213	21.41	38624	0.01856	0.00743	0.01299	0.00905	10.61
49022	32.22	60992	0.01780	0.00696	0.01238	0.00828	11.60
62426	40.40	76480	0.01693	0.00646	0.01170	0.00792	12.11
82188	59.72	113039	0.02033	0.00760	0.01396	0.00711	13.50
101941	68.53	129715	0.01741	0.00634	0.01188	0.00716	13.40
111671	72.43	137104	0.01656	0.00589	0.01122	0.00768	12.50
128947	88.16	166869	0.01822	0.00630	0.01226	0.00752	12.76
142353	98.23	185936	0.01867	0.00632	0.01250	0.00773	12.43

TABLE 5.1 C3

EXPERIMENTAL RESULTS

$\frac{s}{\varepsilon} = 24.2$ $\frac{p}{\varepsilon} = 8$

Re	$\frac{dp}{dx}$ lbf/ft^2/in	$\frac{y_{or}}{s}$	$\frac{y_{mr}}{s}$	$\tau_{\omega r}$ lbf/ft^2	$\tau_{\omega s}$ lbf/ft^2	u_{τ_r} ft/sec	u_{τ_s} ft/sec
10419	0.00064	0.904	0.884	0.00135	0.00014	0.762	0.248
21793	0.00213	0.908	0.895	0.00451	0.00046	1.395	0.444
31902	0.00486	0.990	0.898	0.01030	0.00102	2.109	0.663
50104	0.01195	0.911	0.901	0.02532	0.00247	3.307	1.034
63803	0.01894	0.911	0.904	0.04016	0.00392	4.164	1.302
84001	0.03311	0.912	0.907	0.07026	0.00578	5.508	1.711
104191	0.05085	0.913	0.913	0.10804	0.01030	6.830	2.109
114135	0.06075	0.914	0.916	0.12921	0.01216	7.470	2.291
131792	0.07918	0.915	0.919	0.16859	0.01566	8.533	2.601
145494	0.09829	0.916	0.922	0.20952	0.01921	9.512	2.880

TABLE 5.1 C3 (CONTINUED)

$\frac{s}{\epsilon} = 24.2$ $\frac{p}{\epsilon} = 8$

Re	u_m ft/sec	Rem	f_r	f_s	f	z_{or} in	$\frac{l}{m}$
10419	3.53	6895	0.04083	0.00434	0.02258	0.32263	0.30
21793	6.85	13365	0.03125	0.00317	0.01721	0.29258	0.33
31902	10.84	21165	0.03332	0.00330	0.01831	0.26737	0.36
50104	17.96	35074	0.03321	0.00325	0.01823	0.23870	0.40
63803	23.27	45436	0.03248	0.00317	0.01783	0.22500	0.43
84001	31.63	61748	0.03278	0.00316	0.01797	0.21324	0.45
104191	39.72	77557	0.03277	0.00312	0.01796	0.20750	0.46
114191	43.44	84818	0.03266	0.00307	0.01787	0.20817	0.46
131792	49.89	97414	0.03196	0.00297	0.01746	0.20622	0.47
145494	55.72	108802	0.03259	0.00299	0.01779	0.20597	0.47

TABLE 5.1 D3

EXPERIMENTAL RESULTS

$\frac{s}{\epsilon} = 24.2$ $\frac{p}{\epsilon} = 16$

Re	$\frac{dp}{dx}$ lbf/ft^2/in	$\frac{y_{or}}{s}$	$\frac{y_{mr}}{s}$	$\tau_{\omega r}$ lbf/ft^2	$\tau_{\omega s}$ lbf/ft^2	u_{τ_r} ft/sec	u_{τ_s} ft/sec
10390	0.00053	0.857	0.760	0.00106	0.00018	0.676	0.276
21732	0.00427	0.860	0.761	0.00420	0.00068	1.349	0.544
31813	0.00427	0.863	0.766	0.00857	0.00136	1.926	0.767
49964	0.01126	0.866	0.768	0.02270	0.00351	3.135	1.233
63626	0.01719	0.872	0.774	0.03489	0.00512	3.887	1.489
83767	0.03072	0.874	0.784	0.06247	0.00901	5.201	1.975
103900	0.03891	0.879	0.793	0.07958	0.01096	5.871	2.178
113817	0.05495	0.883	0.800	0.11291	0.01496	6.992	2.545
131425	0.07372	0.886	0.807	0.15199	0.01956	8.113	2.910
145089	0.09010	0.889	0.811	0.18640	0.02327	8.984	3.175

TABLE 5.1 D3 (CONTINUED)

$\frac{s}{\varepsilon} = 24.2$ $\frac{p}{\varepsilon} = 16$

Re	u_m ft/sec	Rem	f_r	f_s	f	z_{or} in	$\frac{l}{m}$
10390	4.50	8755	0.03209	0.00535	0.01872	0.12357	0.78
21732	9.78	19042	0.02920	0.00475	0.01698	0.09739	0.99
31813	14.41	28064	0.02779	0.00441	0.01610	0.08938	1.07
49964	24.59	47886	0.02985	0.00462	0.01724	0.07751	1.24
63626	30.30	59002	0.02830	0.00415	0.01622	0.07965	1.21
83767	41.36	80524	0.02923	0.00421	0.01672	0.07583	1.27
103900	45.91	89397	0.02421	0.00333	0.01377	0.08080	1.18
113817	54.43	105973	0.02862	0.00379	0.01620	0.08274	1.16
131425	62.94	122555	0.02889	0.00372	0.01631	0.08431	1.14
145089	69.19	134716	0.02907	0.00363	0.01635	0.08690	1.11

TABLE 5.1 A4

EXPERIMENTAL RESULTS

$\frac{s}{\epsilon} = 29.5$ $\frac{p}{\epsilon} = 2$

Re	$\frac{dp}{dx}$ lbf/ft^2/in	$\frac{y_{or}}{s}$	$\frac{y_{mr}}{s}$	$\tau_{\omega r}$ lbf/ft^2	$\tau_{\omega s}$ lbf/ft^2	u_{τ_r} ft/sec	u_{τ_s} ft/sec
10493	0.00019	0.517	0.418	0.00027	0.00025	0.341	0.330
20922	0.00065	0.549	0.428	0.00101	0.00083	0.656	0.595
31393	0.00137	0.578	0.443	0.00231	0.00163	0.977	0.835
50003	0.00338	0.608	0.472	0.00581	0.00374	1.577	1.266
63292	0.00476	0.624	0.502	0.00840	0.00506	1.896	1.472
84476	0.00869	0.630	0.517	0.01547	0.00909	2.574	1.972
105556	0.01353	0.638	0.533	0.02441	0.01385	3.233	2.435
116317	0.01550	0.654	0.557	0.02865	0.01516	3.502	2.548
129484	0.01906	0.662	0.565	0.03567	0.01821	3.908	2.793
144033	0.02348	0.674	0.582	0.04474	0.02164	4.377	3.044

TABLE 5.1 A4 (CONTINUED)

$\frac{s}{\varepsilon} = 29.5$ $\frac{p}{\varepsilon} = 2$

Re	u_m ft/sec	Rem	f_r	f_s	f	z_{or} in	$\frac{l}{m}$
10493	6.42	14912	0.01142	0.01067	0.01104	0.00064	150.40
20922	12.43	28885	0.01063	0.00873	0.00968	0.00062	154.51
31393	18.10	42057	0.01047	0.00764	0.00905	0.00076	126.35
50003	28.59	66437	0.01074	0.00693	0.00883	0.00095	101.53
63292	33.58	78026	0.00970	0.00584	0.00777	0.00119	80.57
84476	46.28	107547	0.01002	0.00589	0.00796	0.00110	87.37
105556	58.22	135284	0.01013	0.00575	0.00794	0.00112	85.64
116317	60.86	141413	0.00979	0.00518	0.07049	0.00151	63.61
129484	67.23	156217	0.00984	0.00502	0.00743	0.00164	58.48
144033	73.63	171098	0.00997	0.00482	0.00740	0.00197	48.80

TABLE 5.1 B4

EXPERIMENTAL RESULTS

$\frac{s}{\epsilon} = 29.5$ $\frac{p}{\epsilon} = 4$

Re	$\frac{dp}{dx}$ lbf/ft^2/in	$\frac{y_{or}}{s}$	$\frac{y_{mr}}{s}$	$\tau_{\omega r}$ lbf/ft^2	$\tau_{\omega s}$ lbf/ft^2	u_{τ_r} ft/sec	u_{τ_s} ft/sec
9929	0.00025	0.739	0.602	0.00052	0.00018	0.480	0.285
20768	0.00077	0.750	0.649	0.00163	0.00054	0.852	0.492
30401	0.00179	0.760	0.744	0.00385	0.00122	1.310	0.736
47747	0.00444	0.770	0.754	0.00966	0.00288	2.075	1.134
60803	0.00725	0.790	0.763	0.01622	0.00429	2.688	1.382
80051	0.01195	0.801	0.773	0.02705	0.00672	3.472	1.731
99291	0.01775	0.811	0.782	0.04069	0.00948	4.258	2.056
108768	0.02440	0.821	0.792	0.05664	0.01235	5.024	2.346
125594	0.02935	0.832	0.801	0.06904	0.01394	5.547	2.493
138652	0.03413	0.842	0.811	0.08124	0.01525	6.017	2.607

TABLE 5.1 B4 (CONTINUED)

$\frac{s}{\epsilon} = 29.5$ $\frac{p}{\epsilon} = 4$

Re	u_m ft/sec	Rem	f_r	f_s	f	z_{or} in	$\frac{l}{m}$
9929	5.15	11487	0.02327	0.00822	0.01574	0.02332	4.12
20768	9.39	20954	0.01674	0.00558	0.01117	0.02231	4.30
30401	14.22	31721	0.01848	0.00584	0.01216	0.02738	3.50
47747	23.01	51346	0.01880	0.00562	0.01221	0.02523	3.81
60803	28.60	63816	0.01947	0.00514	0.01231	0.03061	3.14
80051	36.60	81672	0.01873	0.00465	0.01169	0.03222	2.98
99291	44.16	98527	0.01832	0.00427	0.01129	0.03493	2.75
108768	50.89	113549	0.02125	0.00463	0.01294	0.03895	2.46
125594	54.17	120872	0.01942	0.00392	0.01167	0.04554	2.11
138652	56.60	126302	0.01875	0.00352	0.01114	0.05323	1.80

TABLE 5.1 C4

EXPERIMENTAL RESULTS

$\frac{s}{\varepsilon} = 29.5$ $\qquad\qquad$ $\frac{p}{\varepsilon} = 8$

Re	$\frac{dp}{dx}$ lbf/ft^2/in	$\frac{y_{or}}{s}$	$\frac{y_{mr}}{s}$	$\tau_{\omega r}$ lbf/ft^2	$\tau_{\omega s}$ lbf/ft^2	u_{τ_r} ft/sec	u_{τ_s} ft/sec
9980	0.00037	0.900	0.897	0.00093	0.00010	0.652	0.214
20874	0.00123	0.902	0.902	0.00313	0.00034	1.177	0.388
30556	0.00256	0.904	0.904	0.00654	0.00069	1.700	0.554
47990	0.00606	0.906	0.907	0.01553	0.00159	2.620	0.839
61112	0.00981	0.909	0.910	0.02522	0.00252	3.338	1.056
80457	0.01749	0.911	0.911	0.04505	0.00440	4.462	1.395
99795	0.02602	0.913	0.915	0.06717	0.00640	5.449	1.682
112905	0.03447	0.915	0.919	0.08917	0.00828	6.278	1.913
126232	0.04062	0.918	0.920	0.10540	0.00942	6.825	2.040
139356	0.05120	0.921	0.923	0.13329	0.01143	7.676	2.248

TABLE 5.1 C4 (CONTINUED)

$\frac{s}{\varepsilon} = 29.5$ $\frac{p}{\varepsilon} = 8$

Re	u_m ft/sec	Rem	f_r	f_s	f	z_{or} in	$\frac{l}{m}$
9980	2.99	6734	0.04199	0.00467	0.02333	0.39363	0.24
20874	5.95	13388	0.03221	0.00350	0.01786	0.33774	0.28
30556	8.96	20174	0.03139	0.00333	0.01736	0.31042	0.31
47990	14.37	32356	0.03022	0.00310	0.01666	0.28578	0.34
61112	18.62	41907	0.03025	0.00303	0.01664	0.27648	0.35
80457	25.47	57339	0.03117	0.00305	0.01711	0.26284	0.37
99795	31.36	70593	0.03021	0.00288	0.01655	0.25879	0.37
112905	36.06	81176	0.03134	0.00291	0.01712	0.26109	0.37
126232	38.71	87137	0.02963	0.00265	0.01614	0.26911	0.36
139356	42.99	96770	0.03075	0.00264	0.01669	0.27773	0.35

TABLE 5.1 D4

EXPERIMENTAL RESULTS

$\frac{s}{\varepsilon} = 29.5$ $\frac{p}{\varepsilon} = 16$

Re	$\frac{dp}{dx}$ lbf/ft^2/in	$\frac{y_{or}}{s}$	$\frac{y_{mr}}{s}$	$\tau_{\omega r}$ lbf/ft^2	$\tau_{\omega s}$ lbf/ft^2	u_{τ_r} ft/sec	u_{τ_s} ft/sec
10311	0.00022	0.900	0.877	0.00056	0.00006	0.491	0.164
21567	0.00115	0.903	0.880	0.00294	0.00059	1.122	0.368
31570	0.00227	0.906	0.882	0.00581	0.00060	1.577	0.508
49583	0.00546	0.908	0.885	0.01402	0.00142	2.449	0.779
63140	0.00904	0.911	0.888	0.02329	0.00228	3.157	0.987
83128	0.01625	0.913	0.892	0.04195	0.00400	4.236	1.308
103108	0.02346	0.918	0.894	0.06089	0.00544	5.104	1.525
116653	0.03055	0.922	0.896	0.07962	0.00674	5.836	1.698
130422	0.03635	0.925	0.900	0.09505	0.00771	6.377	1.816
144902	0.04437	0.926	0.903	0.11615	0.00928	7.049	1.993

TABLE 5.1 D4 (CONTINUED)

$\frac{s}{\epsilon} = 29.5$ $\frac{p}{\epsilon} = 16$

Re	u_m ft/sec	Rem	f_r	f_s	f	z_{or} in	$\frac{l}{m}$
10311	2.26	5267	0.02457	0.00273	0.01365	0.39234	0.24
21567	5.80	13497	0.02926	0.00314	0.01620	0.31406	0.31
31570	8.41	19556	0.02700	0.00280	0.01490	0.29552	0.32
49583	13.69	31833	0.02639	0.00267	0.01453	0.26751	0.35
63140	17.84	41495	0.02704	0.00264	0.01484	0.26178	0.37
83128	24.44	56865	0.02810	0.00268	0.01539	0.25069	0.38
103108	29.03	67530	0.02651	0.00237	0.01444	0.25969	0.37
116653	32.68	76014	0.02708	0.00229	0.01469	0.26966	0.36
130422	35.09	81606	0.02586	0.00210	0.01398	0.28166	0.34
144902	38.82	90283	0.02560	0.00205	0.01383	0.28209	0.34

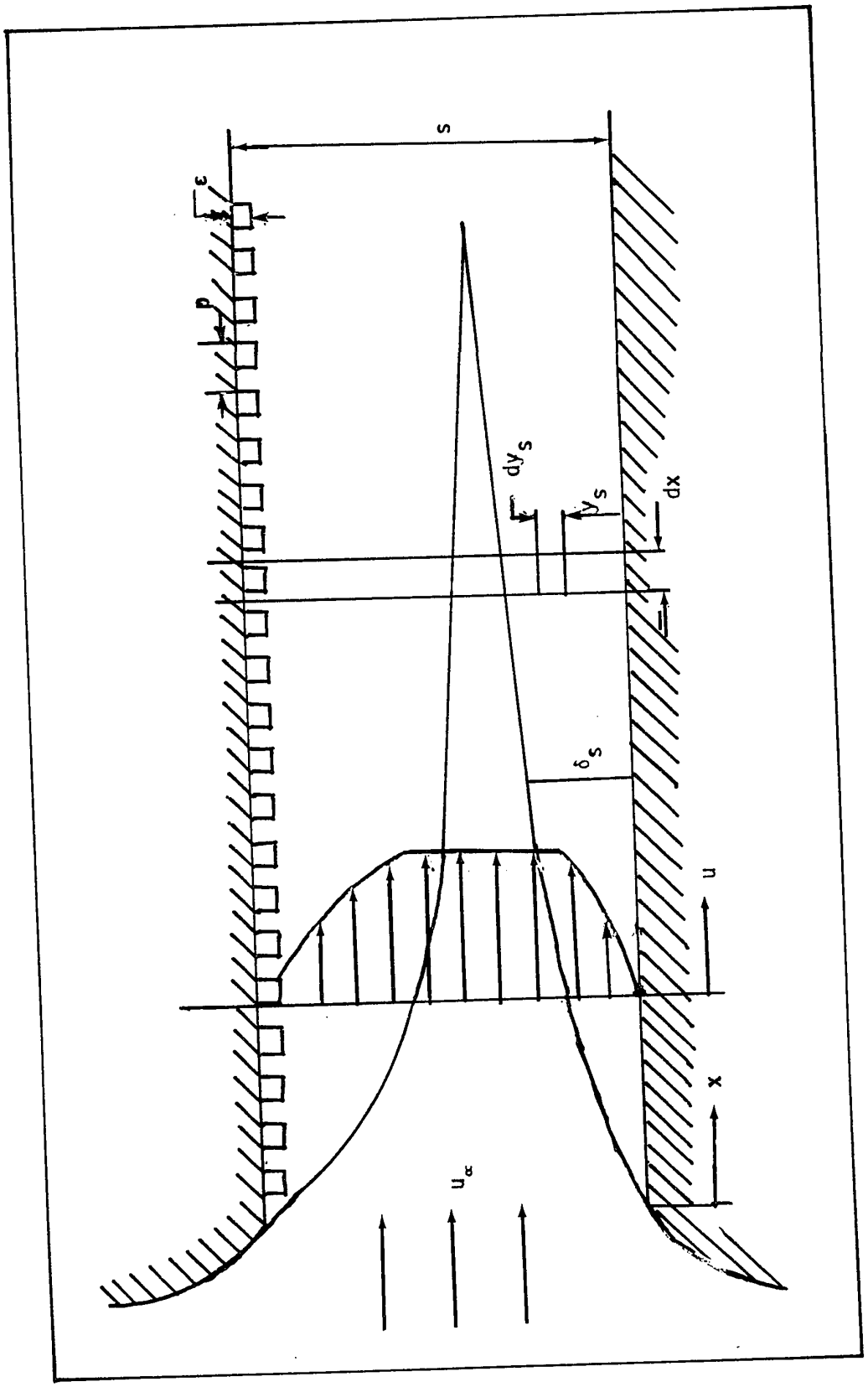

Figure 3.1 Idealized Model

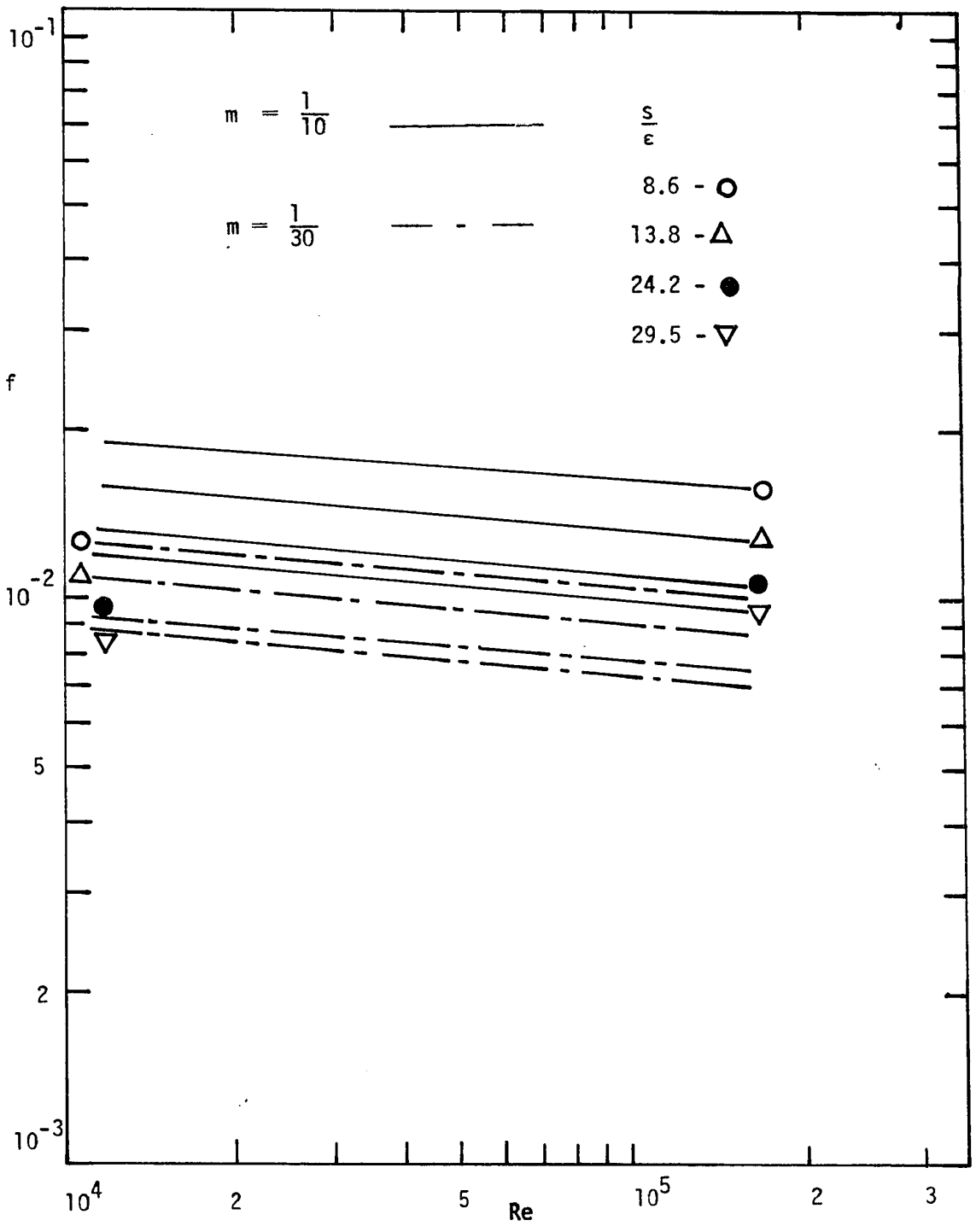

Figure 3.2 Predicted f using constant m

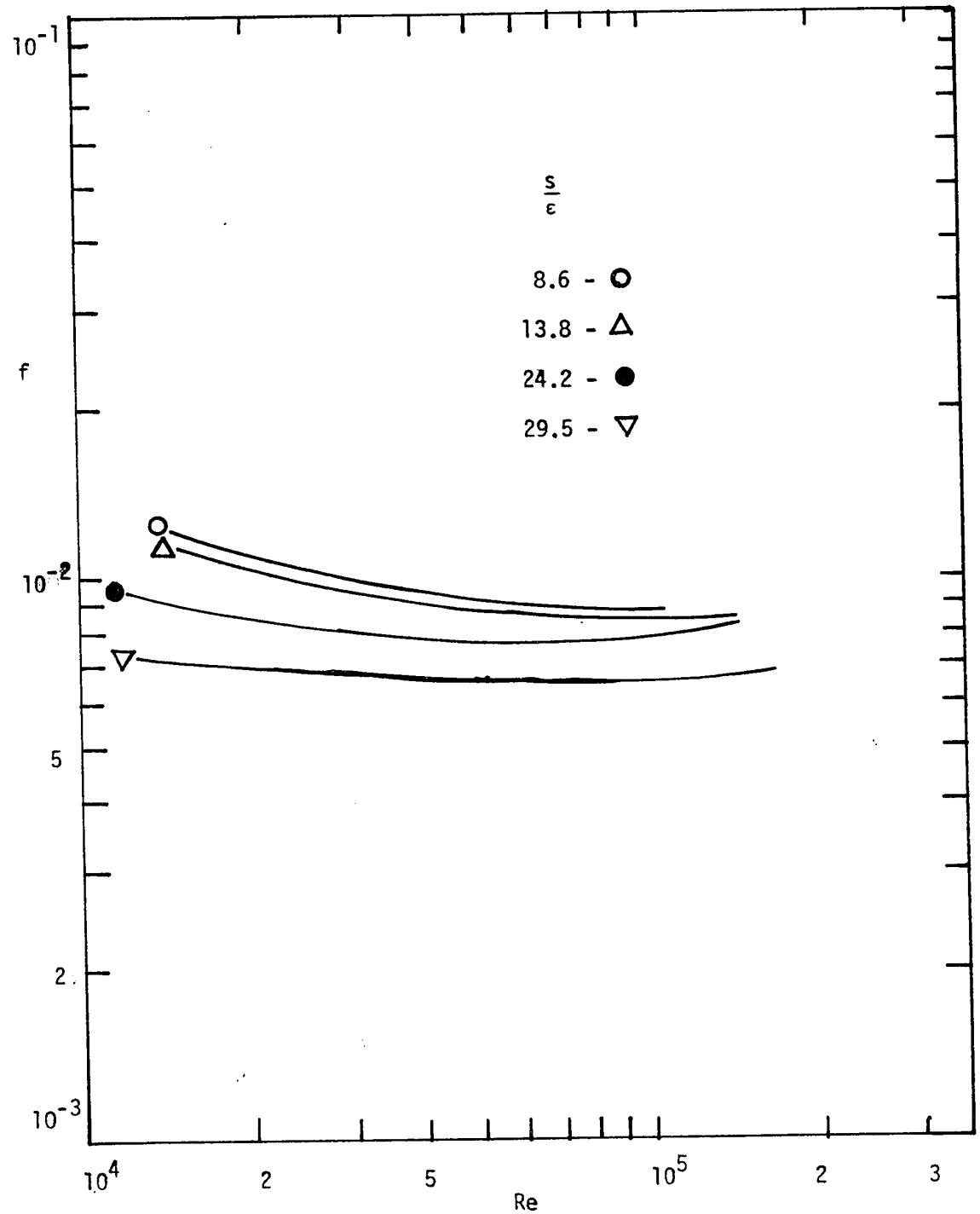

Figure 3.3 Predicted f using variable m

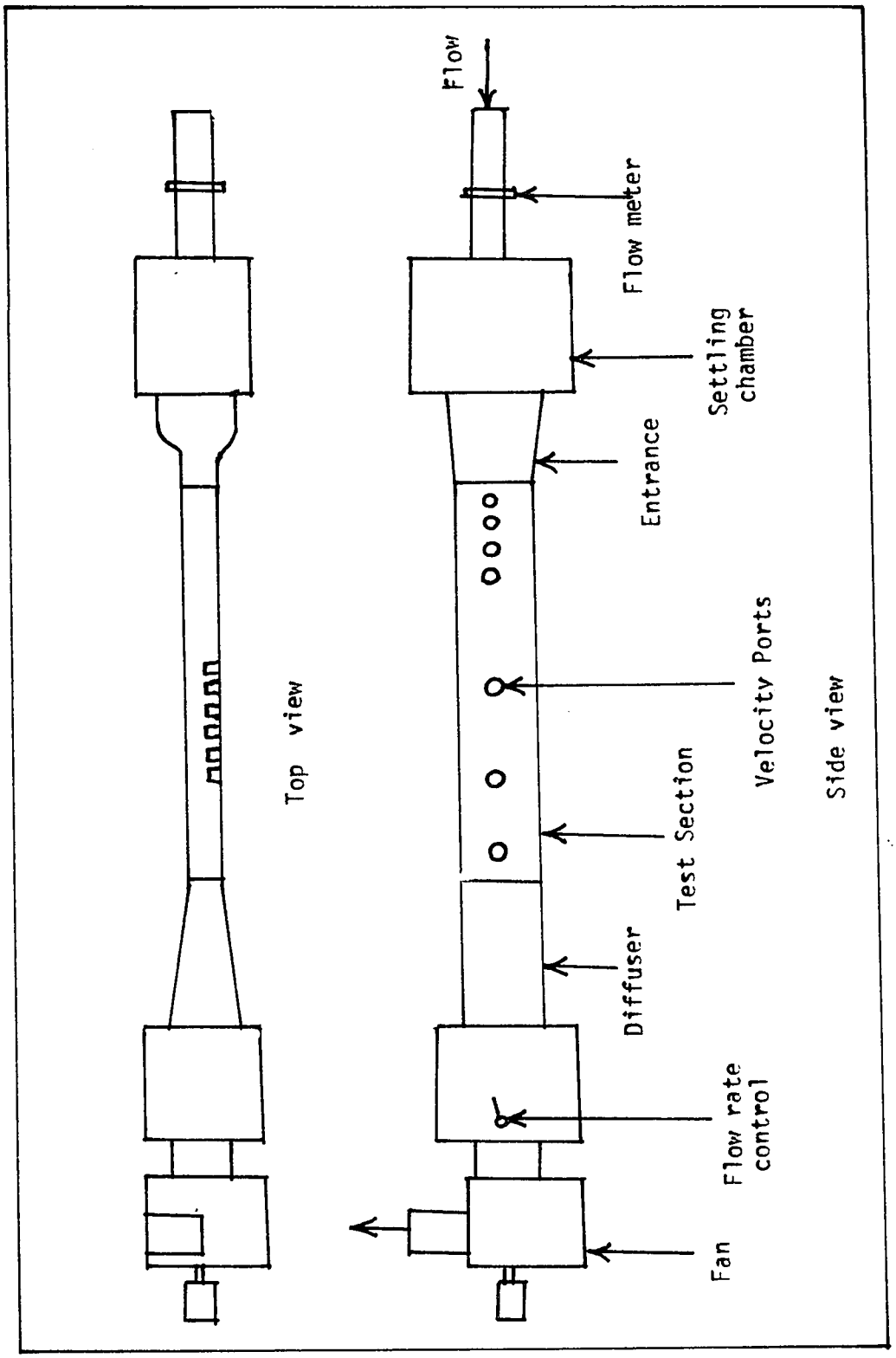

Figure 4.1 Schematical Description of Apparatus

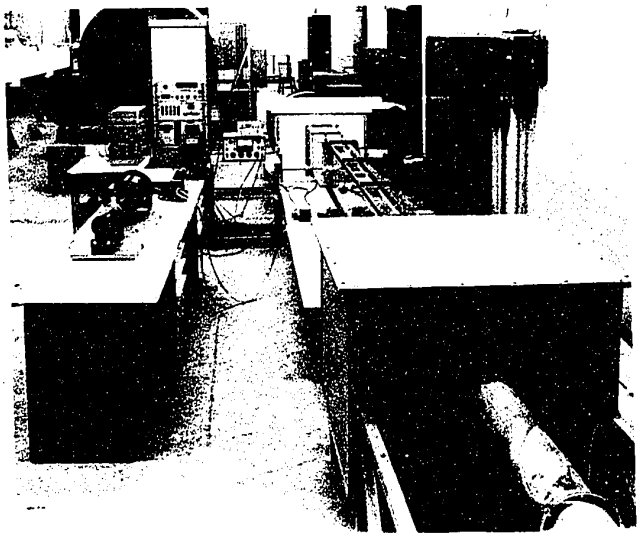

a. General View of Set up

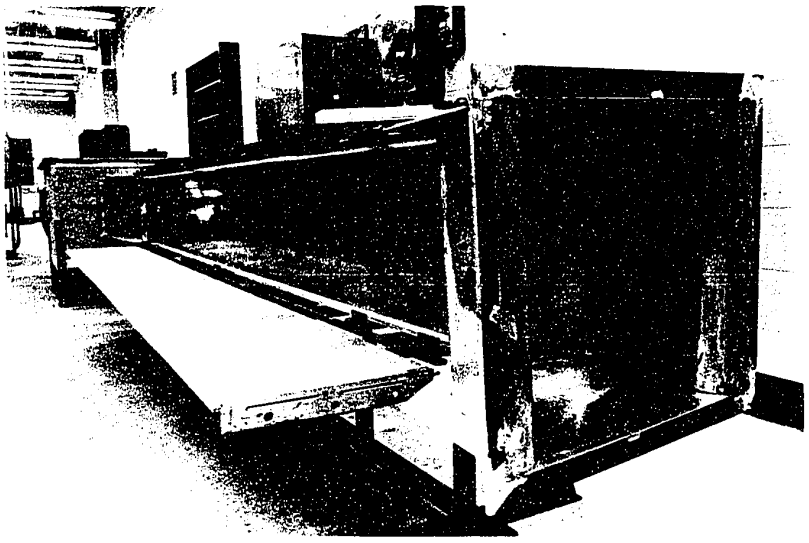

b. Channel Assembly

Figure 4.2 General View of Experimental Apparatus

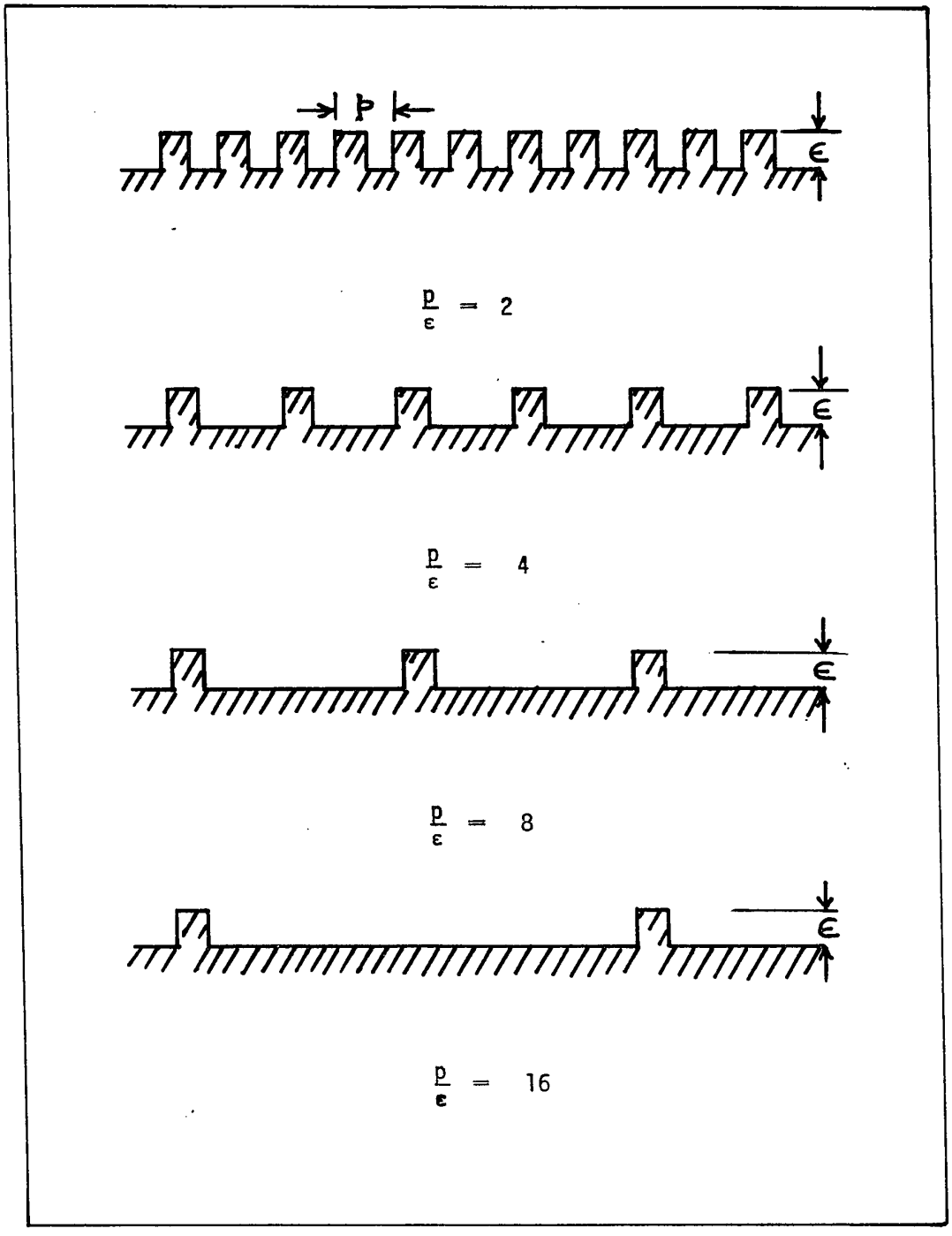

Figure 4.3 Roughness Profile

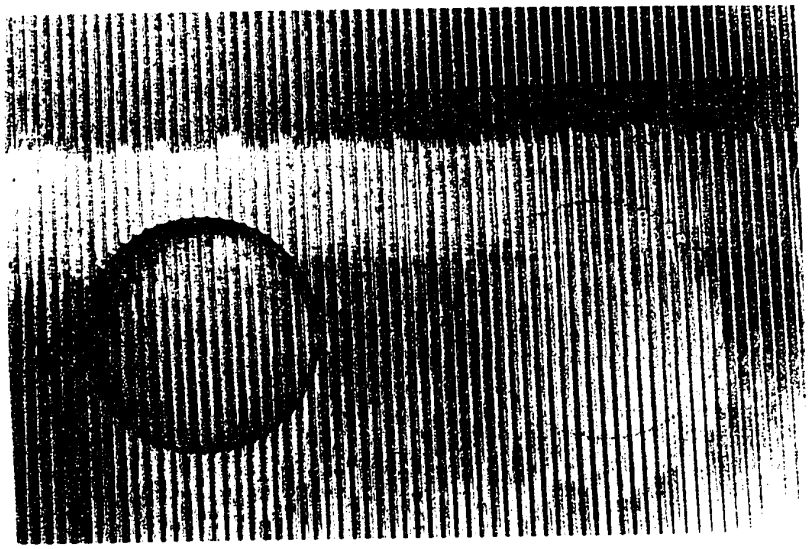

a. Ports with Roughness Profile, $\frac{p}{\epsilon} = 2$

b. Ports with Roughness Profile, $\frac{p}{\epsilon} = 16$

Figure 4.4 Velocity Measuring Ports

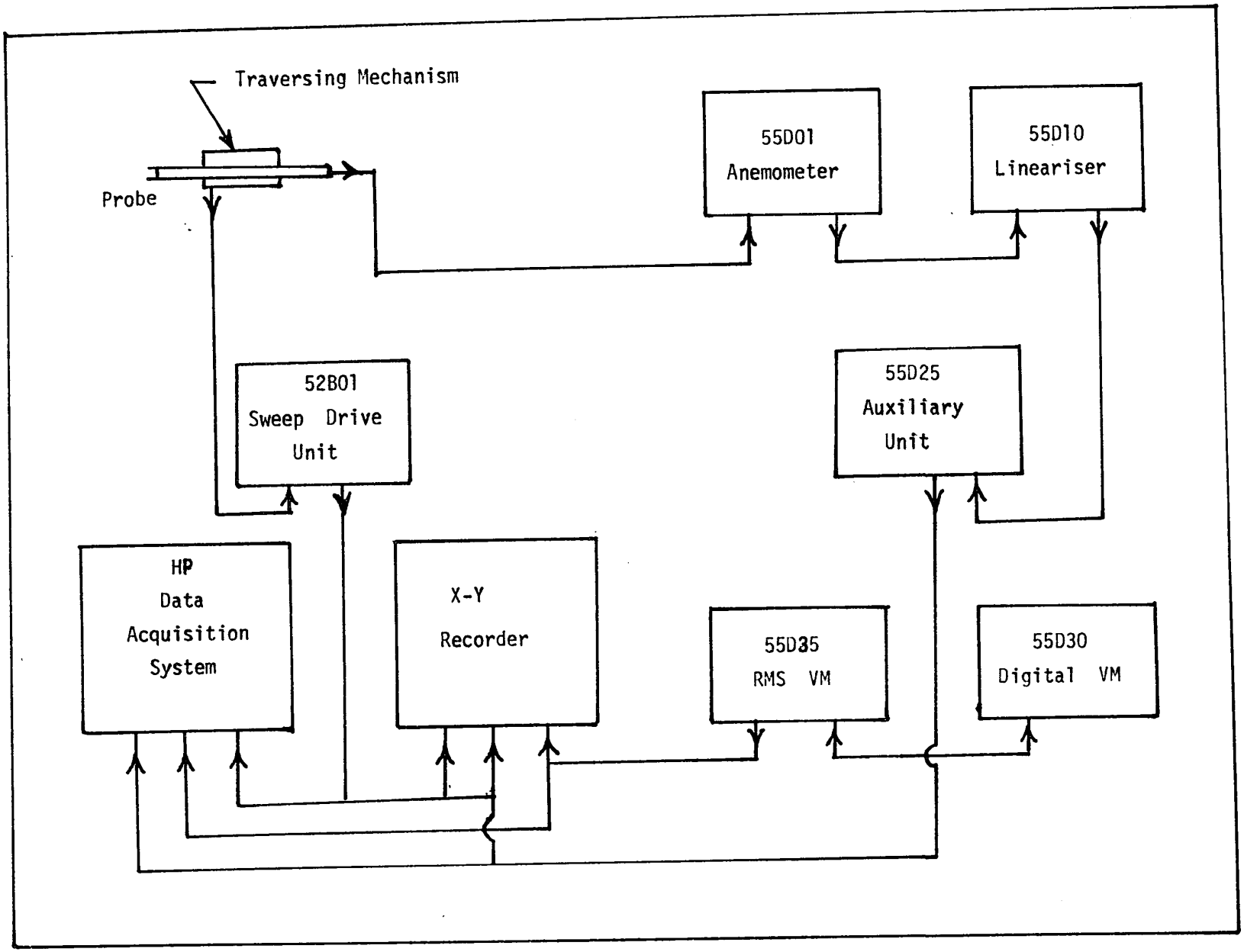

Figure 4.5 Flowchart of Measurements

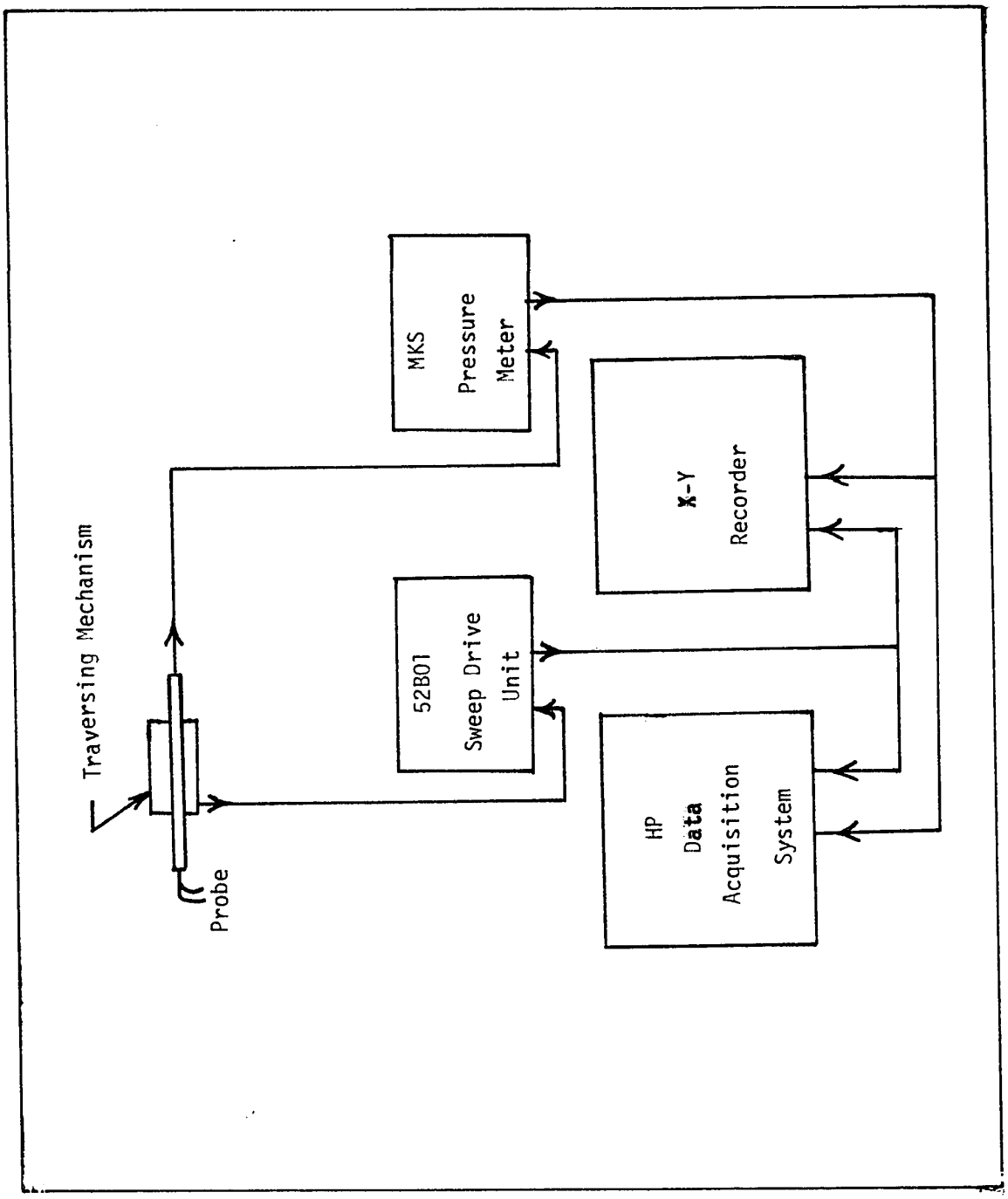

Figure 4.6 Flowchart of Measurements

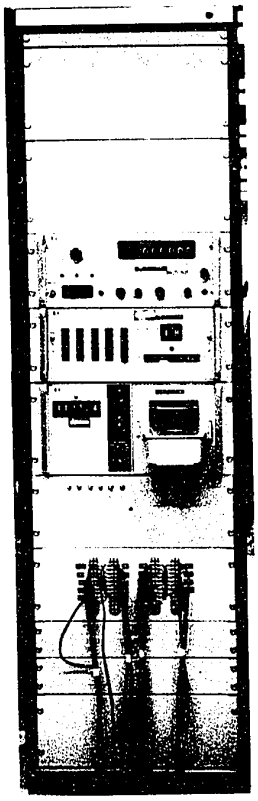

Figure 4.7 Hewlett-Packard Data Acquisition System

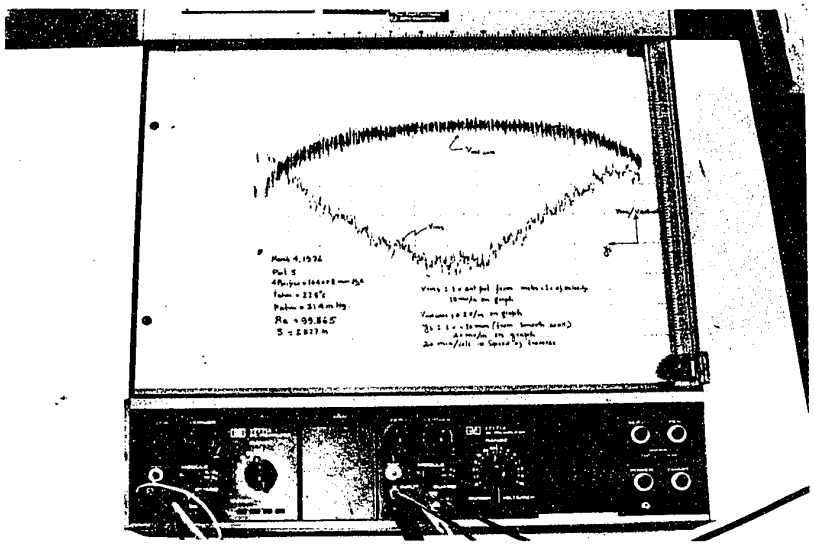

Figure 4.8 Hewlett-Packard X - Y Recorder

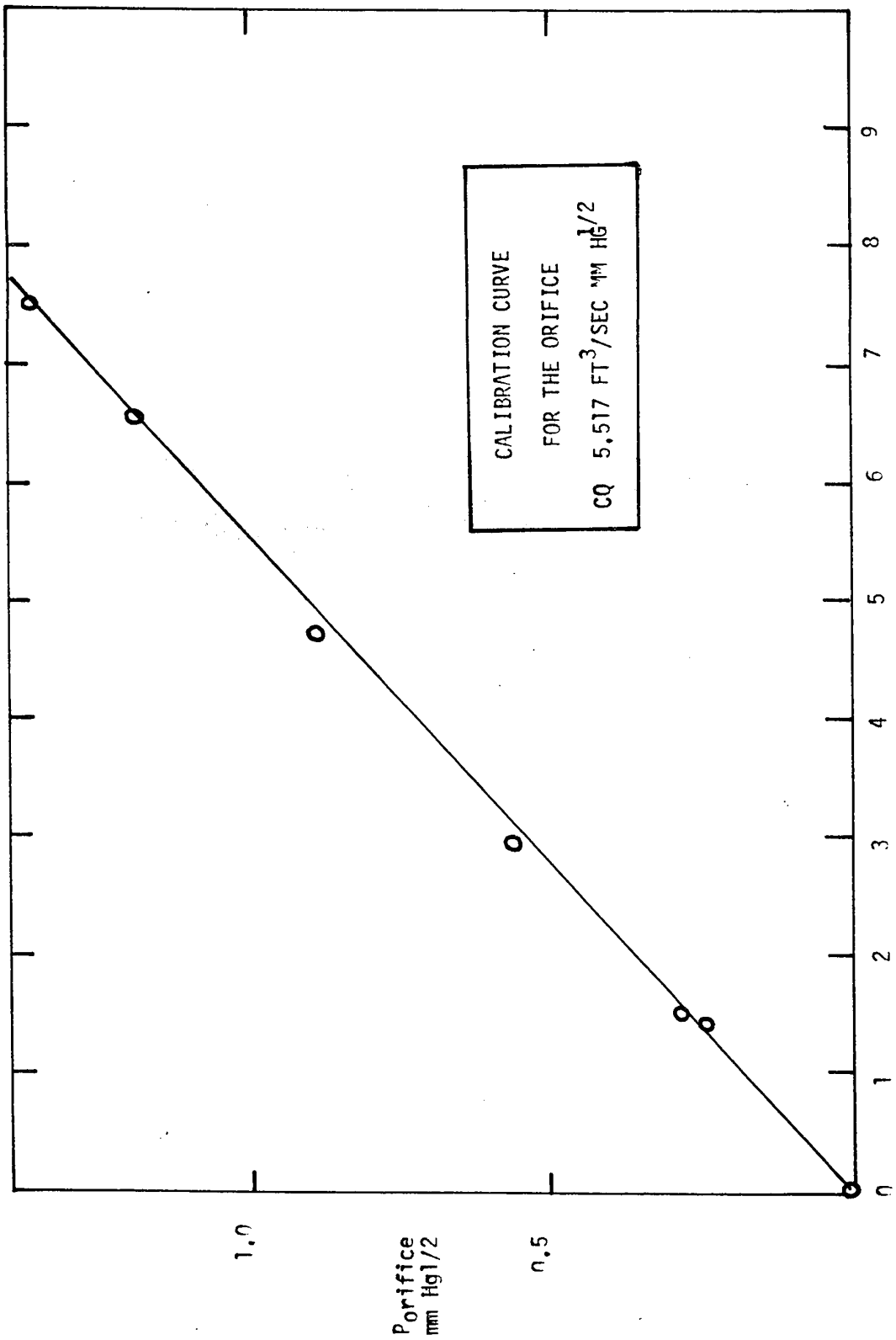

Figure 4.9 Calibration Curve for the Orifice Plate

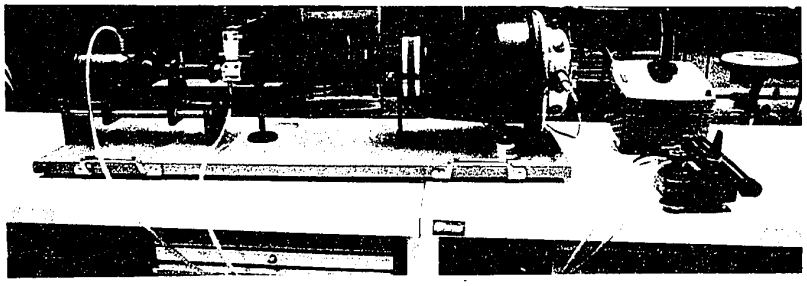

Figure 4.10 Hot-Wire Calibration Apparatus

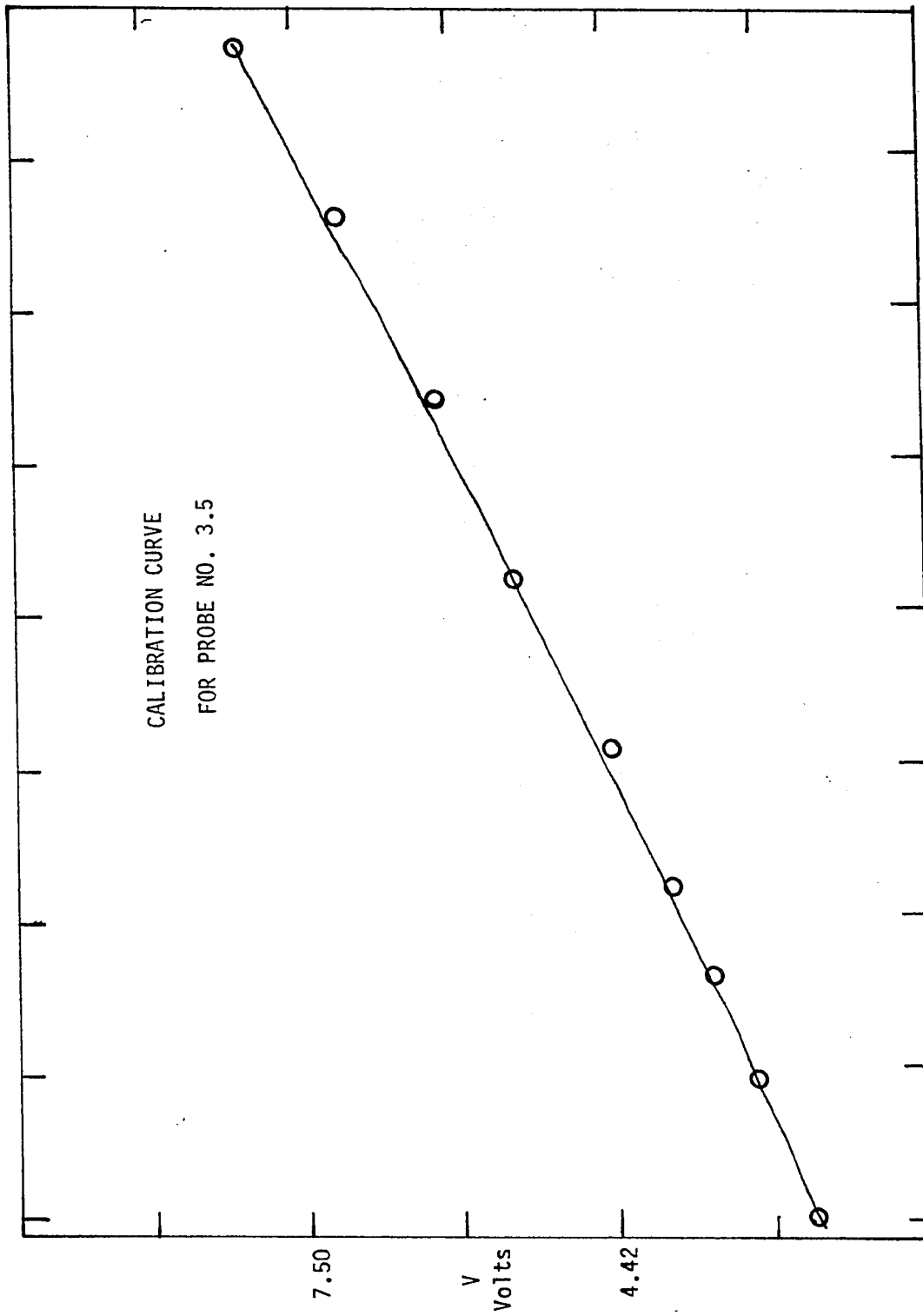

Figure 4.11 Typical Calibration Curve for a Hot-Wire Probe

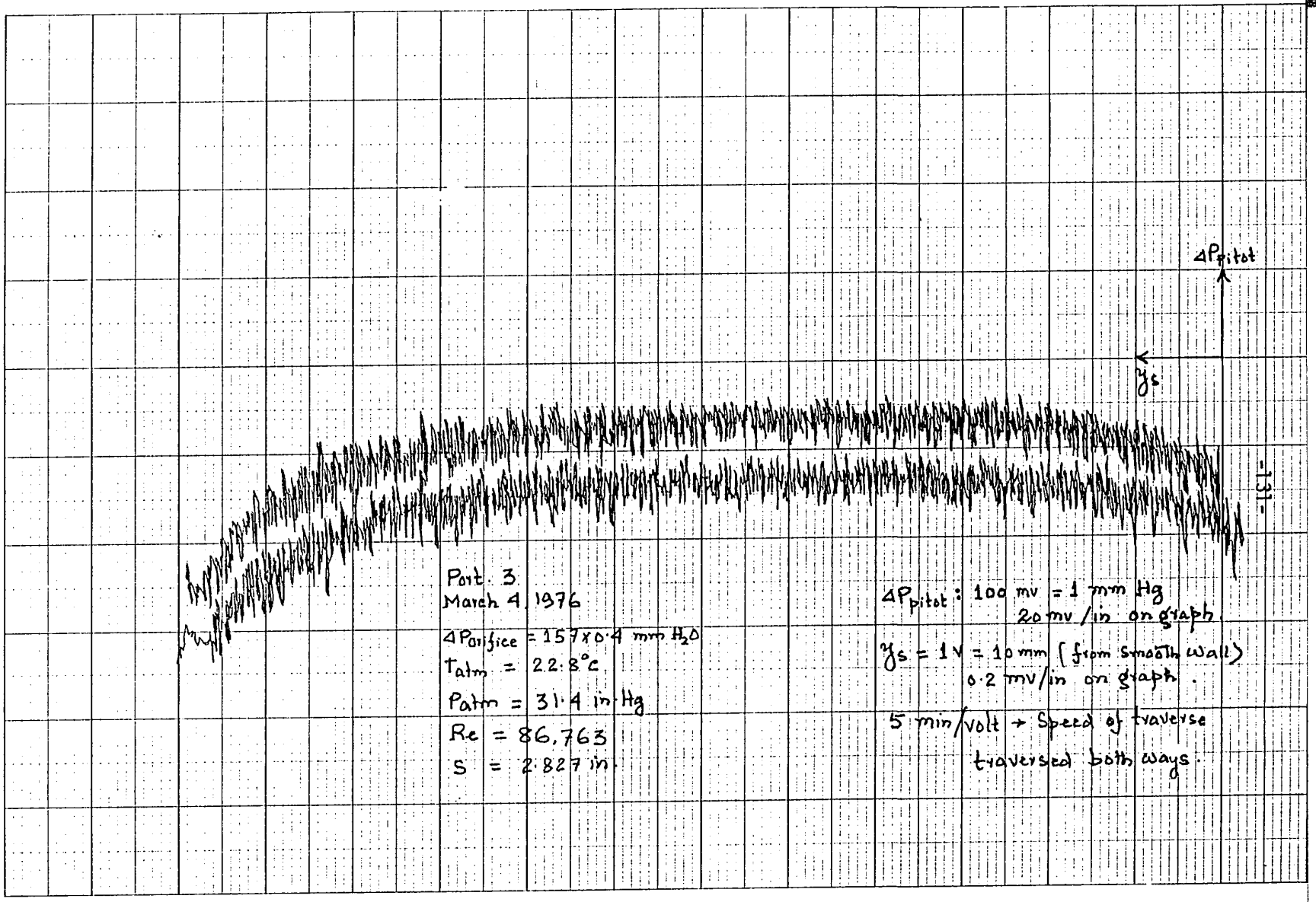

Figure 4.12 Developing Velocity and $\sqrt{\frac{\overline{u'^2}}{\overline{u}}}$ Profiles

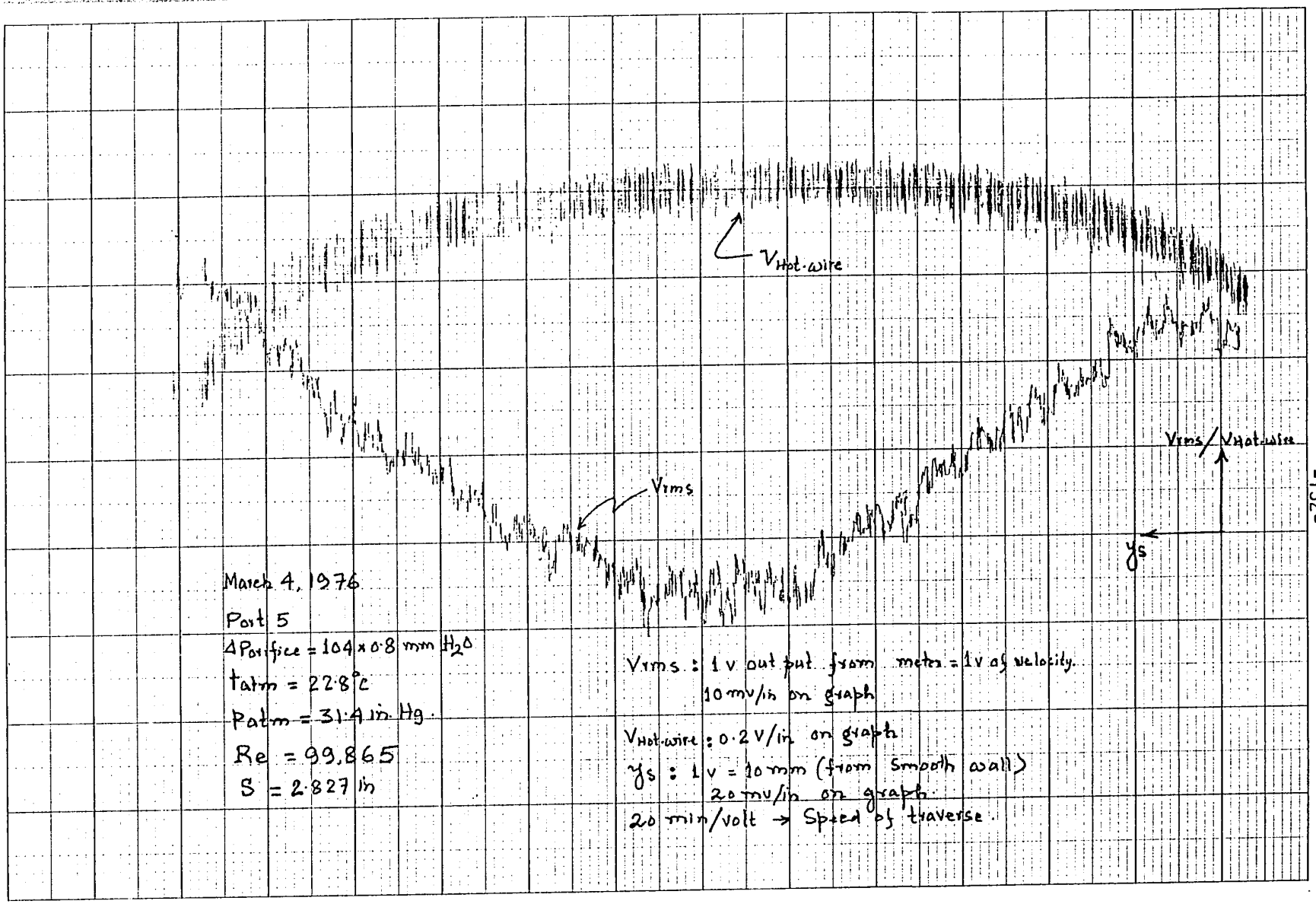

Figure 4.13 Developed Velocity and $\sqrt{\frac{\overline{u}}{\overline{u}}^{T2}}$ Profiles

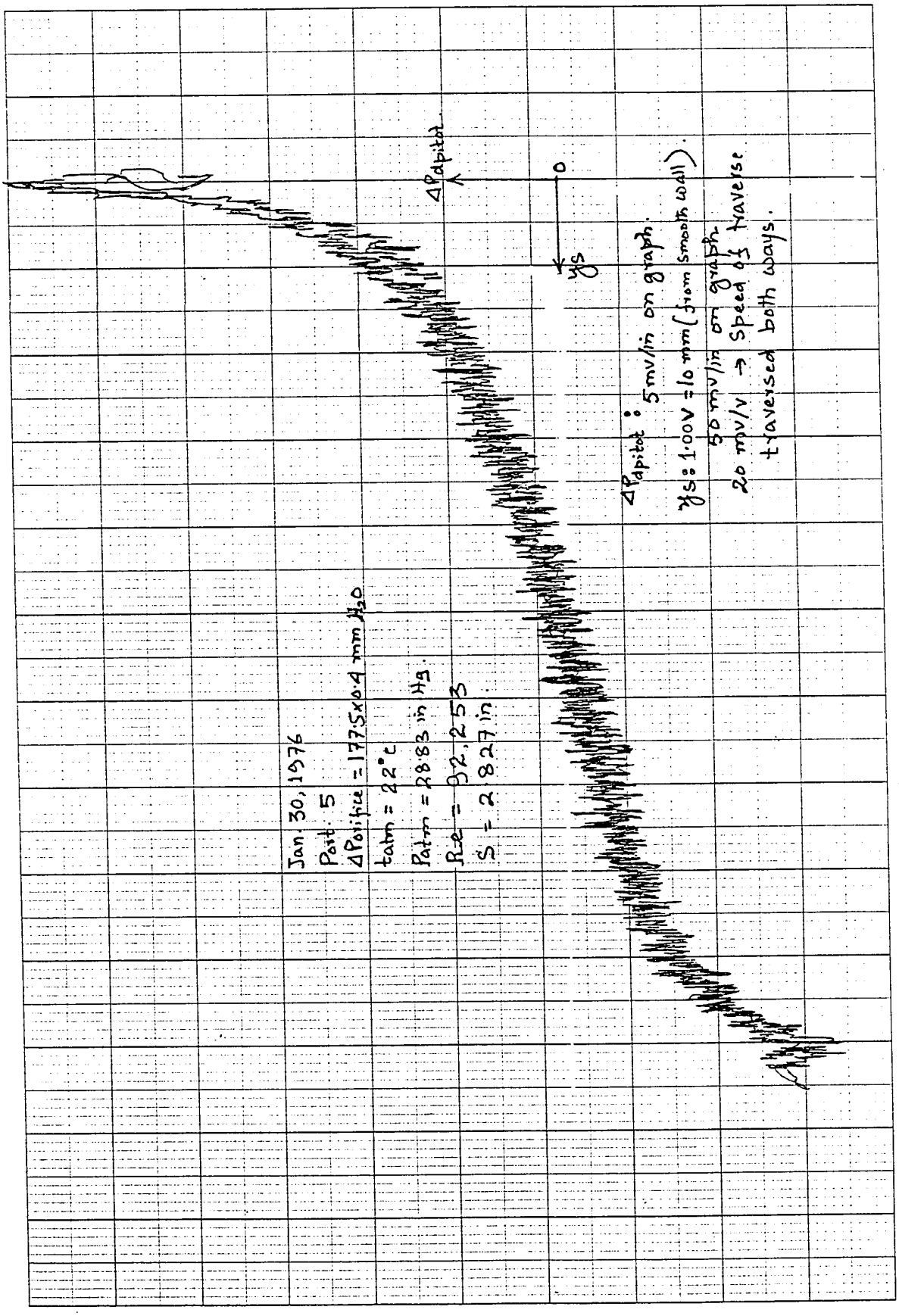

Figure 4.14 Double Pitot Tube Measurement

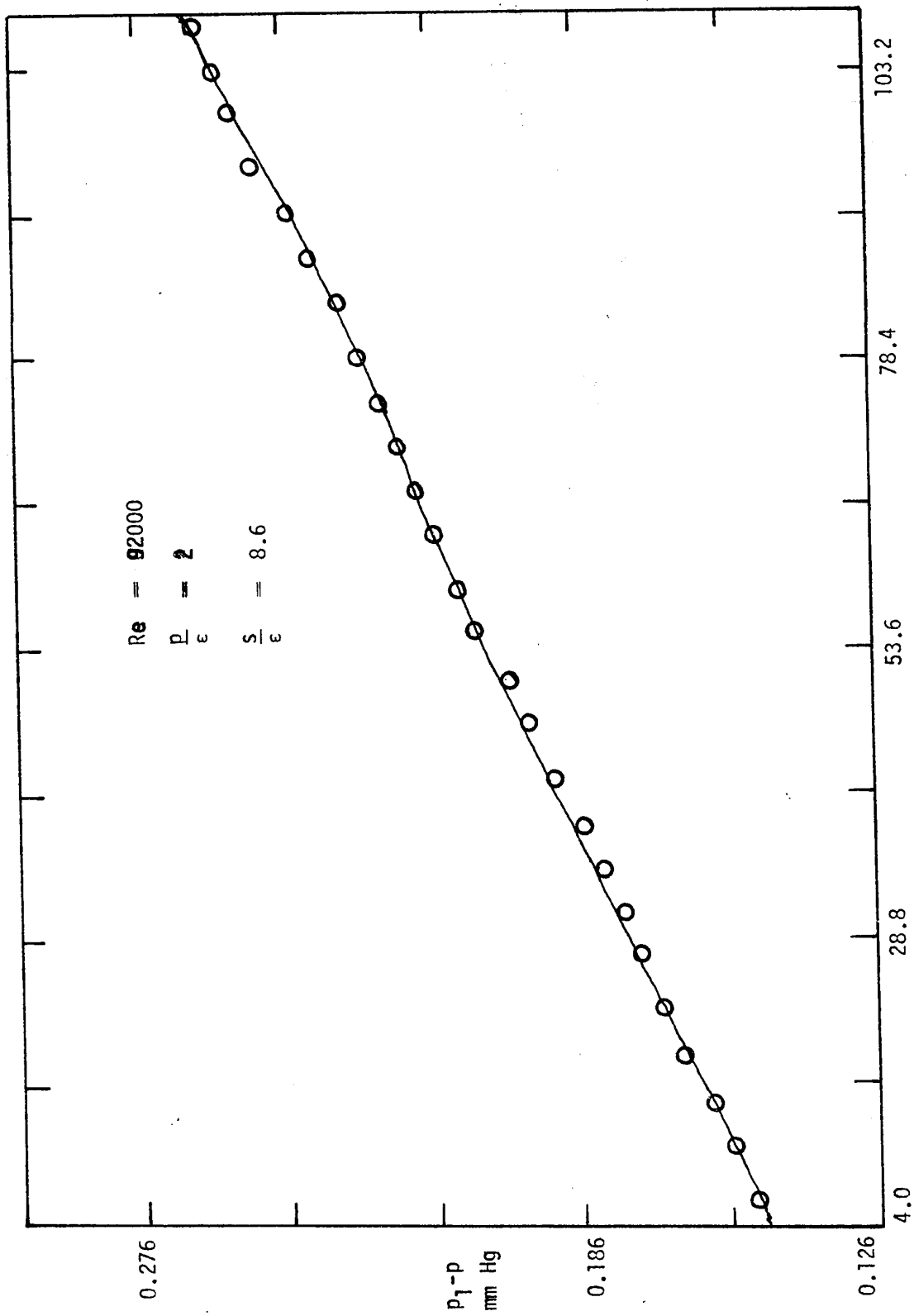

Figure 5.1 Pressure vs Distance

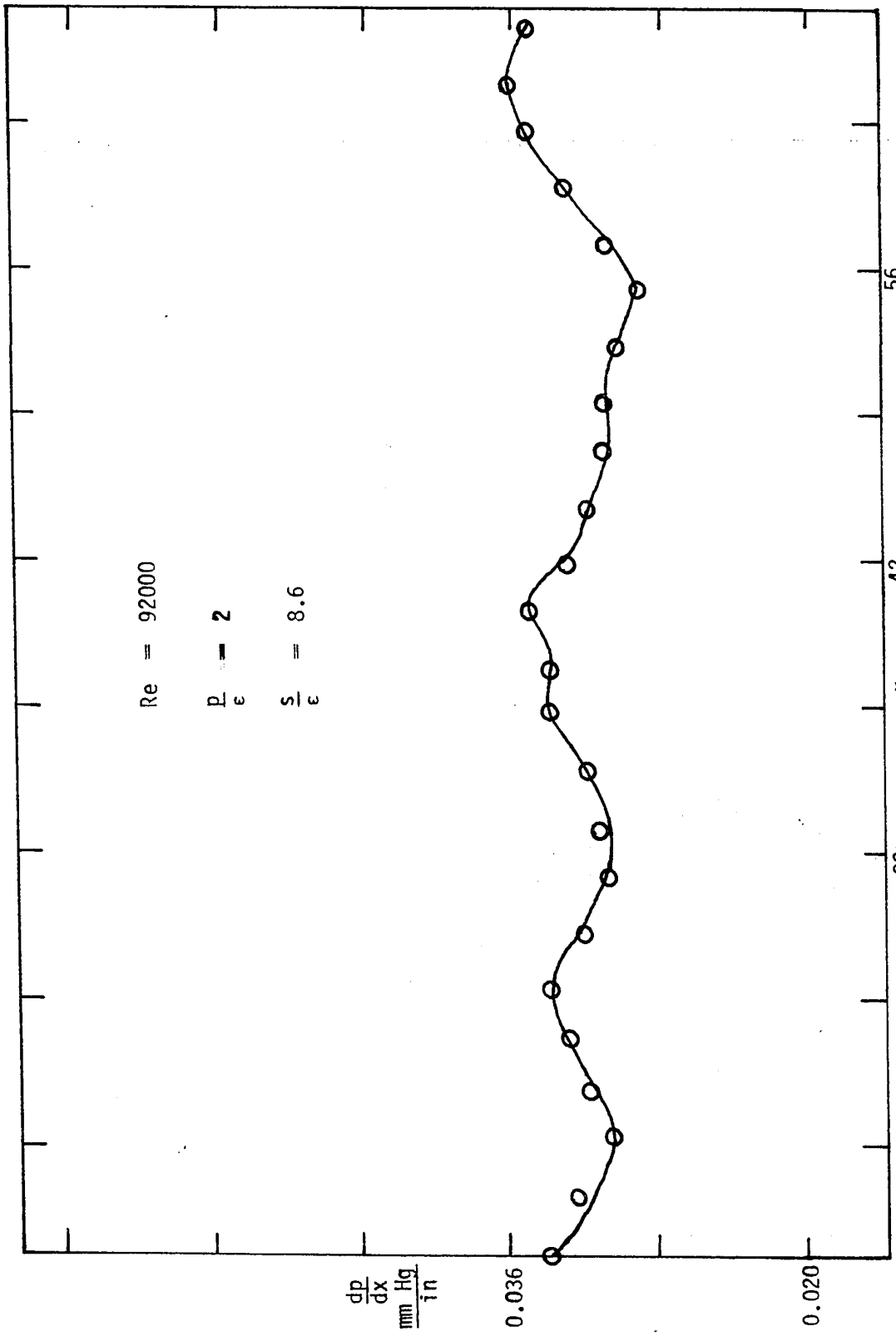
Re = 92000
p/ε = 2
s/ε = 8.6
dp/dx mm Hg/in
0.036
0.020
14
28
42
56
x/D_hyd
dp/dx vs x/D_hyd

Figure 5.2

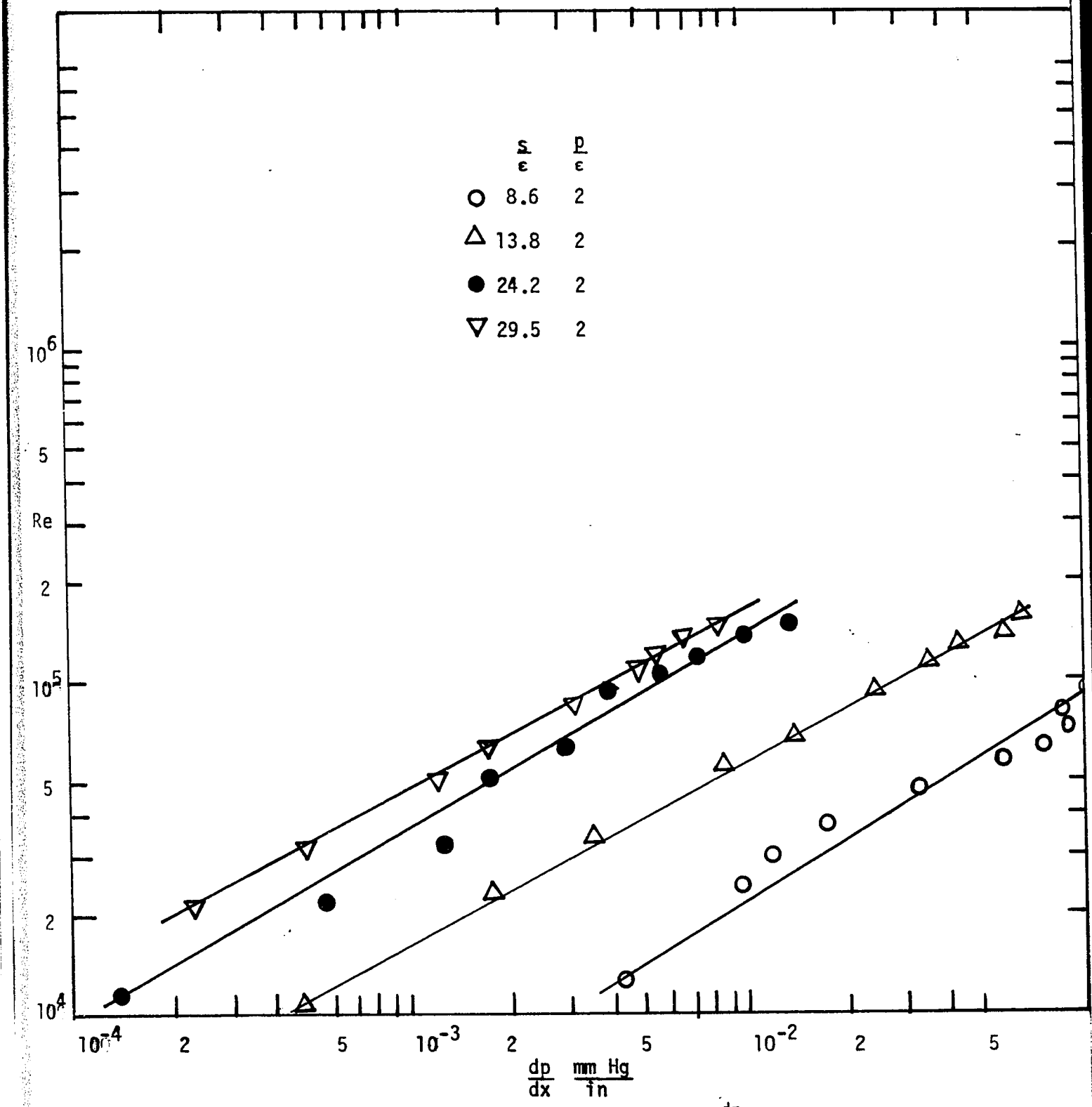

Figure 5.3A Reynolds Number vs $\frac{dp}{dx}$

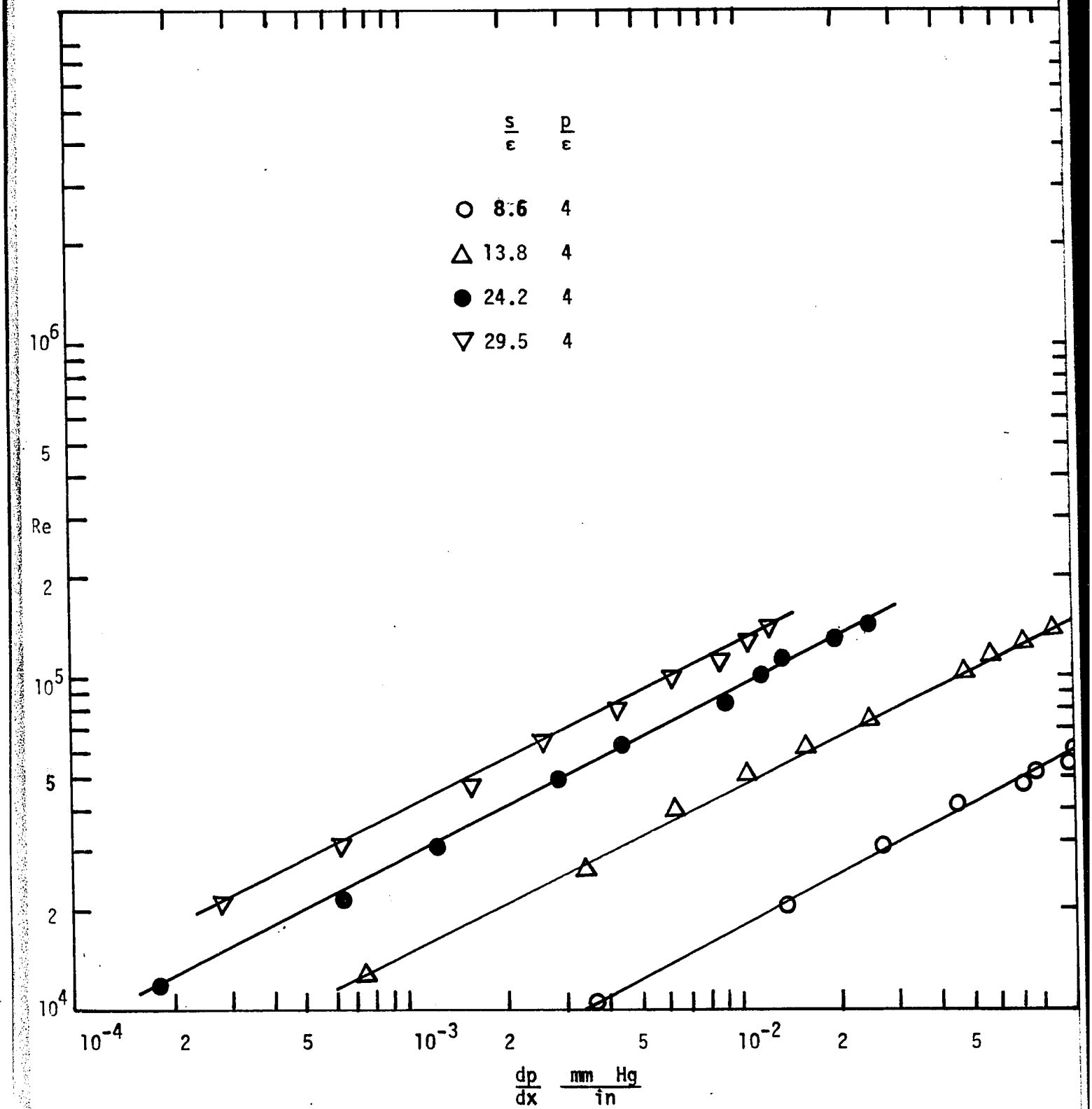

Figure 5.3B Reynolds Number vs $\frac{dp}{dx}$

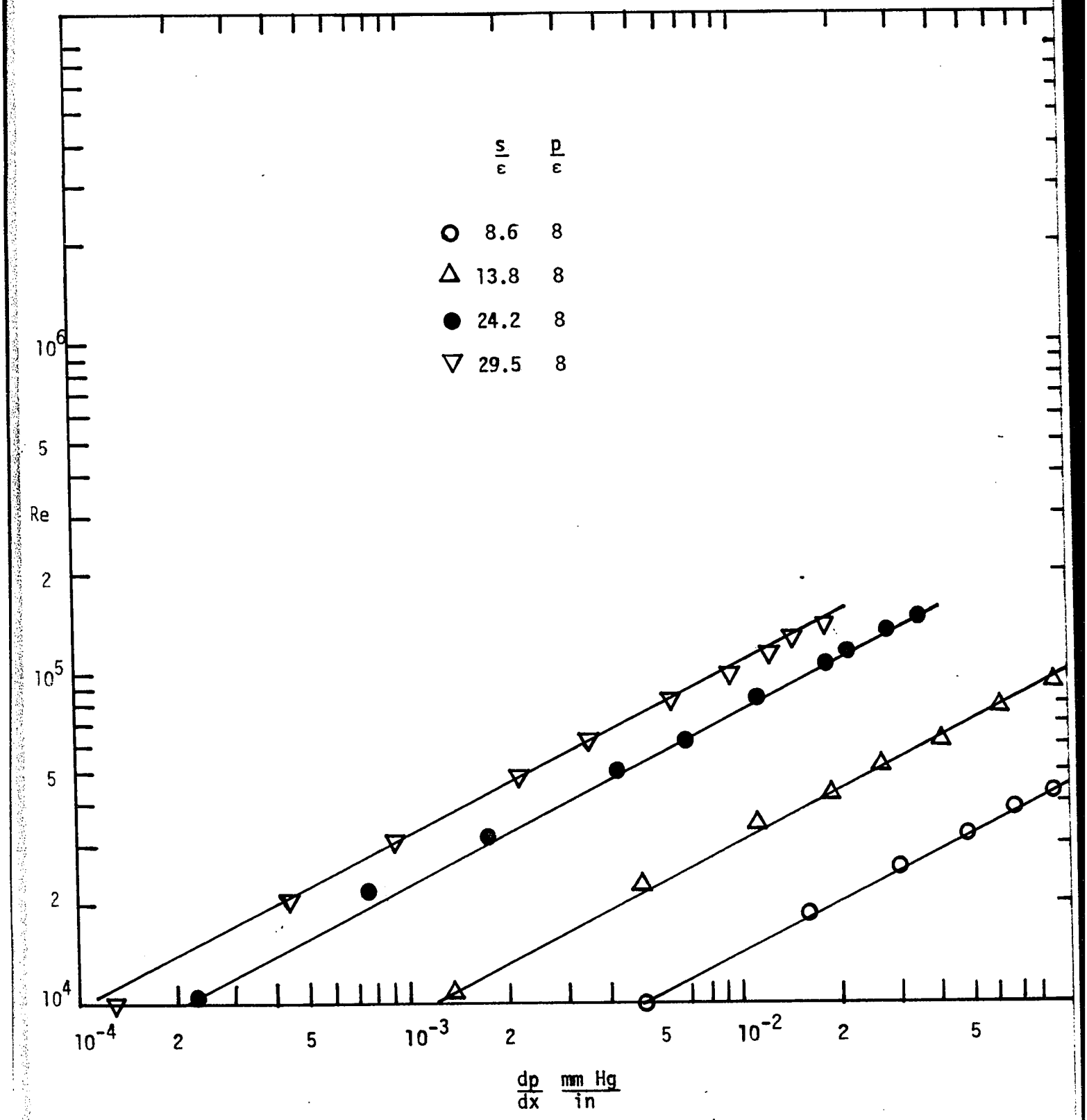

Figure 5.3C Reynolds Number vs $\frac{dp}{dx}$

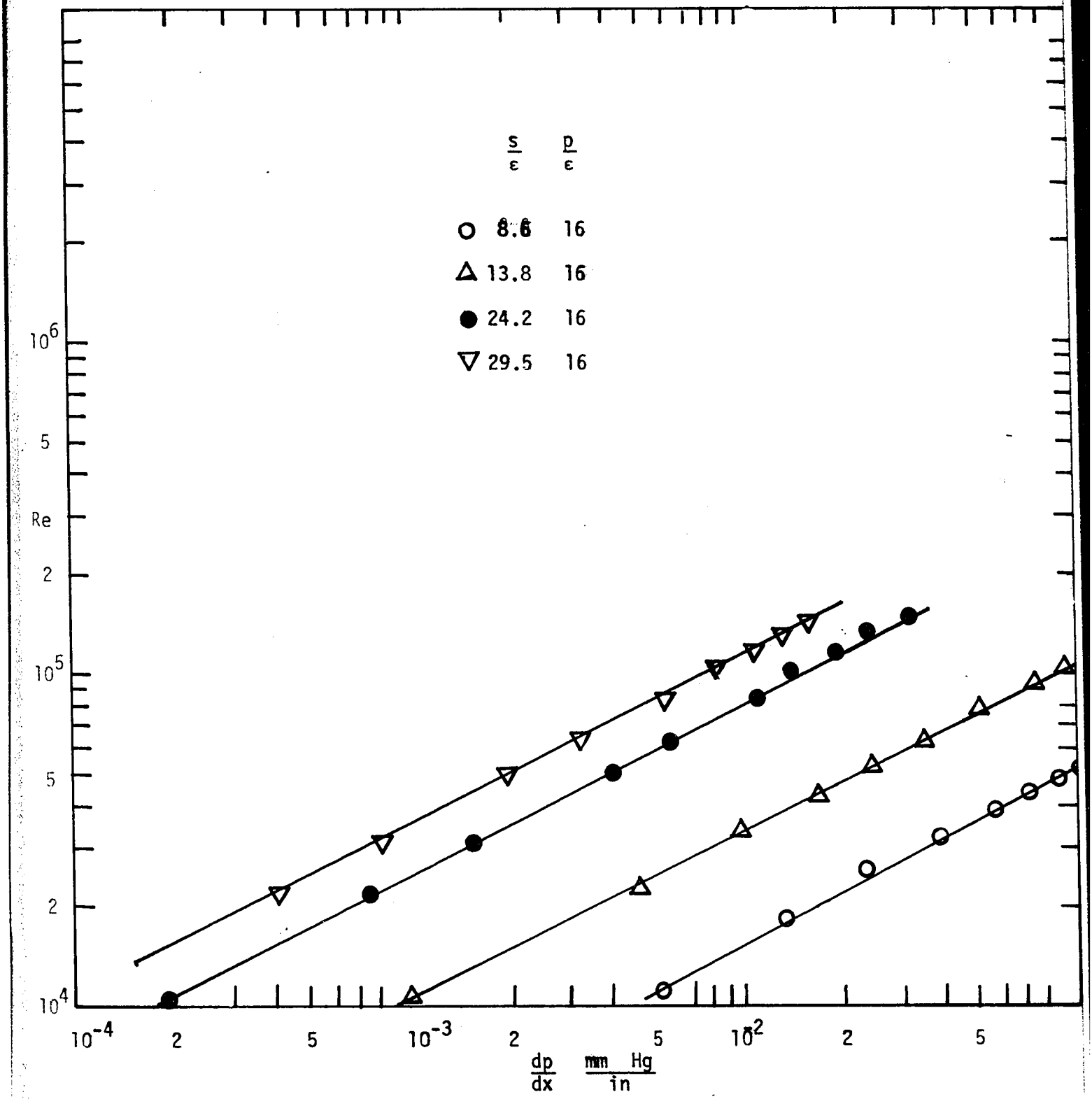

Figure 5.3D Reynolds Number vs $\frac{dp}{dx}$

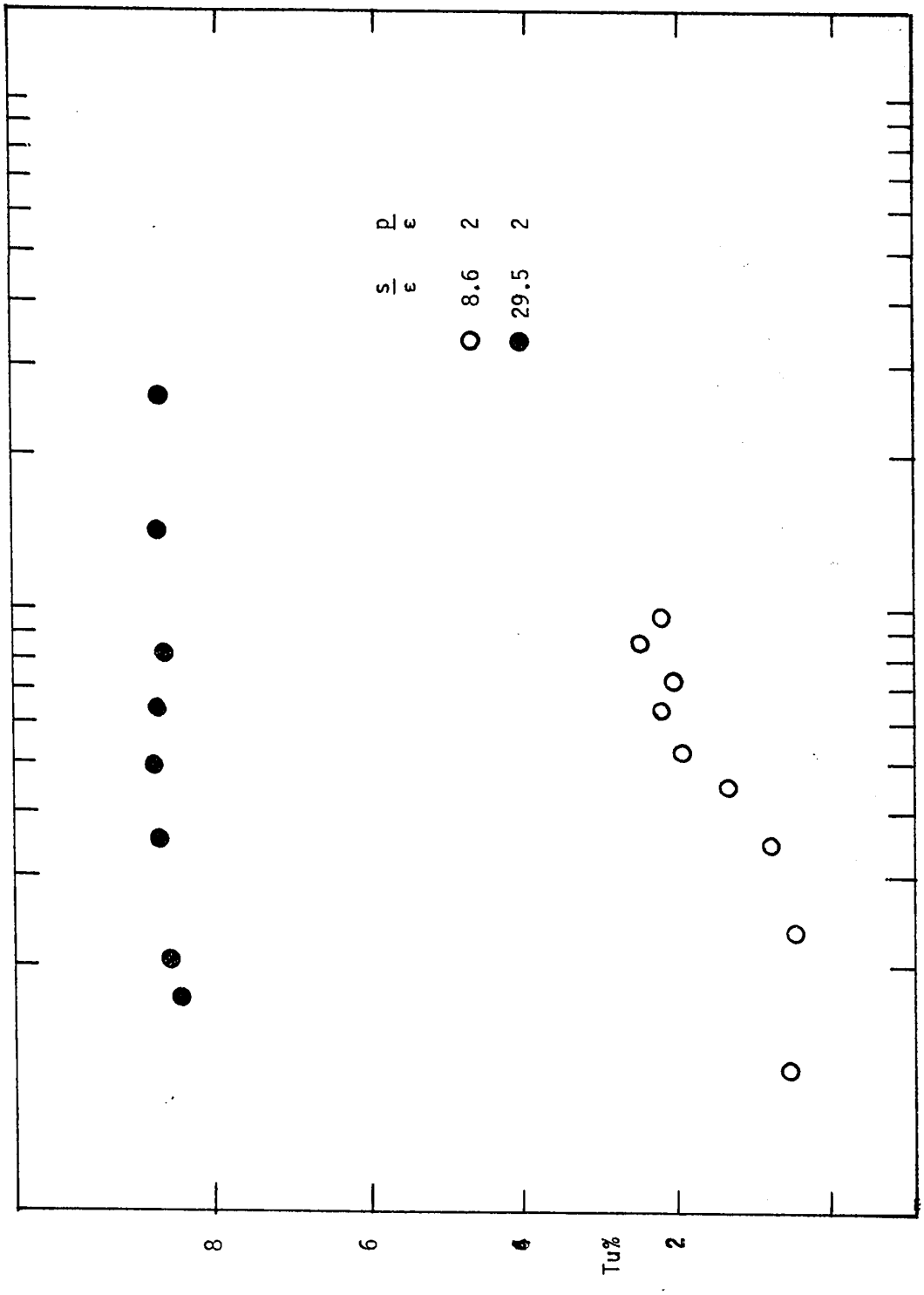

Figure 5.4 Turbulence Intensity vs Reynolds Number

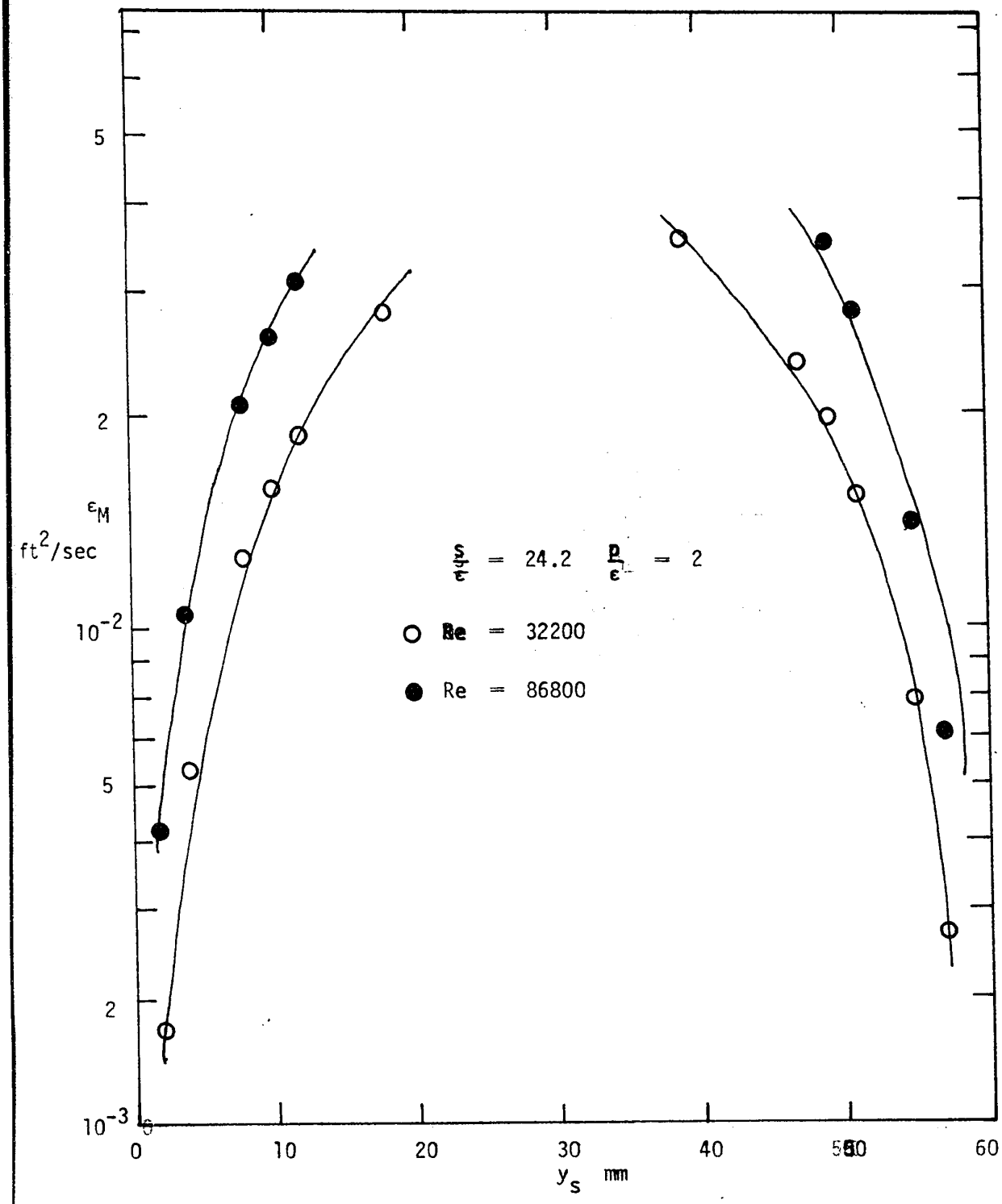

Figure 5.5 Eddy Diffusivity vs Distance

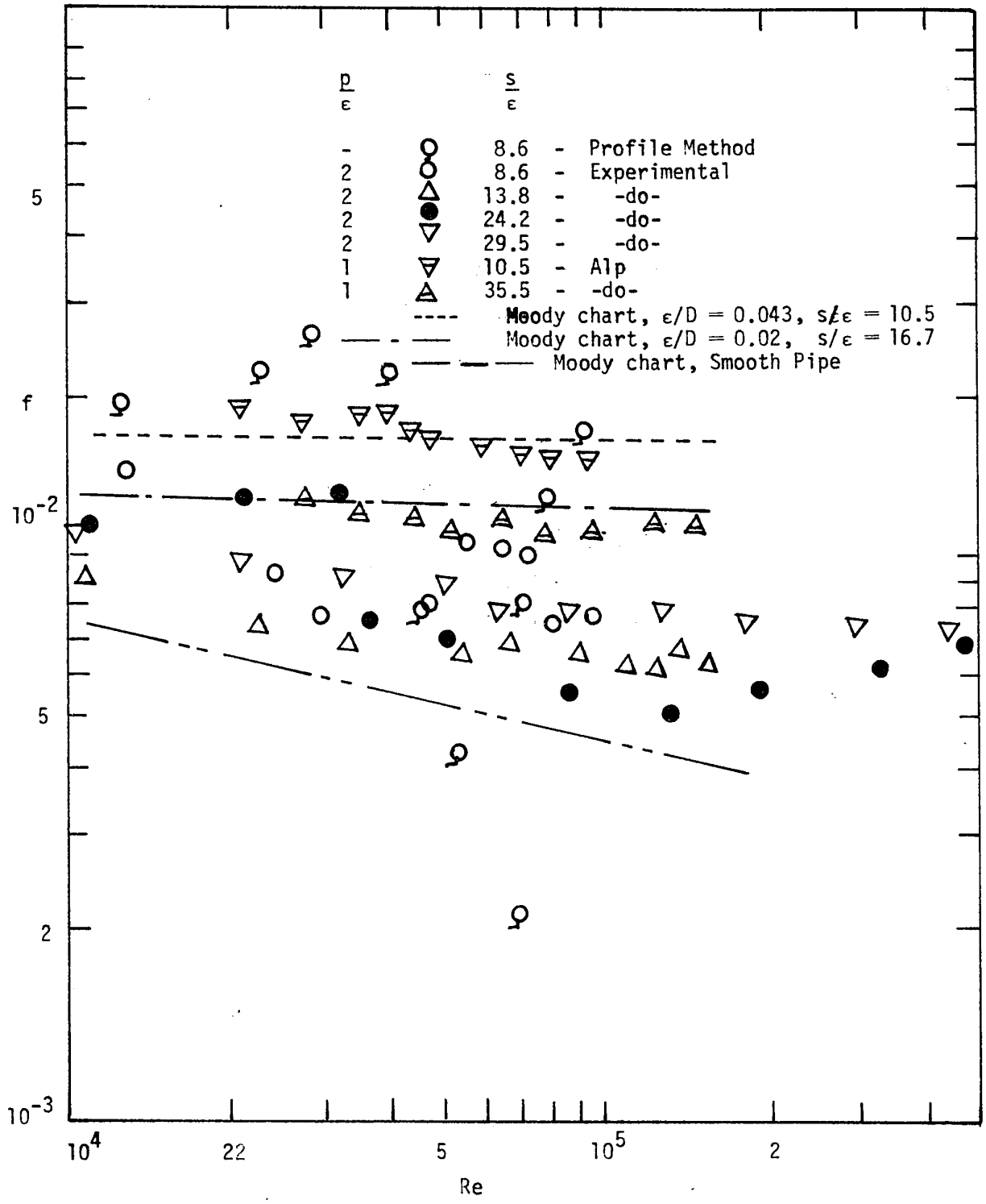

Figure 5.6A Experimental Friction Factor vs Reynolds Number

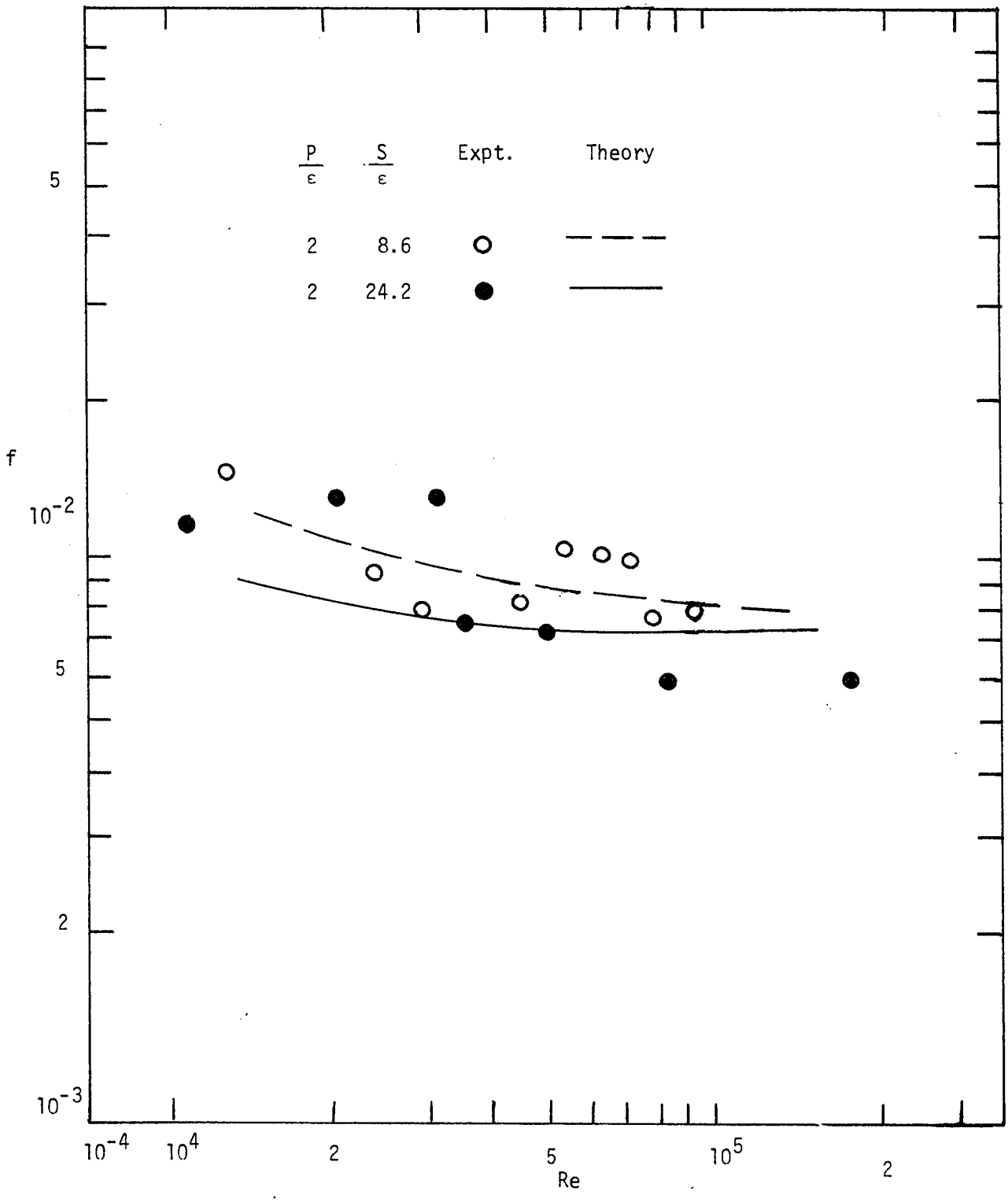

Figure 5.6A$_1$ Experimental Friction Factor vs Reynolds Number

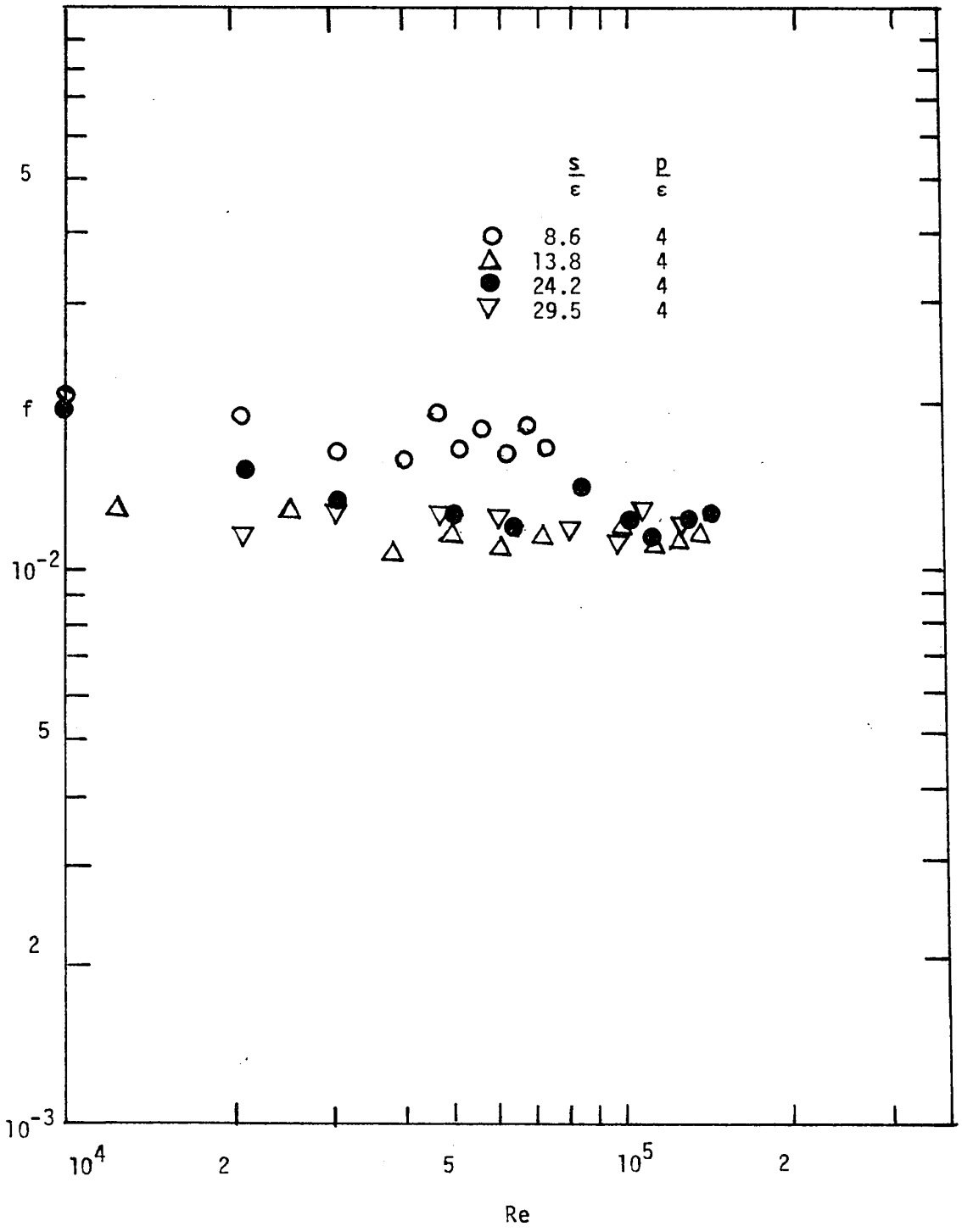

Figure 5.6B Experimental Friction Factor vs Reynolds Number

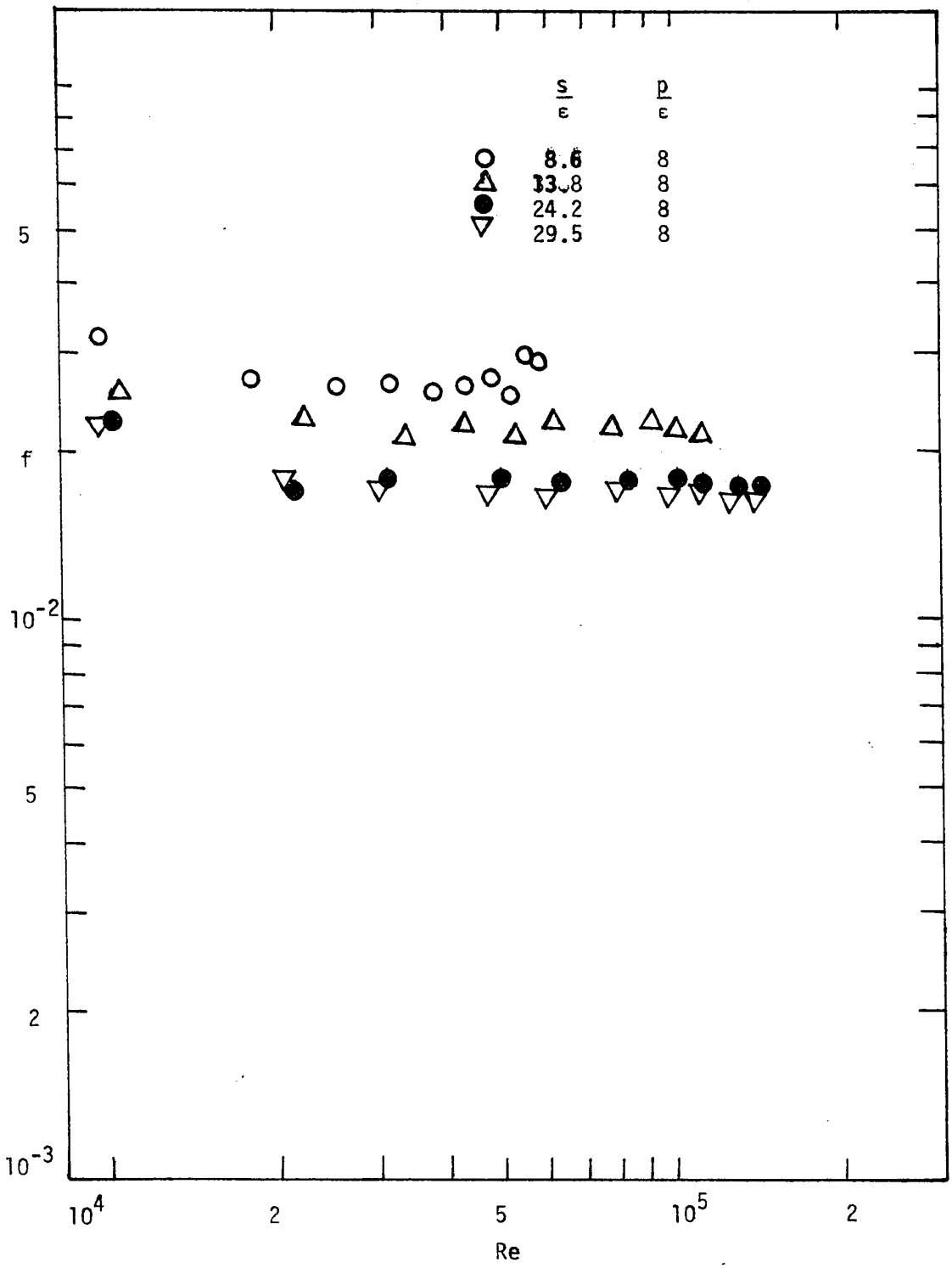

Figure 5.6C Experimental Friction Factor vs Reynolds Number

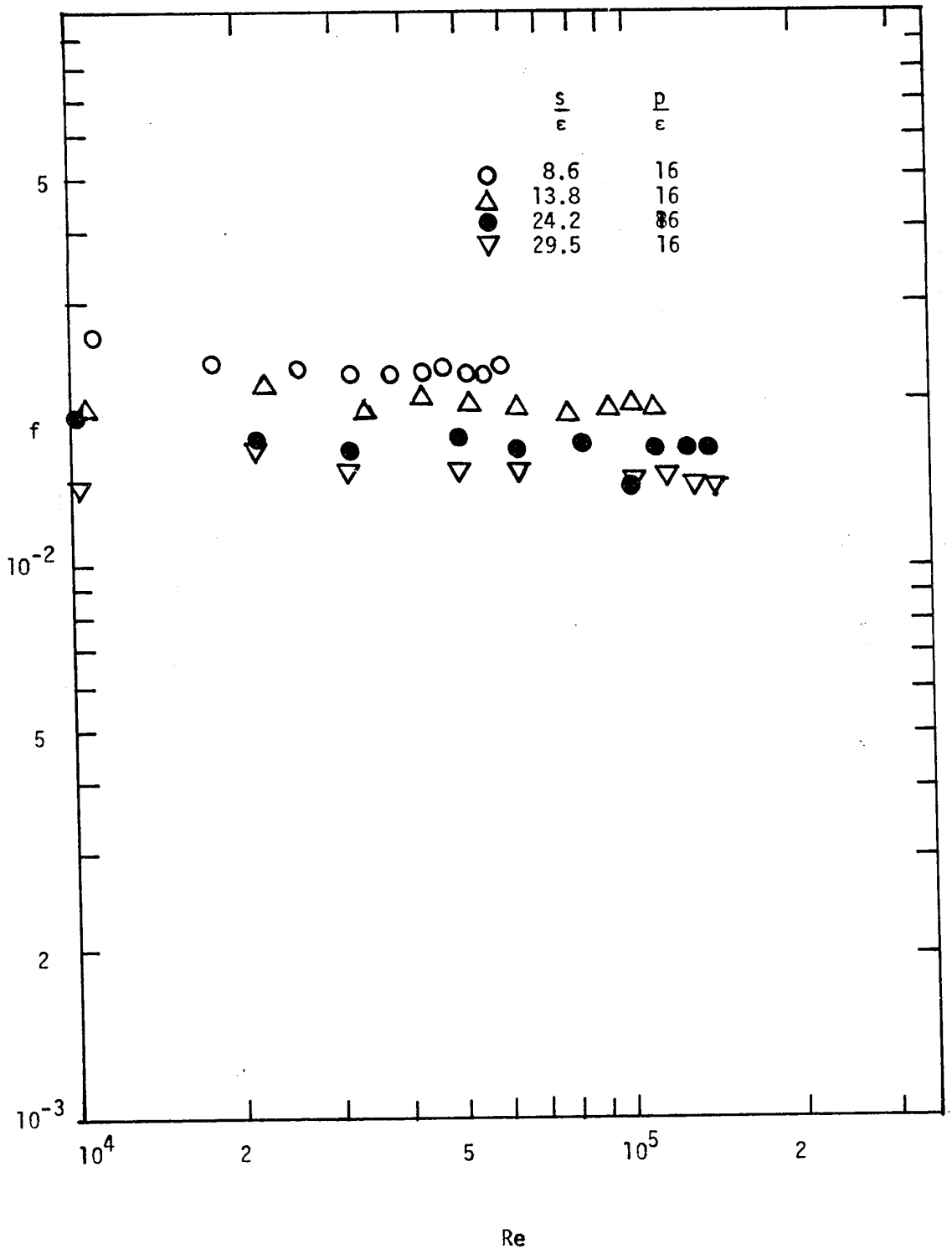

Figure 5.6D Experimental Friction Factor vs Reynolds Number

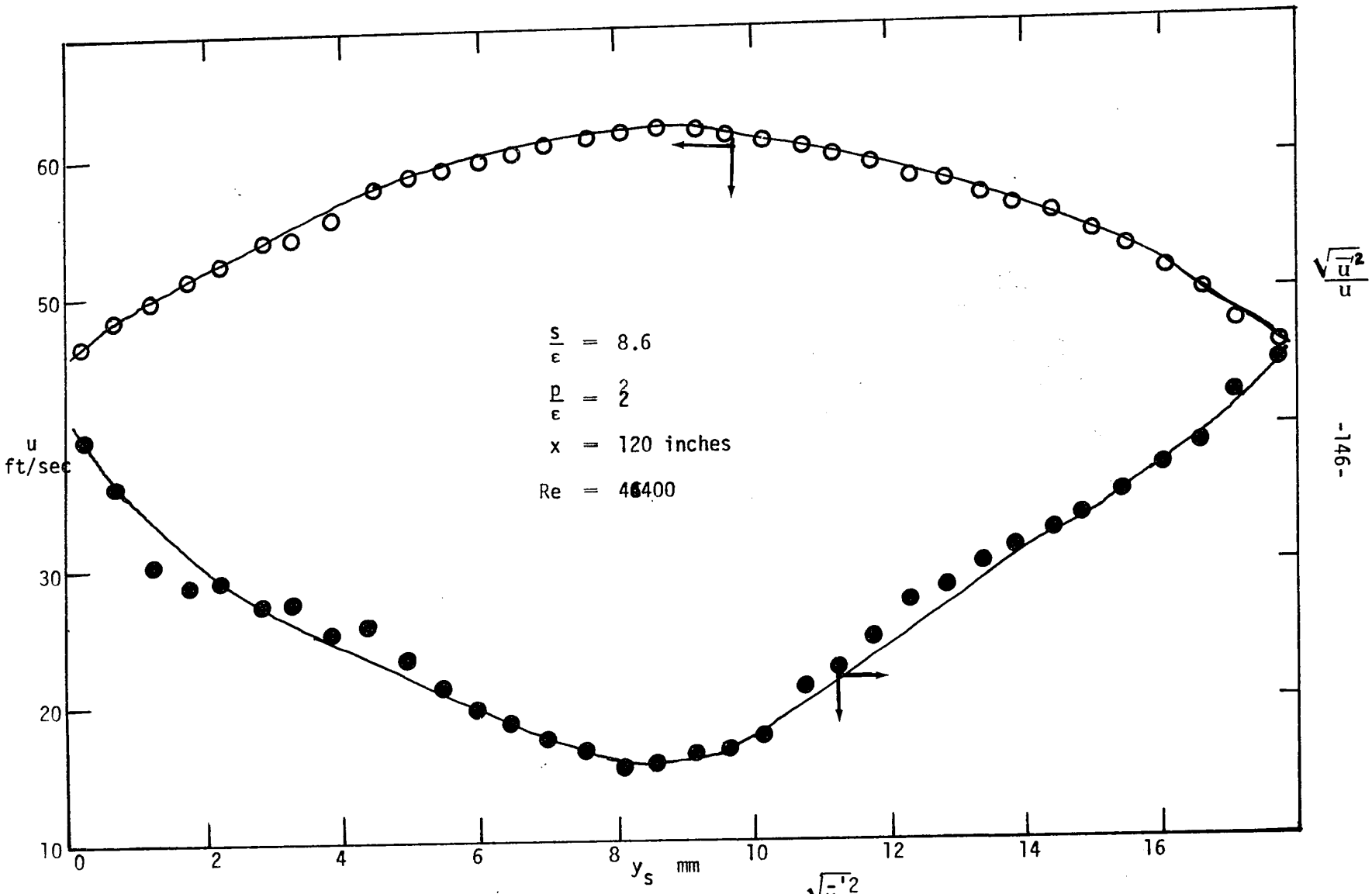

Figure 5.7 Developed Velocity and $\frac{\sqrt{\overline{u'^2}}}{u}$ Profiles

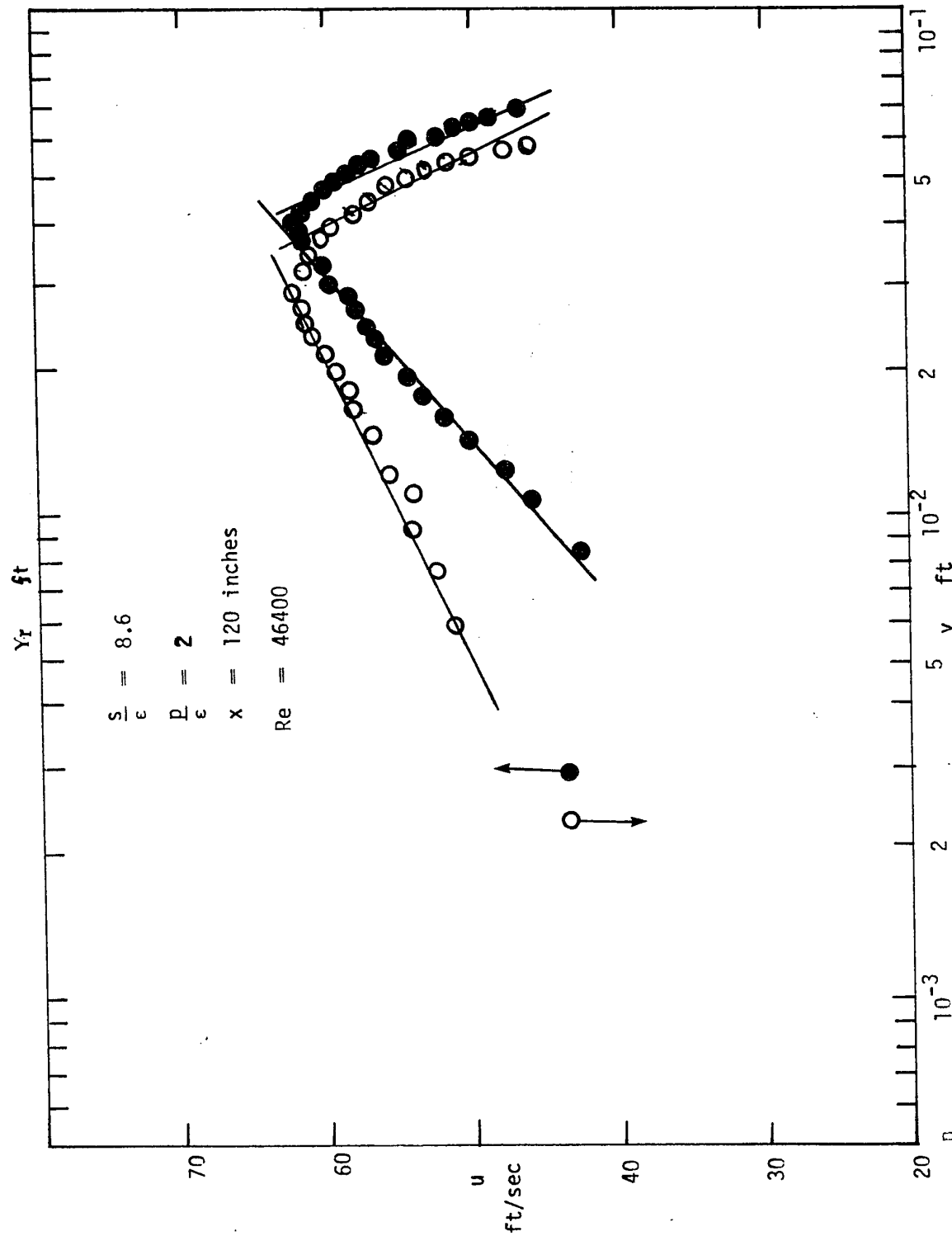

Figure 5.8 Logarithmic Velocity Profiles

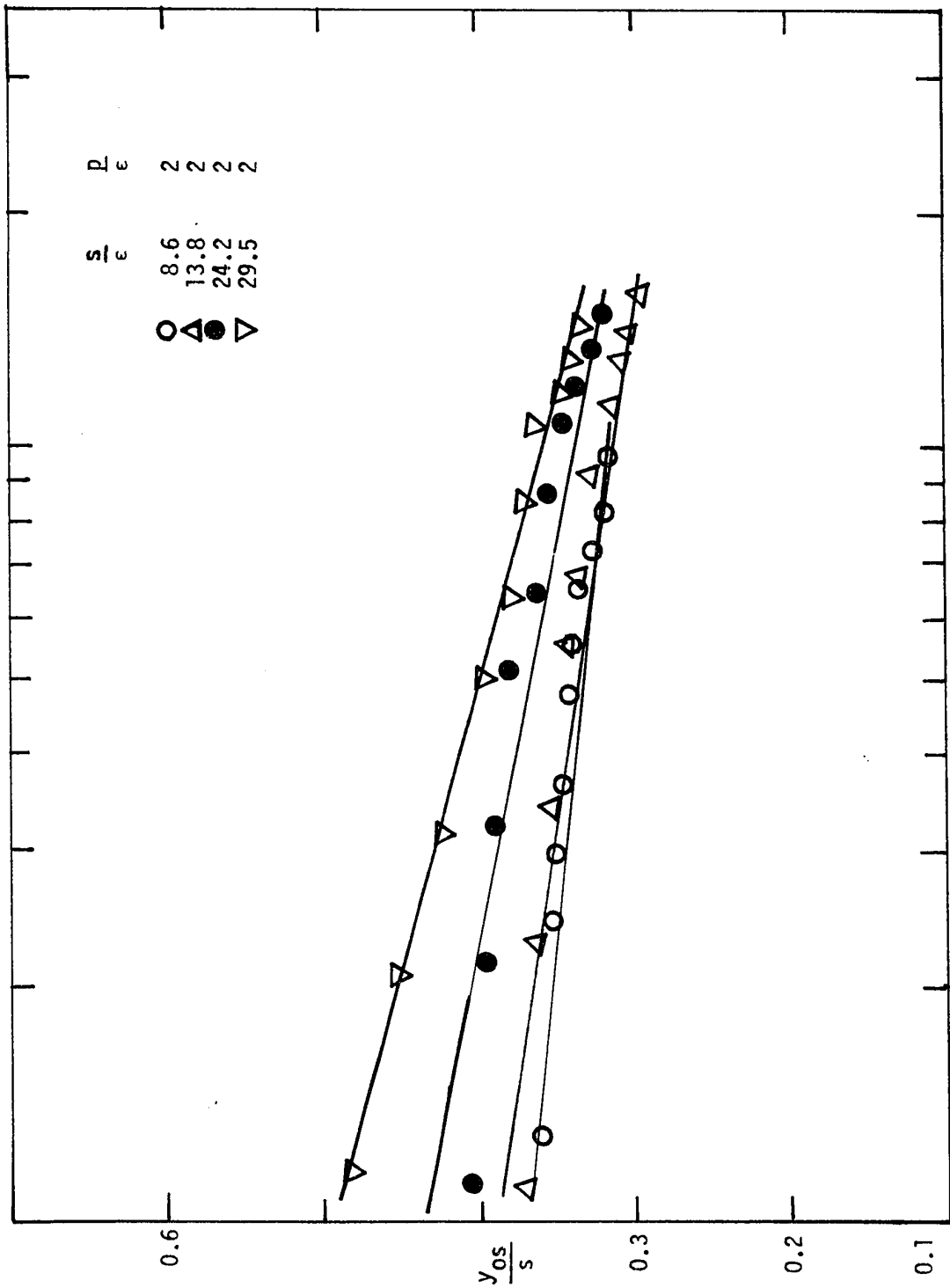

Figure 5.9 Zero Shear Point vs Reynolds Number

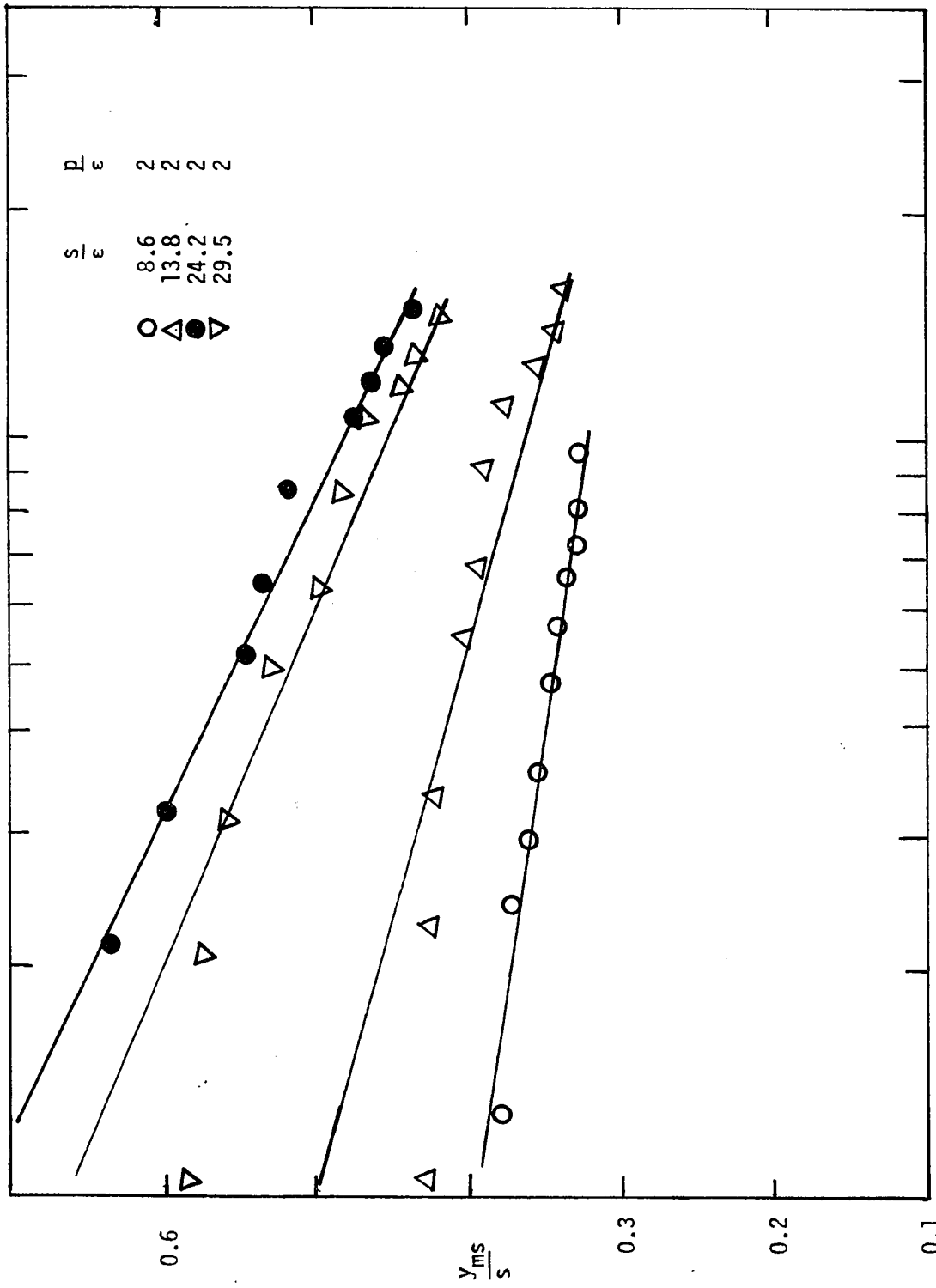

Figure 5.10 Maximum Velocity Point vs Reynolds Number

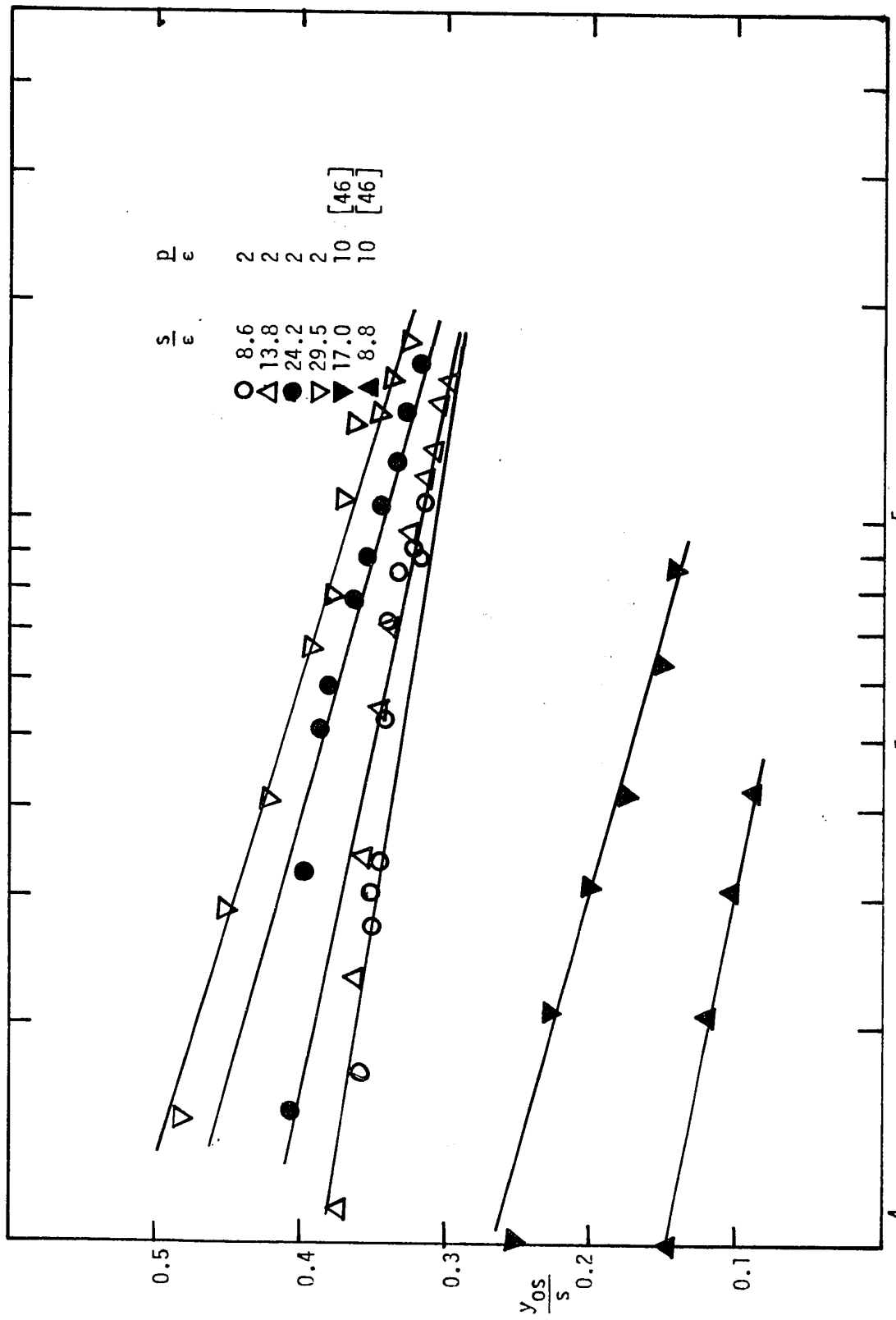

Figure 5.11 Zero Shear Point vs Reynolds Number Based on Maximum Velocity in the Channel

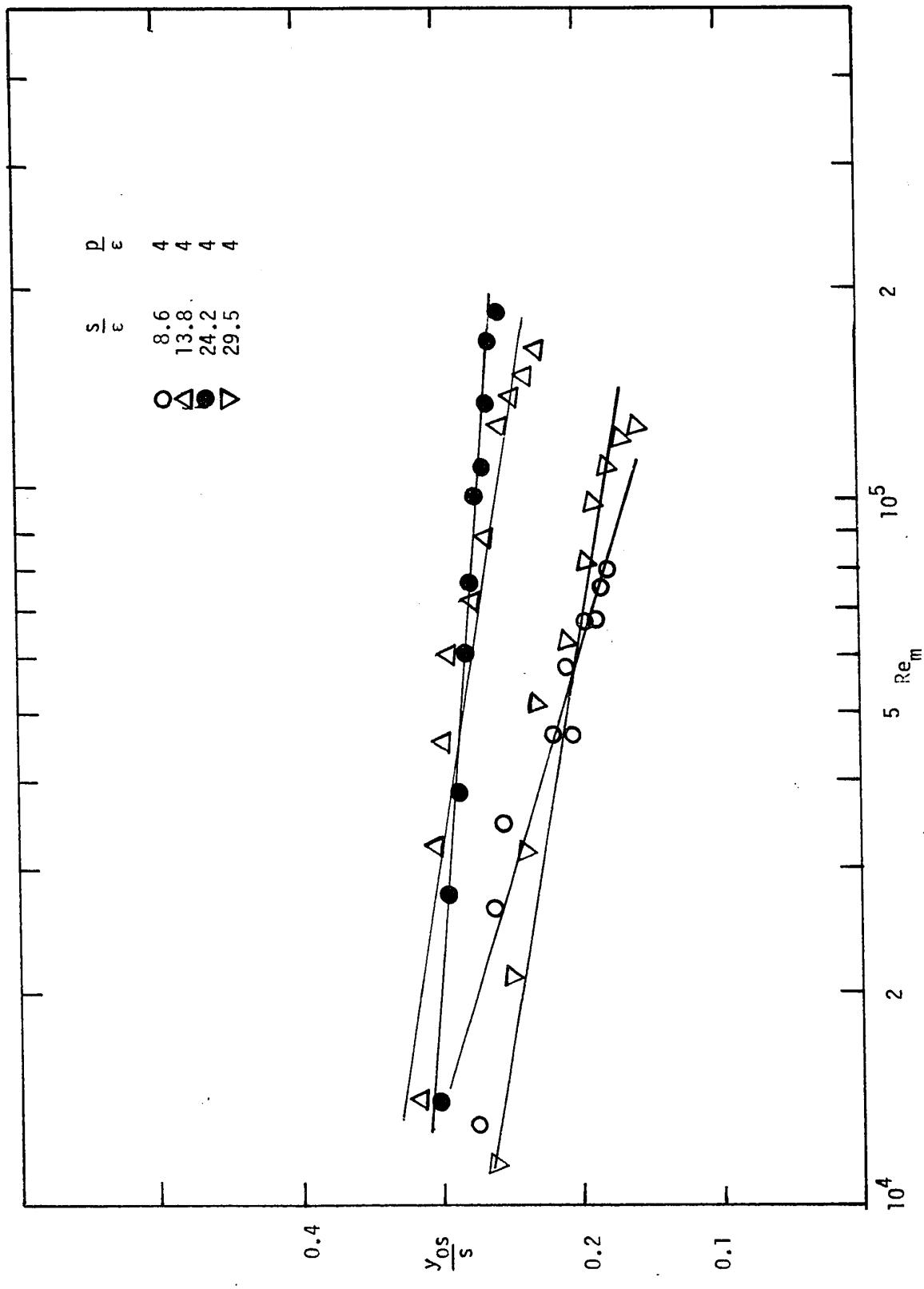

Figure 5.12 Zero Shear Point vs Reynolds Number Based on Maximum Velocity in the Channel

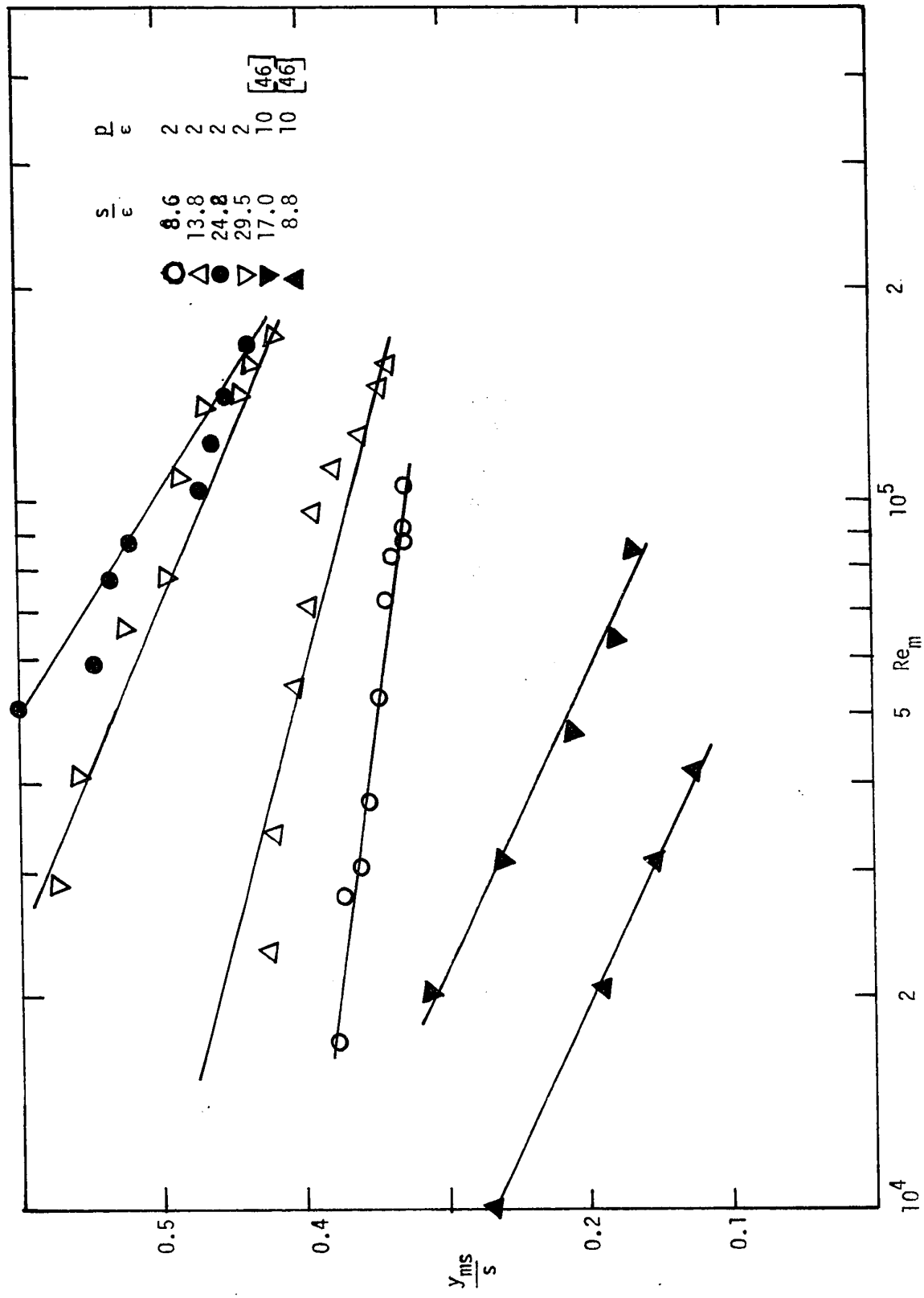

Figure 5.13 Maximum Velocity Point vs Reynolds Number Based on Maximum Velocity in the Channel

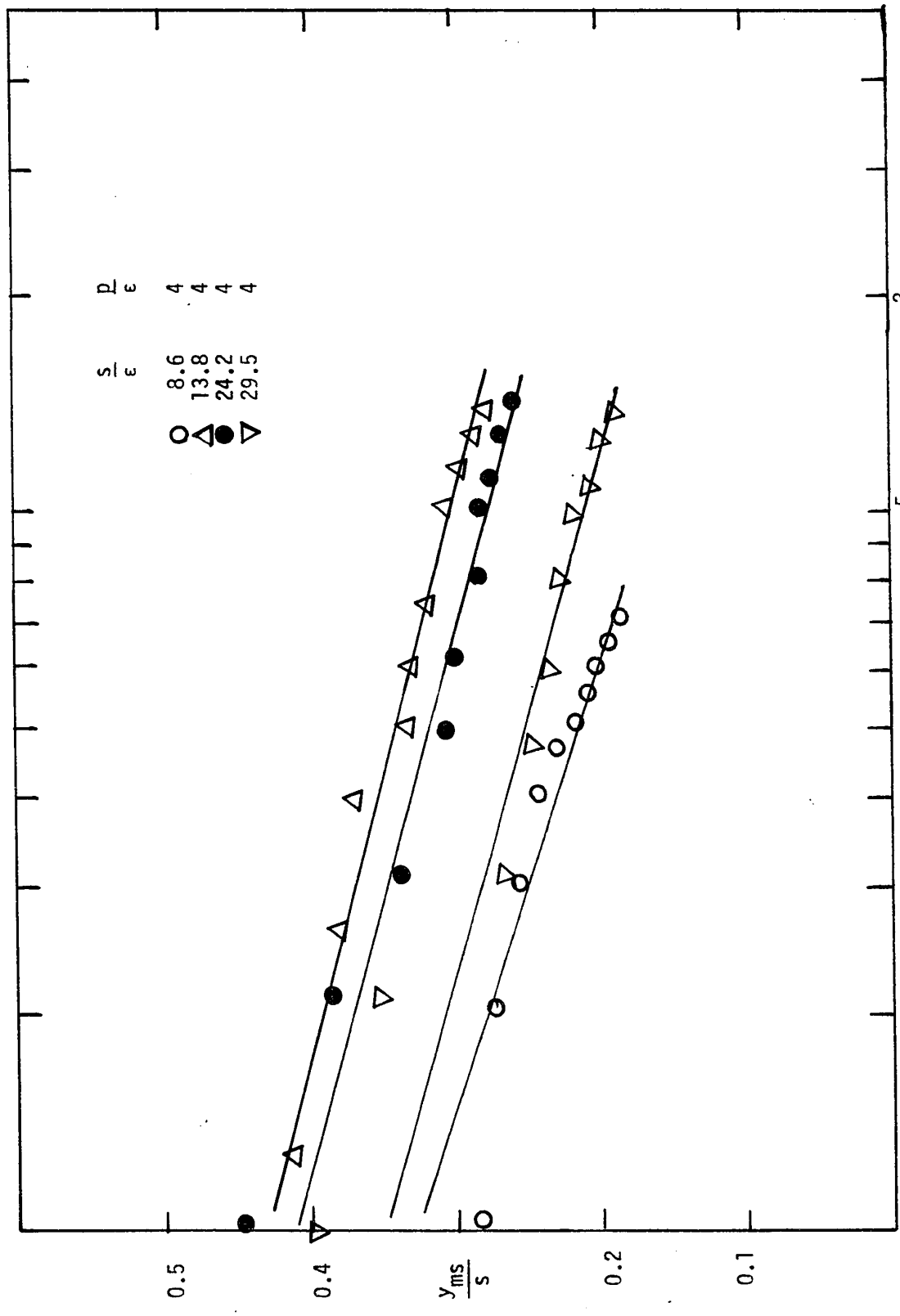

Figure 5.14 Maximum Velocity Point vs Reynolds Number Based on Maximum Velocity in the Channel

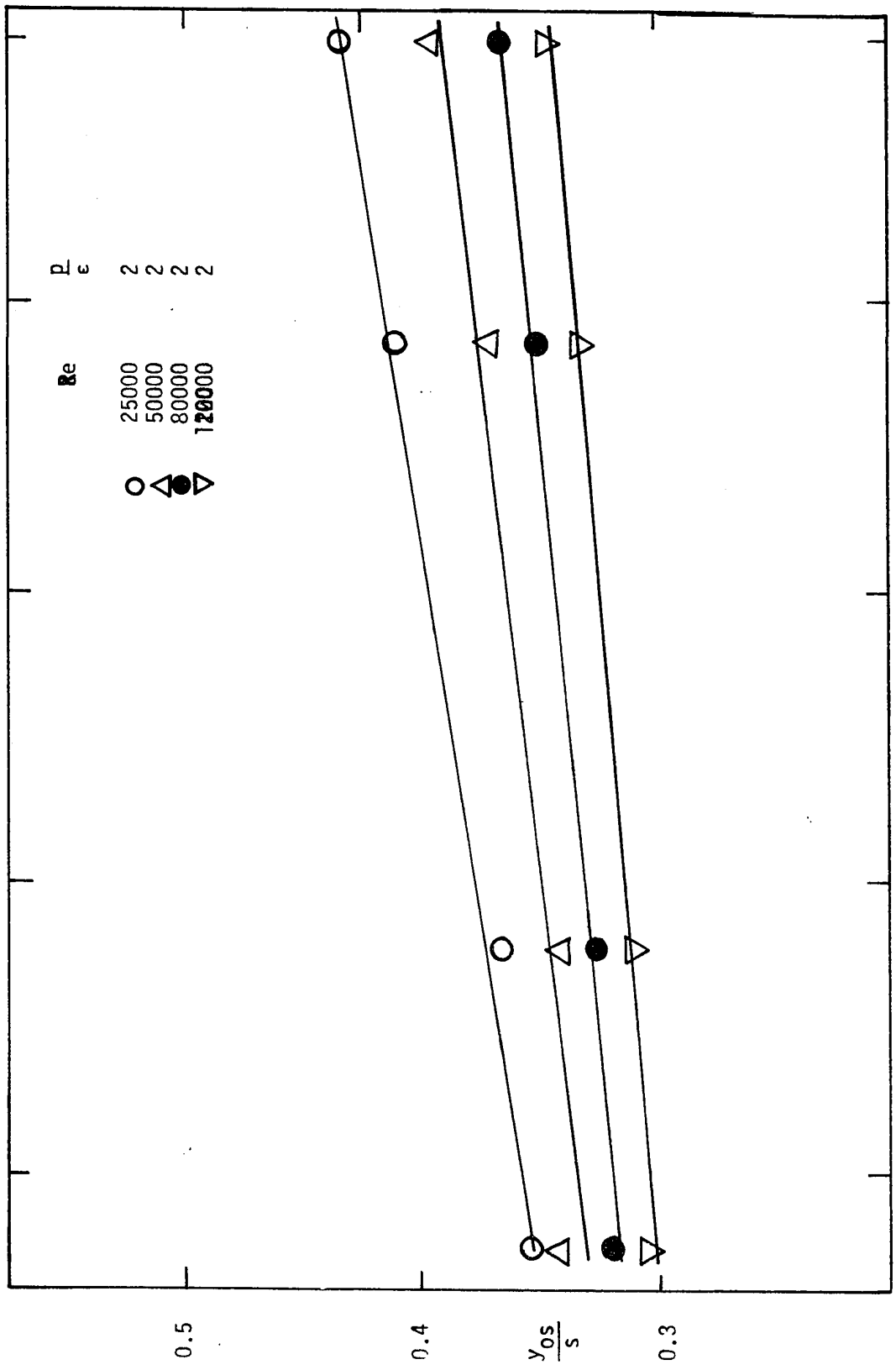

Figure 5.15 Zero Shear Point vs Channel width to Roughness Height Ratio

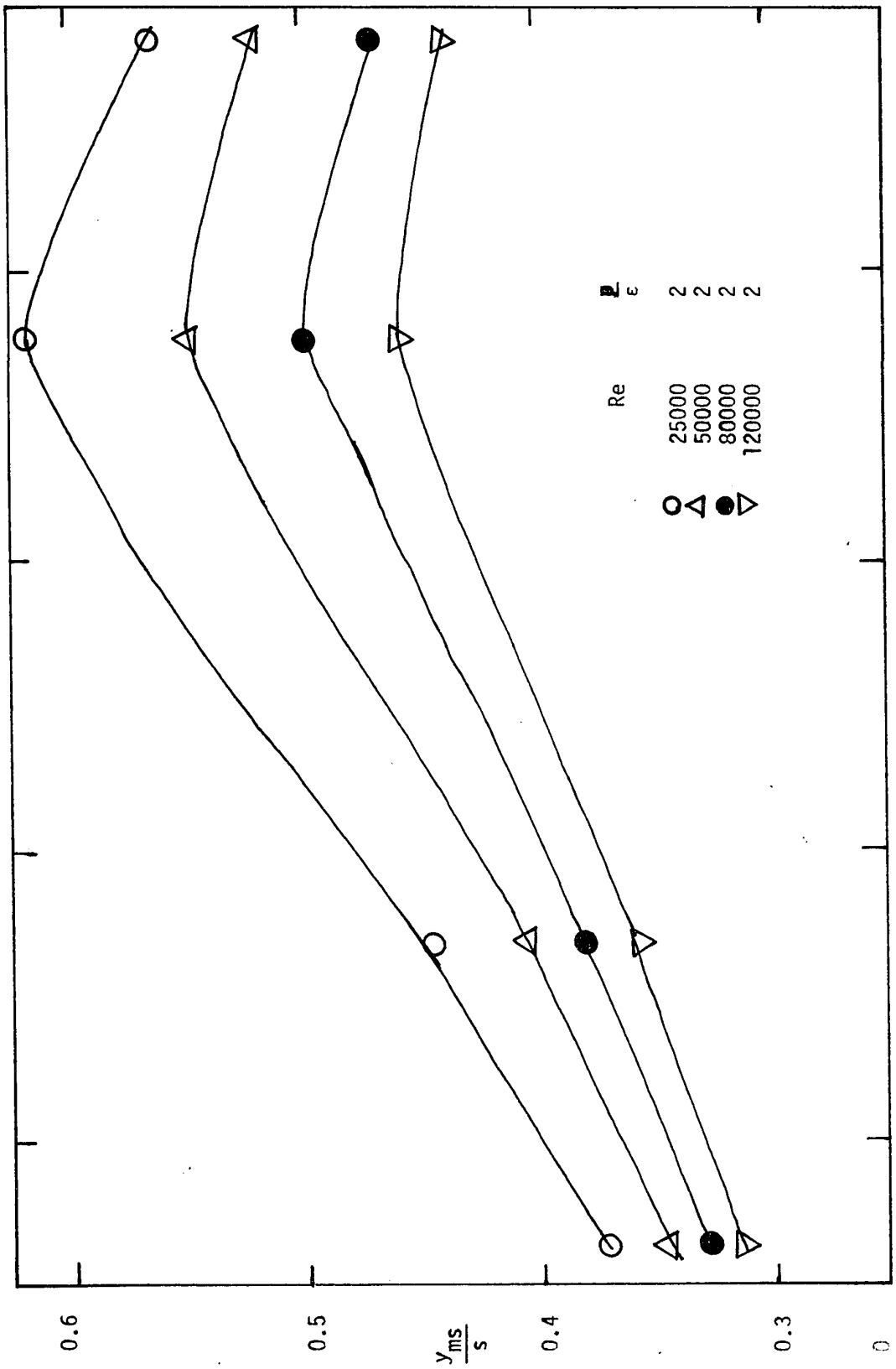

Figure 5.16 Maximum Velocity Point vs Channel width to Roughness Height Ratio

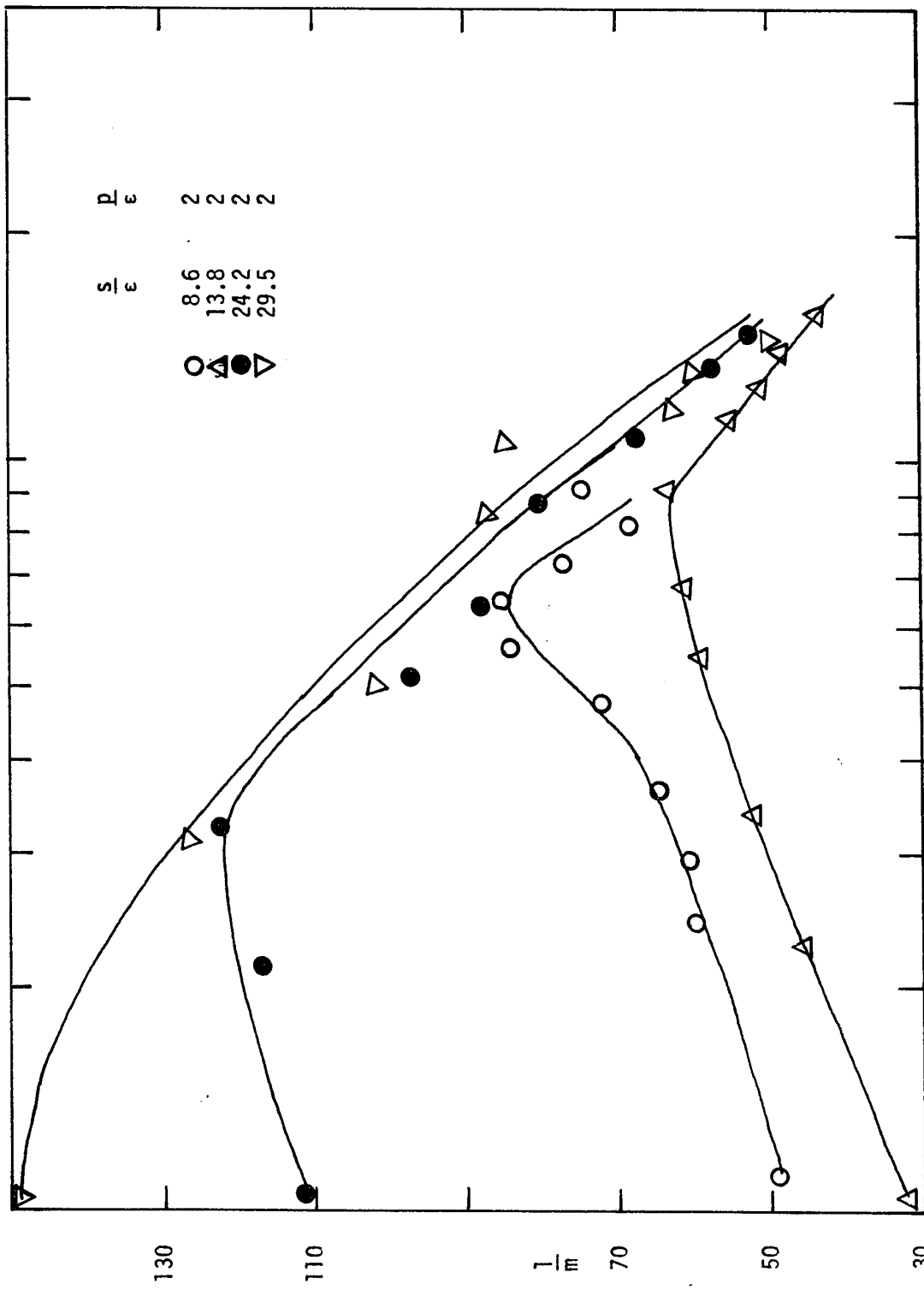

Figure 5.17A $\frac{1}{m}$ vs Reynolds Number

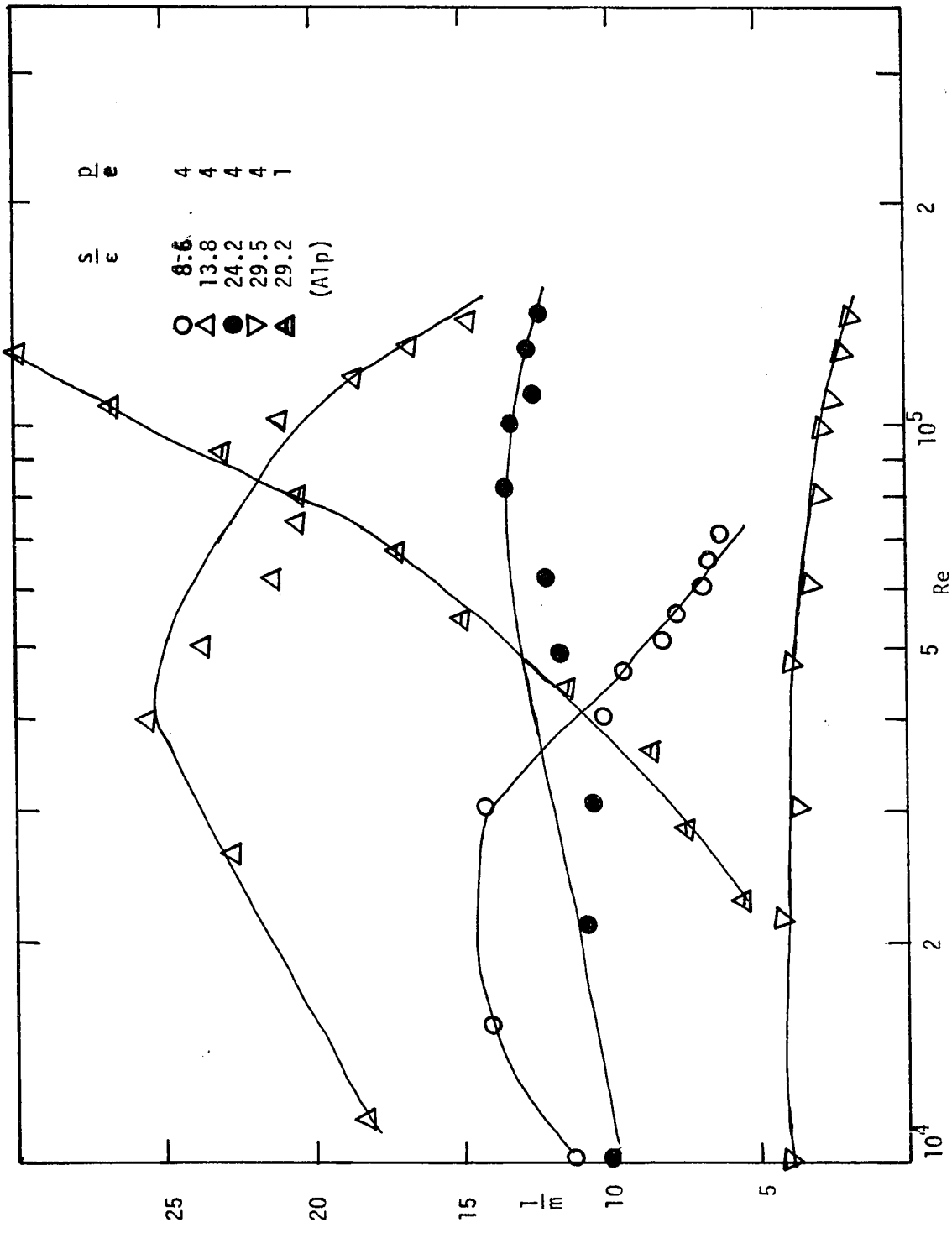

Figure 5.17B $\frac{1}{m}$ vs Reynolds Number

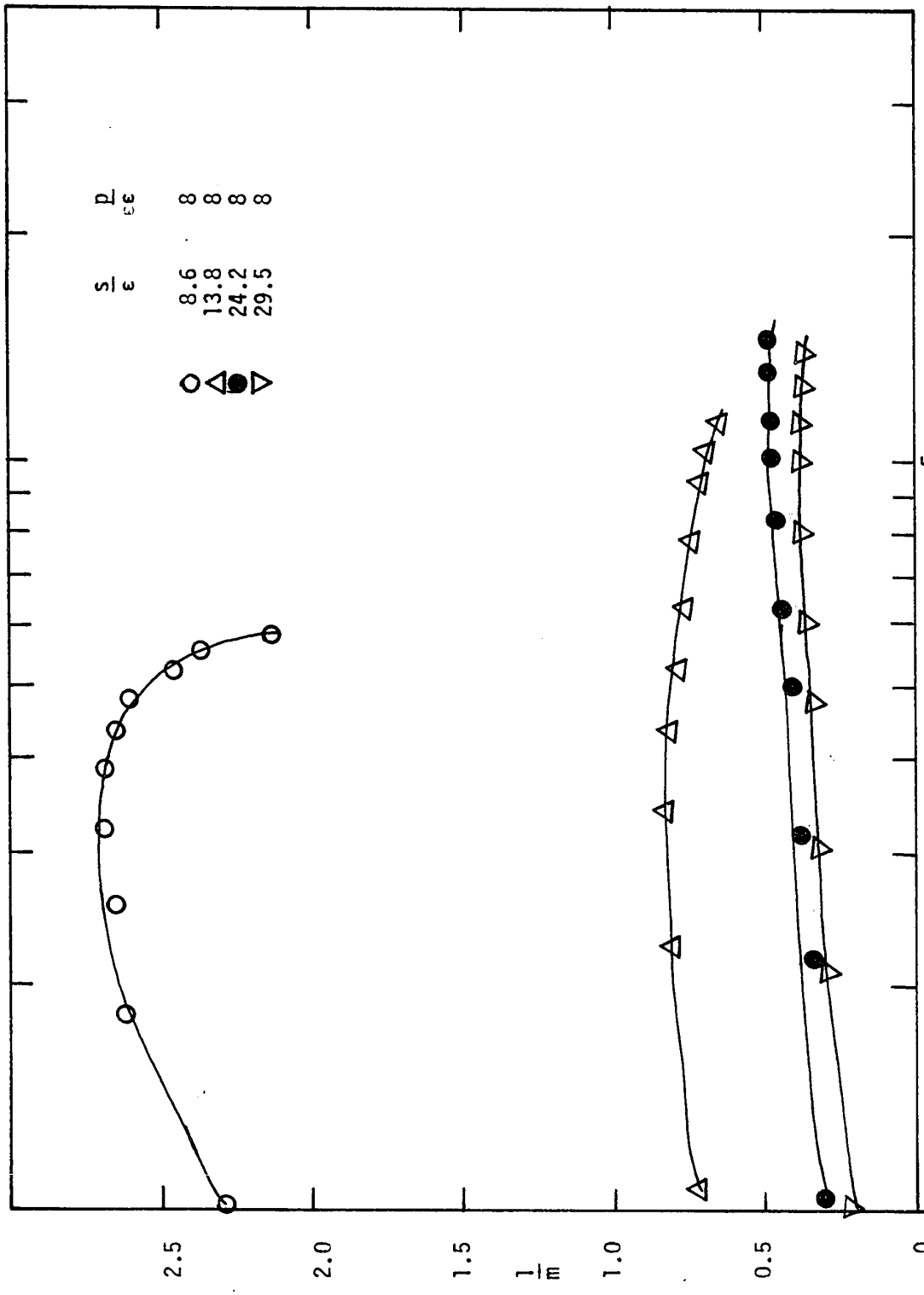

Figure 5.17C $\frac{1}{m}$ vs Reynolds Number

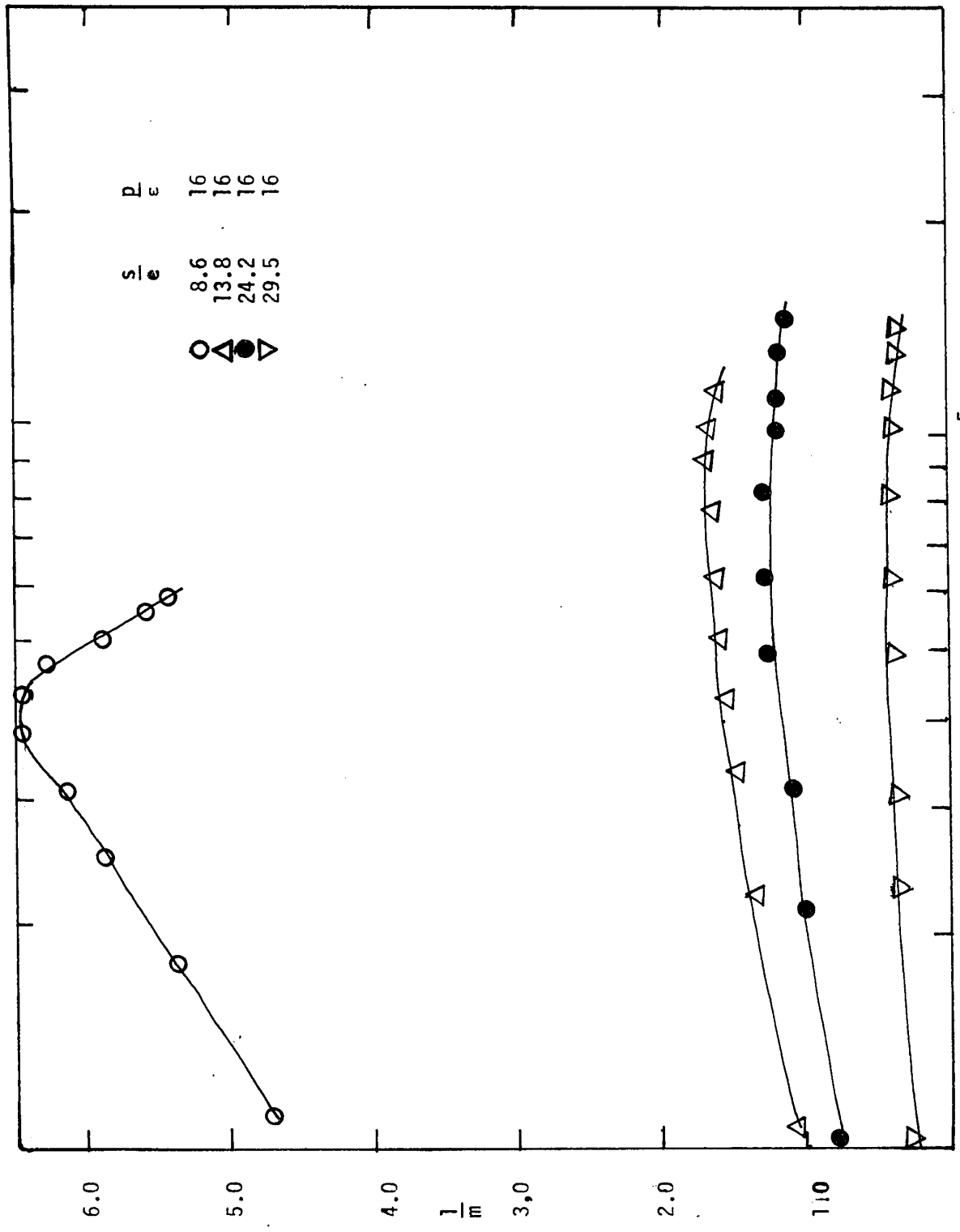

Figure 5.17D $\frac{1}{m}$ vs Reynolds Number

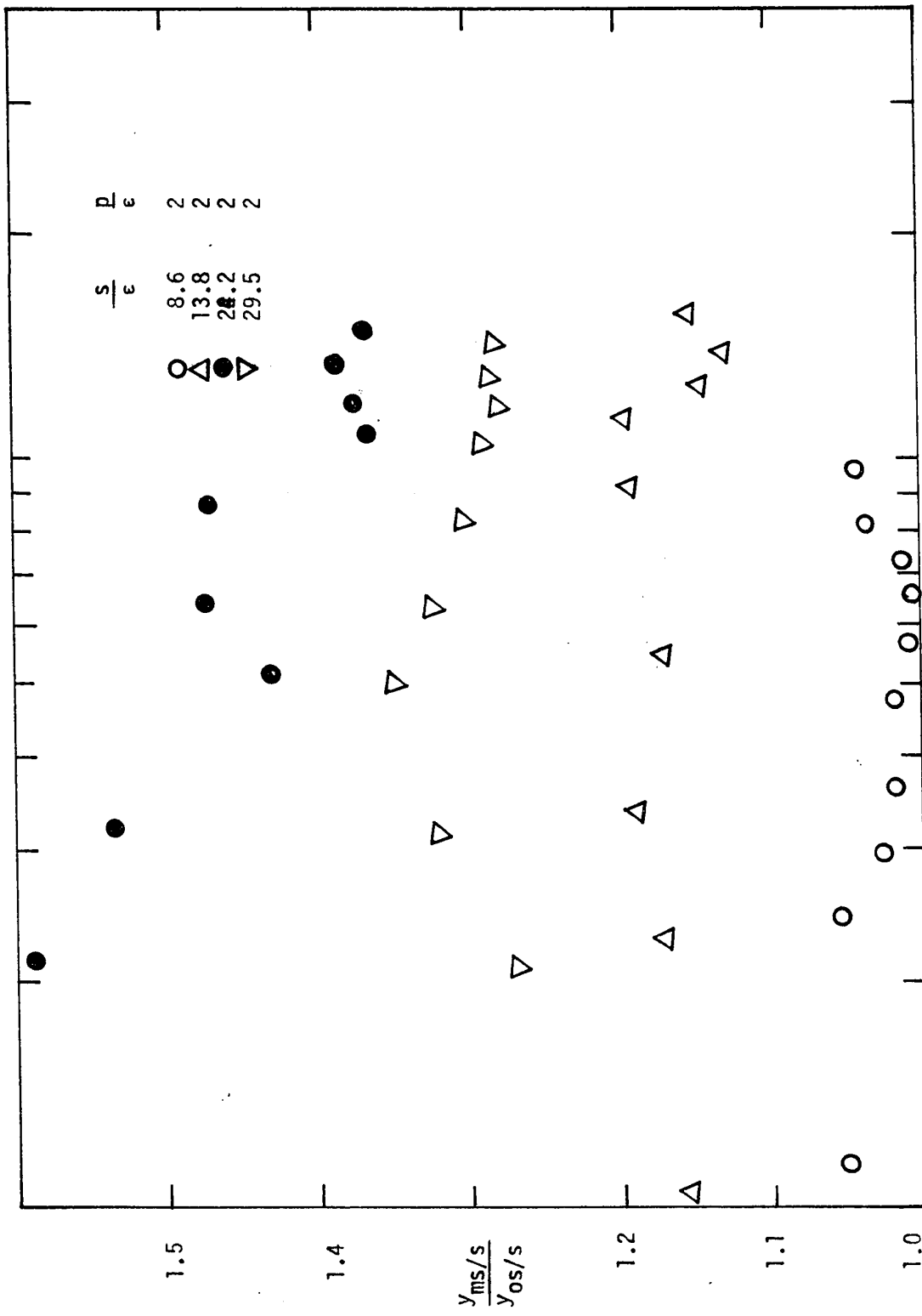

Figure 5.18 $\frac{y_{ms/s}}{y_{os/s}}$ vs Reynolds Number

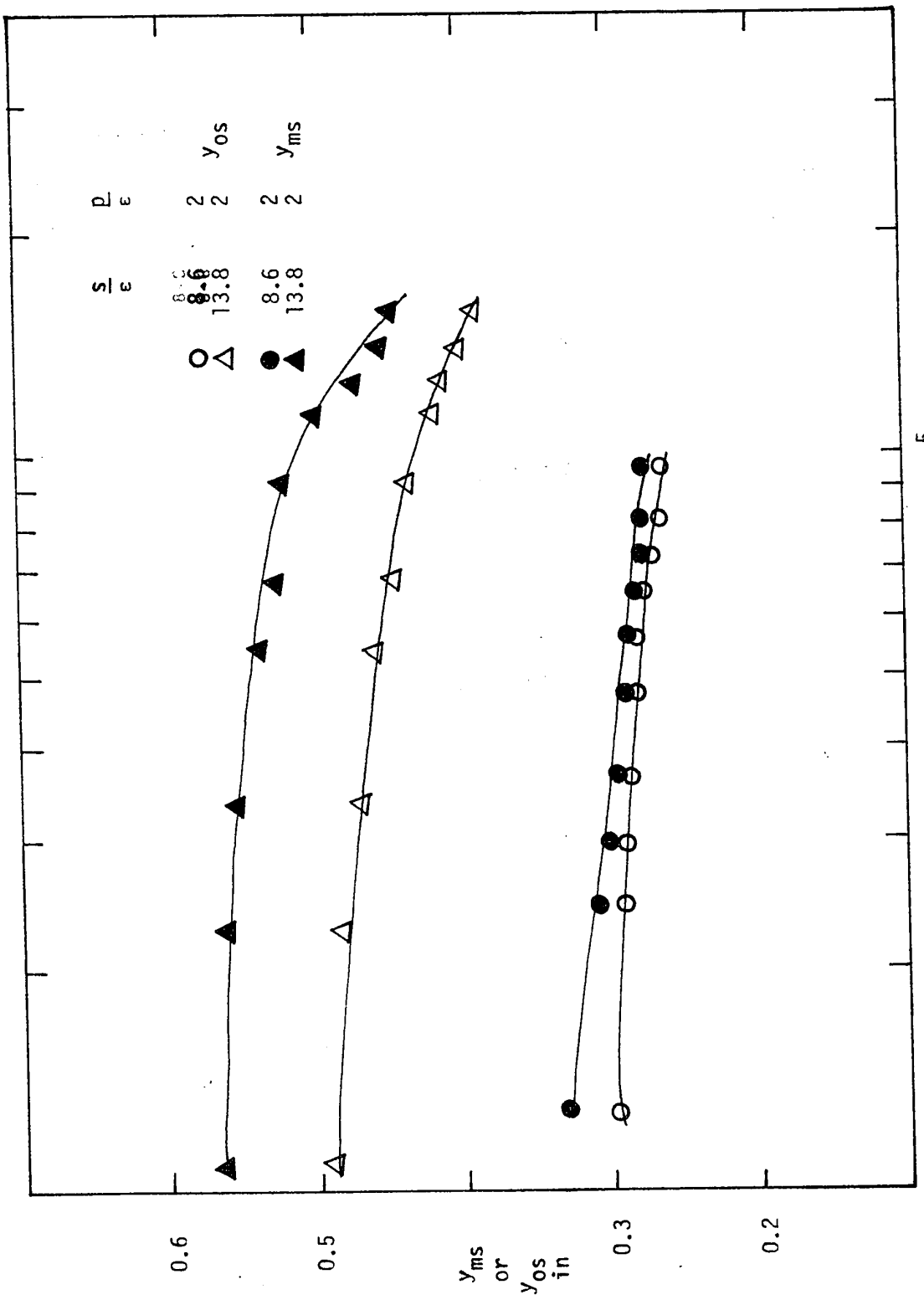

Figure 5.19 Variation of y_m and y_o with Reynolds Number

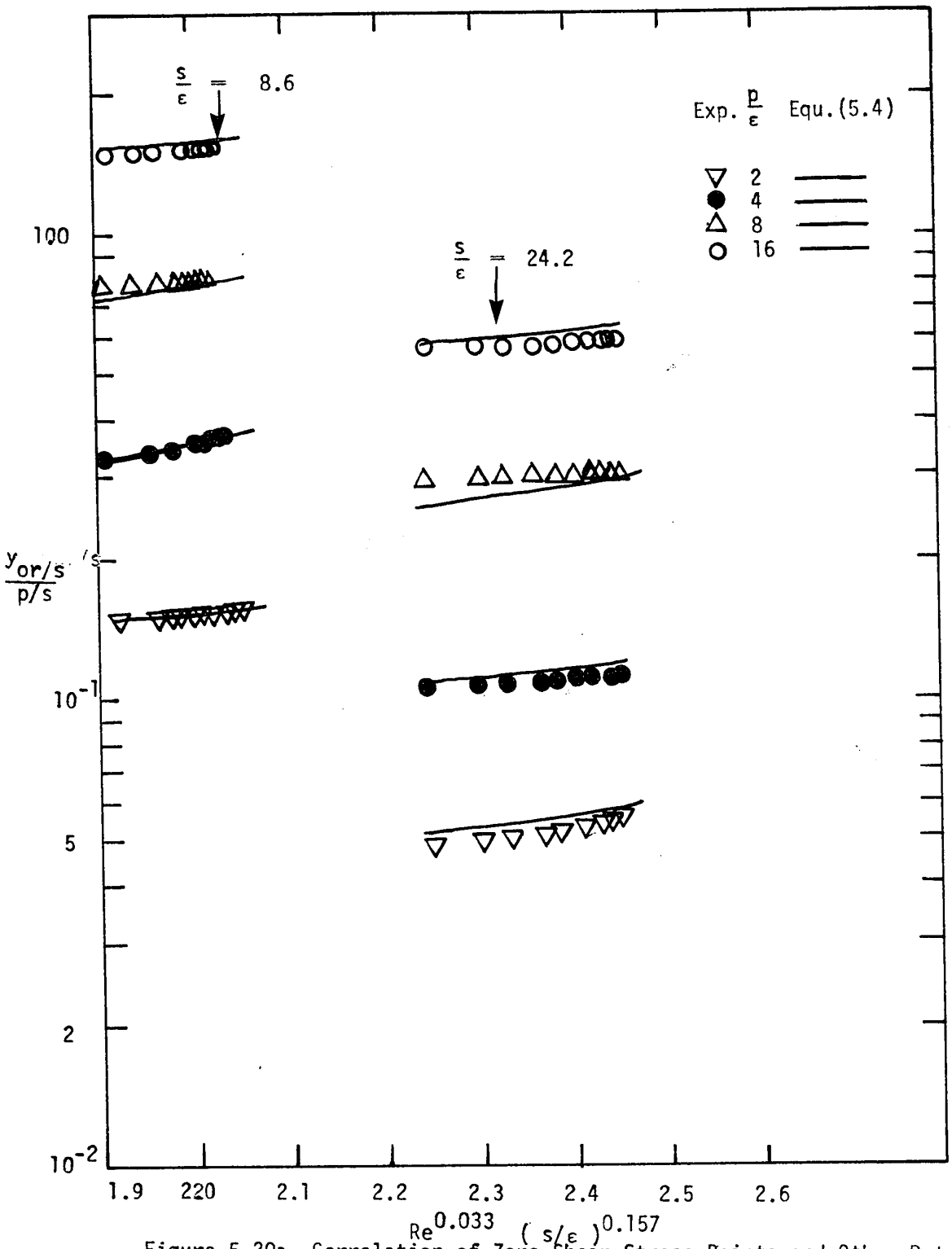

Figure 5.20a. Correlation of Zero Shear Stress Points and Other Data

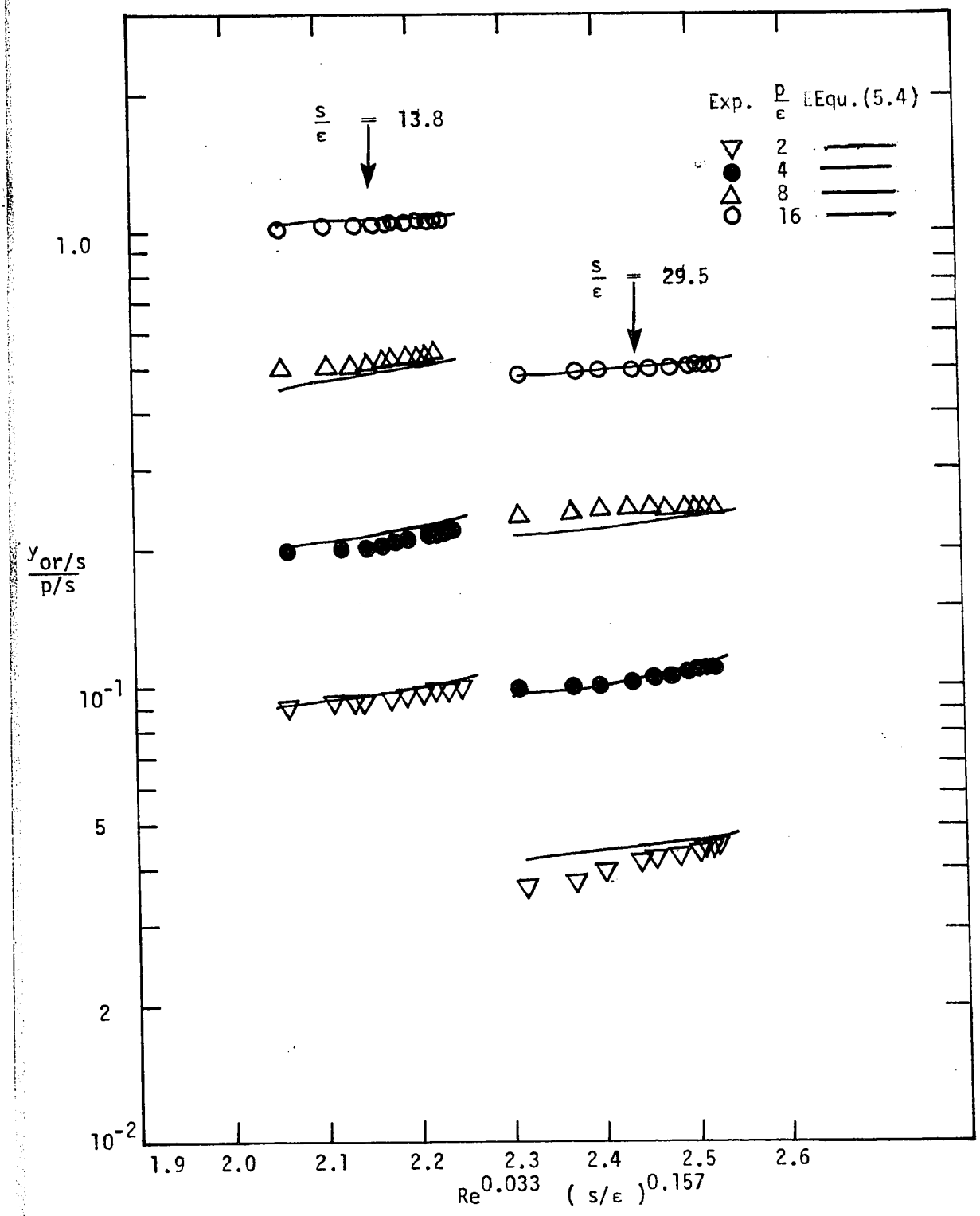

Figure 5.20b Correlation of Zero Shear Stress Points and Other Data

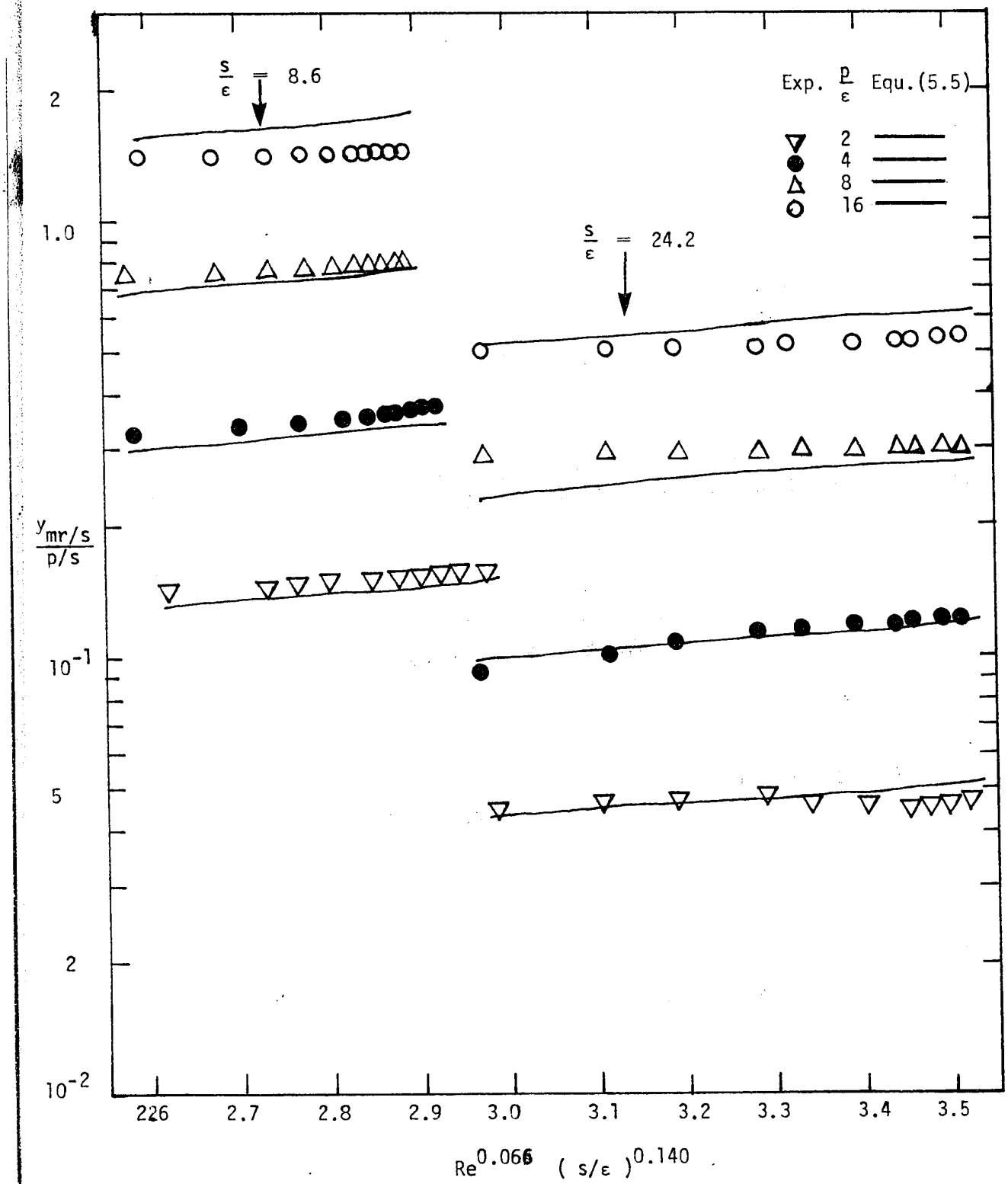

Figure 5.21a Correlation of Maximum Velocity Points and Other Data

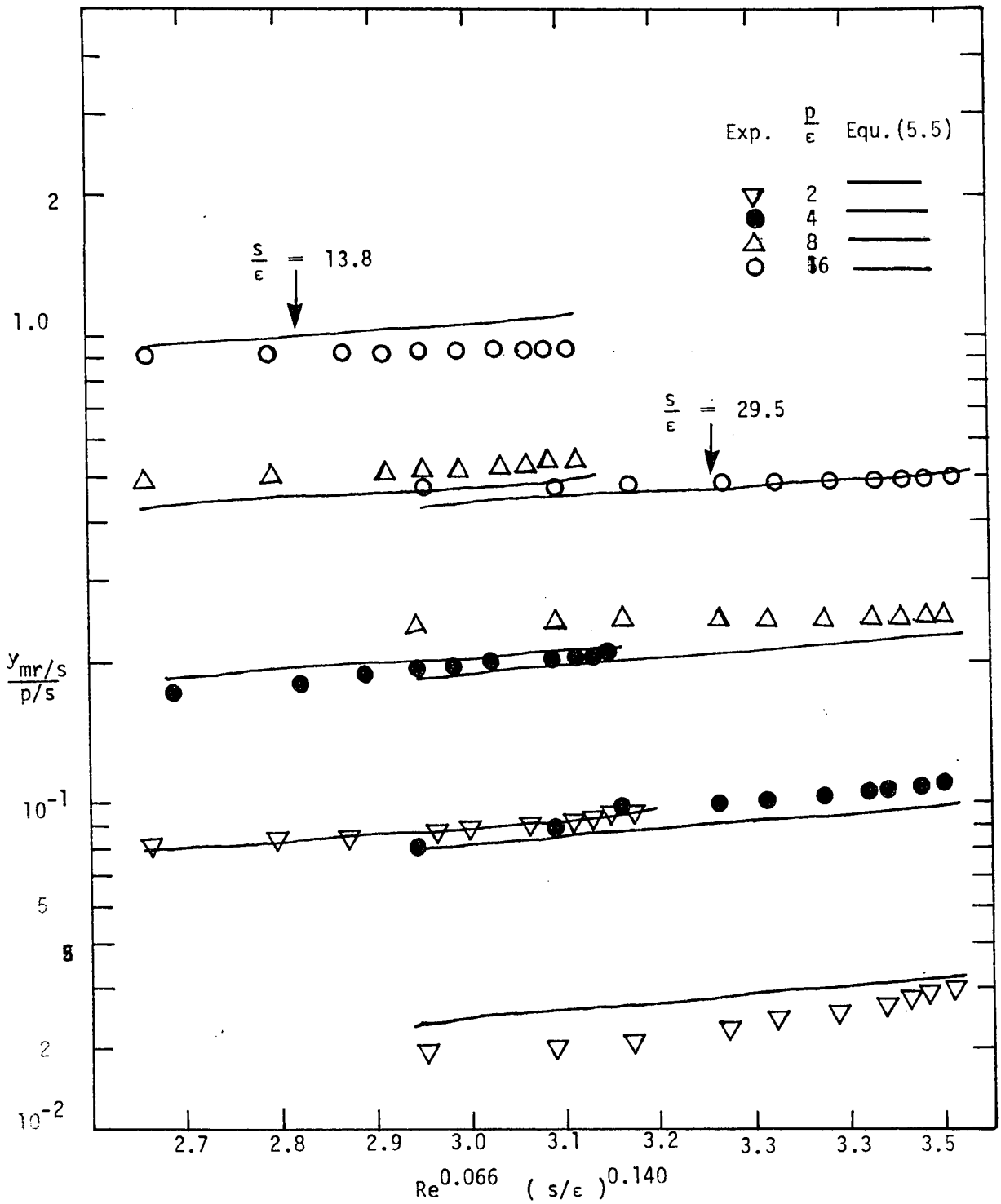

Figure 5.21b Correlation of Maximum Velocity Points and Other Data

REFERENCES

1. Hanjalic, K. and Launder, B.E., " Fully Developed Asymmetric Flow in a Plane Channel ", J. Fluid Mech., v.51,pp. 301-35 (1972).
2. Launder, B.E. and Spalding, D.B., " Mathematical Models of Turbulence ", Academic Press, London and New York (1972).
3. Spalding, D.B. and Patankar, S.V, Heat and Mass Transfer in Boundary Layers ", Morgan-Grampian, London (1967).
4. Deissler, R.G., " Analytical Investigation of Turbulent Flow in Smooth Tubes with Heat Transfer with variable Fluid Properties for Prandtl Number of 1 ", NACA TN 242 (1950).
5. Laufer, J, " The structure of Turbulence in Fully Developed Pipe Flow ", NACA Report, p1174 (1954).
6. Cremers, C.J. and Eckert, E.R.G., " Hot - Wire Measurements of Turbulence Correlations in a Triangular Duct ", J. of Applied Mech., pp. 609-14 (1954).
7. Clark, J.A., " A Study of Incompressible Turbulent Boundary Layers in Channel Flow ", J. of Basic Eng., Trans. ASME, v.90,pp. 455-68 (1968).
8. Barrow, H., " Fluid Flow and Heat Transfer in an Annulus with a Heated Core Tube ", Proc. Inst. Mech. Eng., v.56,p. 1113 (1955) (1955).

9. Lee, Y. and Barrow, H., " Turbulent Flow and Heat Transfer in Concentric Annuli ", Proc. I. Mech. Eng., v.178, pp. 1-16 (1963-64).

10. Brighton, J.A. and Jones, J.B., " Fully Developed Turbulent Flow in Annuli ", J. of Basic Eng., Trans. ASME, Sec. D, v.86,pp. 835-44 (1964).

11. Levy, S.,"Turbulent Flow in Annulus " , J. of Heat Transfer, ASME, v.89,pp. 25-31 (1967).

12. Quarmby, A., " An Experimental Study of Turbulent Flow Through Concentric Annuli ", Int. J. Mech. Sci., v.9,pp. 205-21 (1967).

13. Quarmby, A., " An Analysis of Turbulent Flow in Concentric Annuli ", Appli, Sci. Res., v.19,pp. 250-73 (1968).

14. Michiyoshi, I. and Nakajima, T., " Fully Developed Turbulent Flow in a Concentric Annulus ", J. of Nuclear Sci. and Tech., v.5,pp. 354-59 (1968).

15. Randhava, S.S., " An Analysis of Turbulent Flow in Concentric Annuli ", A.I.CH.E. Jour., v.15,pp. 132-33 (1969).

16. Kjellstrom, B. and Hedberg, S., " On Shear Stress Distributions for Flow in Smooth and Partially Rough Annuli ", Aktiebolaget Atomenergi AE-243, Sweden (1966).

17. Robertson, J.M., Martin, J.D. and Burkhart, T.H., " Turbulent Flow in Rough Pipes ", I/EC Fundamentals, v.7,pp. 253-65 (1968).

18. Deissler, R.G., " Analytical and Experimental Investigation of Adiabatic Turbulent Flow in Smooth Tubes ", NACA TN 2138 (1950).

19. Holdhusen, J.S., " The Turbulent Boundary Layer in the Inlet Region of Smooth Pipes ", Ph.D.Thesis, Univ. of Minesota (1952).

20. Knudsen, J.G. and Katz, D.L., " Fluid Dynamics and Heat Transfer ", Mc Graw Hill Book Co. Inc. (1958).

21. Hatton, A.P. and Walklate, P.J., " A Mixing-Length Method for Predicting Heat Transfer in Rough Pipes ", Int. J. Heat Mass Transfer, v.19,pp. 1425-31 (1975).

22. Van Driest, E.R., " On Turbulent Flow Near a Wall ", Jour. of Aero. Sci., v.23,p. 1007 (1956).

23. Reichardt, H., " Vollstandige Darstellung der Turbulenten Geschwindigkeitsverteilung in Glatten Leitungen ", ZAMM 31, pp. 208-19 (1951).

24. Deissler, R.G., " Turbulent Heat Transfer and Friction in the Entrance Regions of Smooth Passages ", Trans. ASME, pp. 1221-33 (1955).

25. Park, S.D. and Lee, Y., " Diabatic Turbulent Flow in the Entrance Region of Concentric Annuli ", EIC, v.14,n. B-3 (1971).

26. Sparrow, E.M., Eckert, E.R.G. and Minkowycz, W.J., " Heat Transfer and Skin Friction for Turbulent Boundary Layer Flow Longitudinal to a Circular Cylinder ", J. of Appl. Mech., pp. 37-43 (1963).

27. Kays, W.M. " Convective Heat and Mass Transfer ", Mc Graw Hill Book Co. Inc. (1966).

28. Von Karman, T. " The Analogy between Fluid Friction and Heat Transfer ", Trans. ASME 61, p. 705 (1939).

29. Kay, J.M., " Fluid Mechanics and Heat Transfer ", Camb. Univ. Press, London (1957).

30. Rannie, W.D., " Heat Transfer in Turbulent Shear Flow ", Jour. of Aero. Sci., v.23, p. 485 (1956).

31. Spalding, D.V., " Single Formula for the Law of the Wall ", Jour. of Appl. Mech., ASME ' v.28, pp. 455-58 (1961).

32. Wasan, D.T., Tien, C.L. and Wilkie, C.R., " Theoretical Correlation of Velocity and Eddy Viscosity for Flow close to a Pipe Wall ", Jour. of A.I.CH.E., v.9, p. 567 (1963).

33. Plate, E.J., " Aerodynamic Characteristies of Atmospheric Boundary Layers ", TID-25465, AEC Critical Review Series, U.S. Atomic Energy Com. (1971).

34. Barrow, H., " Semi-Theoretical Solution of Asymmetric Heat Transfer in Annular Flow ", Jour. Mech. Eng. Sci., v.2 , p. 331 (1960).

35. Rothfus, R.R., Monrad, C.C. and Senecal, V.E., " Velocity Distribution and Fluid Friction in Smooth Concentric Annuli ", Ind. Eng. Chem., v.42, No.2, p. 2511 (1960).

36. Roll, H.U., " Physics of Marine Atmosphere ", Academic, New York (1965).

37. Sutton, O.G., " Micrometeorology ", Mc Graw Hill Book Co. Inc. (1953).

38. Streeter, V.L., " Frictional Resistance in Artificially Roughened Pipes ", Proc. Amer. Soc. Civil Eng., v.61, p. 163 (1935).

39. Sherrif, N. and Gumley, P., " Heat Transfer and Friction Properties of Surfaces with Discrete Roughness ", Int. J. Heat Mass Transfer, v.9, pp. 1297-1320 (1966).

40. Webb, R.L., Eckert, E.R.G. and Goldstpin, R.J., " Heat Transfer and Friction in Tubes with Repeated-Rib Roughness ", Int. J. Heat Transfer, v. 14, pp. 601-17 (1971).

41. Wilkie, D., Cowin, M., Burnett, P. and Burgoyne, T., " Friction Factor Measurements in a Rectangular Channel with Walls of Identical and Non-identical Roughness ", Int. J. Heat Mass Transfer, v.10, pp. 611-21 (1967).

42. Furber, B.N. and Cox, D.N., " Heat Transfer and Pressure Drop Measurements in Channels with Whitworth Thread Form Roughness ", J. Mech. Eng. Sci., v.9, pp. 339-50 (1967).

43. Hall, W.B., " Heat Transfer in Channels having Rough and Smooth Surface ", J. Mech. Eng. Sci., v.4, p. 287 (1962).

44. Reynolds, O., " On the Dynamic Theory of Incompressible Viscous Fluids and the Determination of Criterion ", Phil. Trans. Roy. Soc., T 186 A123 (1895).

45 Schlichting, H., " Boundary-Layer Theory ", Mc Graw Hill Book Co. Inc., 6th Edition (1968).

46. Eckert, E.R.G., " Introduction to the Transfer of Heat and Mass ", Mc Graw Hill Book Co. Inc., First Edition, p. 74 (1950).

47. Prandtl, L., " Über Flussigkeitsbewegung bei sehr Kleiner Reibung ", Proc. of the Third Intern. Math. Congr. Heidelberg (1904) ; also " Collected Works ", v.3, pp. 575-84 (1961).

48. Prandtl, L., " Über die Ausgebildete Turbulenz ", ZAMM 5, pp. 136-39 (1925); also " Collected Works ", v.2, pp. 736-51 (1961).

49. Von Karman, T., " Über Laminare und Turbulente Reibung ", ZAMM 1, pp. 233-53 (1912) ; also " Collected Works ", v.2, pp. 70-97, London (1956).

50. Reichardt, H., " Messungen Turbulent Schwankungen ", Naturwrssenschaften, p. 404 (1938).

51. Taylor , G.I., " Conditions at the Surface of a Hotbody Exposed to the Wind ", Tech. Rep., Advisory Committee for Aeronantics, v.2, R and M, p. 272 (1916),

52. Prandtl, L., " Bemerkung Über den Wärneübergang in Rohr ", Physik Zeitschr, v.29, (1928).

53. Von Karman, T., " Turbulence and Skin Friction ", J. of the Aero. Sci., V.1., No.1, p.1. (1934).

54. Alp., E., " Asymmetric Turbulent Flow : Analysis and Experiment ", M.A.Sc. Thesis, Dept. of Mech. Eng., Univ. of Ottawa (1974).

55. Shaw, C.Y., " Turbulent Transport Phenomena between a Large Body of Water and Surrounding Atmosphere ", Ph.D. Thesis, Dept. of Mech. Eng., Univ. of Ottawa, (1975).

56. Nikuradse, J., " Strömungsgesetze in Rauhen Rohren ", Forsh, Arb.Ing.-Wes., No.361 (1933).

57. Young, A.D., " The Drag effects of Roughness at High Suberitical Speeds ", Jour. of Roy. Aero.Soc., v.18, p. 534 (1950).

58. Paeshke, W., " Experimentelle Untersuchungen Zum Raughigekeits- und Stabilitätsproblem in der boden nahen Luftschicht ", Z. Geophysik, v.13, p. 14 (1937).

59. Geffroy, J., Jude, P. and Paumard, G., " Contribution a l'etude de la convection forcee par surfaces corruguees ", Fourth Int. Heat Transfer Cont., Fc 5.1, Paris (1970).

60. Simpson, R.L., " A Generalized Correlation of Roughness Density Effects on the Turbulent Boundary Layer ", AIAA Jour., v.2, pp. 242-44 (1973).

61. Hanjalic, K., " Two Dimensional Asymmetric Turbulent Flow in Ducts "., Ph.D. Thesis , Univ. of London (1970).

62. Clauser, F.H., " Turbulent Boundary Layers in Adverse Pressure Gradients ", Jour. of Aero. Sci., v.21, pp. 91-108 (1954).

63. Hama, F.R., " Boundary Layer Characteristics for Smooth and Rough Surfaces ", Trans. of Soc. of Naval Arch. and Marine Eng., v.62, pp. 333-58 (1954).

64. Perry, A.F. and Joubert, P.N., " Rough Wall Boundary Layer in Adverse Pressure Gradients ", J. of Fluid Mech., v.17, pp. 193-211 (1963).

65. Wu, J., " Flow in Turbulent Wall Layer over Uniform Roughness", J. of Appl. Mech.,v.40, pp. 863-67 (1973).

66. Bussinesq, J., " Theorie de L'ecoulement Tourbillant ", Mem. Pres. Acad. Sci. xxlll, 46, Paris (1877); quoted from 5 , Chapter 19.

67. Eskinazi, S. and Yeh, H., " An Investigation on Fully Developed Flows in Curved Channels ", Jour. of Aero. Sci., v.23, pp. 23-24 (1956).

68. Townsend, A.A., " Equilibrium Layers and Wall Turbulence ", J. Fluid Mech., v.11, pp. 97-120 (1961).

69. ISO Recommendation R 540, " Measurement of Fluid Flow by Means of Orifice Plates and Nozzles ", 1st Edition (1967).

70. Spiller, R.L., " The Art and Practice of Orifice Flow Metering ", Instrumentation Technology, v.18, pp.52-56 (1971).

71. Instrumentation Manual, MKS Baratron Type 77, MKS Instruments Inc., Burlington, Massachusetts (1967).

72. Durst, F., Launder, B.E. and Akesson, H., " The Determination of the Position of Maximum velocity in Turbulent Shear Flow ", Aero. J. Roy. Aero. Soc., v.75, pp. 196-99 (1971).

73. DISA Hot-Wire Anemometer System Instruction and Service Manuals, DISA Electronik A/S, Denmark (1968 , 1973).

74. Park, S.D., " Developing Turbulent Flow and Heat Transfer in Concentric Annuli, an Analytical and Experimental Study ", Ph.D. Thesis, Dept. of Mech. Eng., Univ. of Ottawa (1971).

75. Massey, B.S., " Mechanics of Fluids ", Van Nostrand Reinhold Co., London (1971).

76. IBM SSP / 360 Manual (1970).

77. Eckert, E.R.G. and Drake, R.M. Jr., " Heat and Mass Transfer ", Mc Graw Hill Book Co. Inc., Appendix of Property Values (1959).

78. Rampf , H. and Feurstein, G., " Wärmeübergang und Druckverlust an Dreiecksformigen Roughigkeiten in Turbulenter Rengspaltströmung ", Fourth Int. Heat Transfer Conf., FC 5.3,Paris (1970).

79. Williams, F. and Watts, J., " The Development of Rough Surfaces with Improved Heat Transfer Performance and a study of the

Mechanisms Involved ", Fourth Int. Heat Transfer Conf., FC 5.5, Paris (1970).

80. Wang, J. and Tullis, J.P., " Turbulent Flow in the Entry Region of a Rough Pipe ", ASME Paper 73-WA/FE-3 (1973).

81. Tennekes, H., and Lumley, J.L., " A First Course in Turbulence ", The MIT Press, Cambridge, Massachusetts, and London, England (1972).

82. Nie, N.H., Hull, C.H., Jenkins , J.G., Steinbrenner, K. and Bent, D.H., " Statistical Package for the Social Sciences ", Second Edition, Mc Graw Hill Book Co., New York (1975).